Impact of Climate Change on Canadian Water Resources: A Continental-Scale Hydrologic Modelling Study Using Multiple RCM Projections

by

Jianming Chen

A thesis
presented to the University of Waterloo
in fulfillment of the
thesis requirement for the degree of
Doctor of Philosophy
in
Earth Sciences

Waterloo, Ontario, Canada, 2015

AUTHOR'S DECLARATION

I hereby declare that I am the sole author of this thesis. This is a true copy of the thesis, including any required final revisions, as accepted by my examiners.

I understand that my thesis may be made electronically available to the public.

Abstract

Evidence of climate change is mounting and there is nowadays an increasing international scientific consensus that current climate change is, in part, induced by anthropogenic emissions of greenhouse gases. Climate change will have significant impacts on the water cycle and hence on both quantity and quality of our limited and valuable water resources. Quantifying the potential hydrologic responses to a range of plausible future climates is the key for assessing the linkage between future climate change and water resources. There have been a large number of hydrologic impact studies addressing this challenging issue in the literature. Most of the studies, however, bear one or more of the following deficiencies: 1) global-scale GCM data are directly used as the forcing for the hydrologic model; 2) Future climate projections are derived based on only one emission scenario; 3) Future climate projections are derived based on only one climate model; 4) The future climate scenario is hypothetical, e.g. based on an arbitrary assumed change factor relative to the present-day climate scenario, instead of using a climate model output; 5) The hydrologic model does not simulate both surface water and groundwater in a physically-based manner and 6) The model domain is too small, e.g. a catchment or river basin scale. In this study, a continental-scale modelling framework free of the above caveats is developed to predict the potential future climate change effects on Canadian water resources. To the best of my knowledge, this study is one of the first of its kind in the literature.

HydroGeoSphere, a physically-based fully-coupled surface-subsurface flow and transport simulator, is selected to perform hydrologic modelling in this study. The study domain

covers the Northern half of North America continent, consisting of six super watersheds. The study domain is discretized into a triangular mesh, with refinement along hydrologically important features. After discretization, the 3D prism grid has 15 vertical layers and about one million nodes. In total 11 hydrostratigraphic units are represented in the 3D geology model which is constructed based on sediment thickness, permafrost distribution and surficial geological data. In this work, net precipitation data are used as the forcing to drive the HydroGeoSphere model. Present-day net precipitation is computed using observed total precipitation data in conjunction with high-resolution RCM outputs. The hydrologic model is initially used to reproduce present-day hydrology and the simulation results show good agreement against observed hydrologic data.

After calibration and validation, the HydroGeoSphere model is used to assess hydrologic impacts of future climate changes assuming that, except for net precipitation, all parameters and boundary conditions remain unchanged. Multiple high-resolution outputs obtained with three reputable RCMs (CRCM, HRM and WRF) under two IPCC emission scenarios (A2 and A1B) are used to estimate future net precipitation. This is determined based on the RCM projected changes between the future periods (2011-2040, 2041-2070 or 2071-2100) and the control period (1971-2000) using a hybrid approach. The long-term evolution of hydrologic responses to future climate changes over the 21st century is explored using three 30-year-period CRCM data. Efforts are also made to quantify the two main uncertainties in simulation results that are associated with the climate models and the emission scenarios using four RCM outputs for the period of 2041-2070. Simulation results suggest that rivers in the North are likely to observe a steady increase in streamflow and streamflows of the major

rivers in the South are predicted to remain more or less unchanged over the 21st century. The water table is predicted to rise in mountainous regions in the NW, decrease in the prairies and remain relatively unchanged for most of the remaining areas where the terrains are relatively flat. Sensitivity analyses indicate that the hydrologic responses are more sensitive to the different climate models than they are to the different emission scenarios.

This modelling study demonstrates that a fully-coupled surface and subsurface flow hydrologic simulation at the continental-scale is possible and could be made operational. The good skill exhibited by the HydroGeoSphere model for the present-day hydrology simulation suggests that high-resolution RCM outputs are effective surrogate data for actual ET estimation when observed climate data are insufficiently available. Based on the RCM projections used in this work, future climate may have significant hydrologic impacts in some regions of this study domain such as in the North and the prairies. However, simulation results should be interpreted with cautions due to the inconsistencies and sometimes even opposite predictions between the outputs of different RCMs.

Acknowledgements

There are many people I should thank and acknowledge here, but first and foremost I have to thank my supervisor Ed Sudicky. No words can express my gratitude and appreciation enough to him. In my view, I have been given everything that a student can expect from his/her supervisor. I am truly grateful for the great research topic, great financial support and the motivations along the way. I am also indebted to my co-supervisor Dick Peltier, who provided constructive and helpful feedbacks on the interim modelling results. Also, Dick and his team provided the WRF and permafrost data for this work. I would also like to thank my other committee members: Martin Ross, Dave Rudolph, Chin Man Mok, James Craig and David Hyndman. They all contributed significantly to this work. Martin and his team should also be acknowledged for compiling the surficial geological data.

I must also acknowledge my great indebtedness to Young-Jin Park and Rob McLaren for their invaluable technical assistance throughout the duration of my Ph.D. study. Special thanks should go to Jonathan Gula (for the WRF data), Lev Tarasov (for the permafrost data), and Matthew Schumacher (for the surficial geological data). Finally, I would like to thank my family, fellow students and friends for their moral support.

This work was funded by a grant from the Canadian Water Network, by a Natural Sciences and Engineering Research Council of Canada Discovery Grant, and by a Canada Research Chair in Quantitative Hydrogeology (Tier I) awarded to E.A. Sudicky. Additional funding for this work was provided by multiple scholarships from the Ontario Graduate Scholarship (OGS) and the UW President's Graduate Scholarship (PGS) programs awarded to the author.

Table of Contents

AUTHOR'S DECLARATION ii
Abstract iii
Acknowledgements vi
Table of Contents vii
List of Tables ix
List of Figures x
Chapter 1 Introduction 1
1.1 Background 1
1.2 Previous Studies 5
1.3 HydroGeoSphere 11
1.4 Objectives 16
1.5 Overall Modelling Approach 17
1.6 Thesis Organization 18
Chapter 2 Hydrologic Model Descriptions 20
2.1 Study Domain 20
2.2 Three-Dimensional Geology Model 21
2.2.1 Thickness of Sediments 22
2.2.2 Surficial Geology (Top 5.0 m) 23
2.2.3 Permafrost 23
2.2.4 Final Product 25
2.3 Model Parameter Estimation 25
2.4 Land Surface Elevation 27
2.5 Numerical Discretization 28
2.6 Boundary Conditions 29
2.7 Initial Conditions 30
Chapter 3 Climate Data 41
3.1 Observed Climate Data 41
3.1.1 Total Precipitation 41
3.1.2 Temperature 42
3.2 IPCC SRES Emission Scenarios 42
3.3 Dynamical Downscaling 44

3.4 Main Characteristics of Global Climate Models 46
3.5 Main Characteristics of Regional Climate Models 47
3.5.1 CRCM 47
3.5.2 HRM 48
3.5.3 WRF 48
3.6 Descriptions of RCM Outputs 49
3.6.1 Present-day Results of P, AET and T 51
3.6.2 Predicted Changes in P, ET and T during the 21st Century 52
Chapter 4 Present-day Steady-State Hydrologic Simulation 68
4.1 Present-day Net Precipitation 68
4.2 Observed Hydrologic Data 70
4.2.1 Streamflow Data 71
4.2.2 Lake Surface Elevation Data 71
4.3 Results and Discussions 72
4.3.1 Surface Flow Results 72
4.3.2 Subsurface Flow Results 74
4.3.3 Water Budget Analysis for the Great Lakes 75
4.3.4 Comments on Transient Annual Cycle Simulations 78
Chapter 5 Hydrologic Impacts of Future Climate Change 93
5.1 Key Assumptions and Their Justifications 93
5.2 Future-Time Net Precipitation 95
5.3 Results and Discussions 98
5.3.1 Evolution of Hydrologic Responses to Three Incremental CRCM Projections during the 21st Century 99
5.3.2 Hydrologic Responses to Various RCM Projections by 2041-2070 101
5.3.3 Sensitivity/Uncertainty Analysis 108
Chapter 6 Discussions and Conclusions 123
Bibliography 128

List of Tables

Table 2-1: Values for the fully-saturated hydraulic conductivity, total porosity and specific storage. 32

Table 2-2: Values for van Genuchten parameters, Manning roughness coefficient and coupling length. 32

Table 3-1: Major characteristics of three GCMs used in this study. Table is adapted from Randel [2007]. 56

Table 3-2: Major characteristics of the three RCMs used in this study. This table is adapted from NARCCAP (http://www.narccap.ucar.edu/data/rcm-haracteristics.html). 57

Table 3-3: Attributes of each RCM output used in this study. 58

Table 3-4: Summaries of the attributes and data application purposes about the climate datasets used in this study which are derived from the RCM outputs described in Table 3-3. The datasets are the mean values of the entire data period indicated in the table. 59

Table 4-1: Information on streamflow gauging stations used in this study. 79

Table 4-2: Observed mean annual surface elevations of 10 largest lakes in study domain. 80

Table 4-3: Present-day (1961-2000) simulated mean annual water budget components for the Great Lakes. 81

Table 5-1: Predicted changes in water budget components for the Great Lakes by 2041-2070 based on four RCM future projections. (a) CRCM (A2); (b) HRM (A2); (c) WRF (A2) and (d) WRF (A1B). 110

Table 5-2: Standard deviation of hydrologic responses to the differences between RCMs and SRES scenarios. All data are for the future 2041-2070 period. 114

List of Figures

Figure 2-1: Geographical location of the study domain and the topography of North America. Elevation data is from HYDRO1K [U.S. Geological Survey, 2000]. The region within the blue line represents the model domain. 33

Figure 2-2: Super watersheds, major rivers, 10 largest lakes and 20 representative gauging stations selected for streamflow study within the simulation domain. Gauging station numbers are the same as those in Figure 4-3 and Figure 5-4. 34

Figure 2-3: Thickness of sediments and sedimentary rocks. Maps are produced based on a global sediment thickness dataset [Laske and Masters, 1997]. (a) Thickness of unconsodidated sediments, up to 2,000 m; (b) Thickness of combined unconsodidated sediments and sedimentary rocks. 35

Figure 2-4: Top 5.0 m surficial geology across study domain. Unit classification is based on the hydraulic property of each formation, with Unit 1 having the lowest permeability and Unit 5 having the highest k. This map is produced based on Ross et al. [2010]. 36

Figure 2-5: Simulated 3D distribution of present-day permafrost across North America by Tarasov and Peltier [2007]. 37

Figure 2-6: 3D Geology model in (a) plan view and (b) fence view. 1: basement rocks; 2: fractured basement rocks; 3: sedimentary rocks; 4: unconsolidated sediments; 5: upper 5 m unit 1; 6: upper 5 m unit 2; 7: upper 5 m unit 3; 8: upper 5 m unit 4; 9: upper 5 m unit 5; 10: discontinuous permafrost; 11: continuous permafrost. 38

Figure 2-7: Cell volume (m^3) distribution of the 3D triangular prism grid in (a) plan view and (b) fence view. Cell volume is indicative of the elemental segment length and layer thickness. 39

Figure 2-8: A close-up look at the 3D triangular prism grid along Great Lakes region. Red color represents high elevation and blue color represents low elevation. 40

Figure 3-1: Observed present-day (1960-2000) mean annual total precipitation (mm/year) across the study domain. The plotting is based on a 0.5 degree by 0.5 degree gridded global dataset compiled by Matsuura and Willmott (2009a). 60

Figure 3-2: Observed present-day (1961-2000) mean annual air temperature (Celsius) across the study domain. The plotting is based on a 0.5 degree by 0.5 degree gridded global dataset compiled by Matsuura and Willmott (2009b). 61

Figure 3-3: Global carbon dioxide emissions due to energy and industry from 1900 to 1990 and for the 40 SRES scenarios from 1990 to 2100. Data are shown as an index (1990 = 1). The dashed

time-paths represent the individual SRES scenarios and the blue-shaded area illustrates the total SRES database range. This figure is after the IPCC Emission Scenario Special Report. 62
Figure 3-4: Model domains for the three RCMs (CRCM, HRM and WRF) relative to study domain and North America. 63
Figure 3-5: Simulated present-day (1971-2000) mean annual total precipitation (mm/year), mean annual actual evapotranspiration (mm/year), and mean annual temperature (Celsius) by three RCMs (CRCM, HRM and WRF). 64
Figure 3-6: RCM predicted changes in mean annual total precipitation (mm/year). A positive change means an increase and a negative change represents a decrease. 65
Figure 3-7: RCM predicted changes in mean annual actual evapotranspiration (mm/year). A positive change means an increase and a negative change represents a decrease. 66
Figure 3-8: RCM predicted changes in mean annual temperature (Celsius). Positive changes indicate an increase. 67
Figure 4-1: Present-day (1961-2000) mean annual net precipitation patterns (mm/year) across the study domain. 82
Figure 4-2: Present-day (1961-2000) mean annual actual evapotranspiration (mm/year) across the study domain. 83
Figure 4-3: HydroGeoSphere simulated and observed present-day (1961-2000) mean annual streamflow for the major rivers in the study domain. Locations of the gauging stations can be found in Figure 2-2 according to the numbers in parentheses. 84
Figure 4-4: HydroGeoSphere simulated and observed present-day (1961-2000) mean annual lake surface elevations for the 10 largest lakes in the study domain. See Figure 2-2 for the location of each lake. 85
Figure 4-5: HydroGeoSphere simulated present-day (1961-2000) surface water drainage patterns and mean annual surface water depth distribution across the study domain. 86
Figure 4-6: An inter-comparison of present-day (1961-2000) mean annual infiltration / exfiltration results (mm/year) across the study domain between HydroGeoSphere and CCSM3. (a) HydroGeoSphere computed infiltration (negative) / exfiltration (positive) results. (b) CCSM3 computed infiltration results. 87
Figure 4-7: Present-day (1961-2000) mean annual depth to water table across the study domain. This map is produced using HydroGeoSphere computed watertable elevation data in conjunction with high resolution land surface elevation data. 88

Figure 4-8: HydroGeoSphere simulated present-day (1961-2000) mean annual hydraulic head distribution on the land surface (m). A-A' and B-B' are two cross-sectional profiles shown in Figure 4-9 and Figure 4-10. 89
Figure 4-9: A cross-sectional view of the present-day (1961-2000) mean annual hydraulic head distribution (m) and quasi-2D flow net across the Rocky Mountain area (see Figure 4-8 for the location of A-A'). Vertical scale is exaggerated 25 times. 90
Figure 4-10: A cross-sectional view of the present-day (1961-2000) mean annual hydraulic head distribution (m) and quasi-2D flow net across the Great Lakes area (see Figure 4-8 for the location of B-B'). Vertical scale is exaggerated 50 times. 91
Figure 4-11: Laurentian Great Lakes and their drainage basins. This map is from Environment Canada (https://www.ec.gc.ca/grandslacs-greatlakes/). 92
Figure 5-1: RCM based changes in mean annual net precipitation (mm/year) during the 21st century. Data are adjusted using the hybrid method described in this Chapter. 115
Figure 5-2: Predicted percentile changes in mean annual streamflow relative to present-day values based on CRCM (A2) projections. Further information of each gauging station can be found in Figure 2-2 and Table 4-1. 116
Figure 5-3: Predicted change in major lake surface elevations (cm) over the 21st century based on CRCM (A2) projections. Numbers on top of the bars denote the 10 largest lakes within the study domain as follows. 1: Athabasca; 2: Erie; 3: Great Bear; 4: Great Slave; 5: Huron; 6: Michigan; 7: Ontario; 8: Reindeer; 9: Superior; 10: Winnipeg. 117
Figure 5-4: Predicted relative change in mean annual streamflow based on RCM future climate projections. Refer to Figure 2-2 for the location of each gauging station based on the number in parentheses. 118
Figure 5-5: Predicted absolute change in surface water depth (m) based on RCM future climate projections. A positive change means an increase in surface water depth and a negative change represents a decrease in surface water depth. 119
Figure 5-6: Predicted change in major lake surface elevations (cm) over the Mid-21st century (2041-2070) based on four RCM projections. Numbers on top of the bars denote the 10 largest lakes within the study domain as follows. 1: Athabasca; 2: Erie; 3: Great Bear; 4: Great Slave; 5: Huron; 6: Michigan; 7: Ontario; 8: Reindeer; 9: Superior; 10: Winnipeg. 120

Figure 5-7: Predicted absolute change in watertable elevation (m) based on RCM future climate projections. A positive change means a rise in water table and a negative change represents a decline in water table. 121
Figure 5-8: Predicted absolute change in rates of groundwater recharge (mm/yr) based on RCM future climate projections. A positive change means an increase in groundwater recharge and a negative change represents a decrease in groundwater recharge. 122

Chapter 1
Introduction

1.1 Background

Climate is generally defined as the average weather over a long period, e.g. 30 years as suggested by the World Meteorological Organization (WMO). The climate of a region is generated by a complex and interactive climate system consisting of five major components: the atmosphere, the hydrosphere, the cryosphere, the land surface and the biosphere. These interconnected components involve a large number of physical, chemical and biological processes. The climate is never static and it varies from place to place and time to time. Over the last 4.5 billion years, the earth's climate slowly changed as the earth evolved. However, the earth's climate has changed at an alarming speed since the 19^{th} century, especially after 1970. The rapid climate change in the last few decades has become evident by the observations of: the global mean temperature rise, the global mean sea level (GMSL) rise, the ice melting around the globe, the increasing frequency of extreme weather events and the acidification of sea water. In addition to the influence of its own internal dynamics, continental drift, variation of solar radiation, volcanic eruptions, and the change in earth's tilt are the prominent natural external factors causing climate change. Nevertheless, none of the aforementioned natural forcing can sufficiently explain the recent global warming and climate change. With significant progress being made in understanding the climate system over the last few decades, it is now generally believed within the scientific community that

the human-induced perturbation of atmospheric composition is mainly responsible for the recent global warming.

The majority of the gases in earth's atmosphere are nitrogen and oxygen, and greenhouse gases (GHGs) make up only a minute portion of the atmosphere. However, these GHGs have large effects on climate, acting as a radiation blanket that helps keep the Earth's surface warm. This warming effect is known as the greenhouse effect, and this effect makes our planet warm enough for human and many other species to inhabit. Water vapor is the most abundant GHG in the atmosphere, but its atmospheric concentration is mainly controlled by temperature and is not directly influenced by human activities. On the other hand, many other GHGs, such as carbon dioxide (CO_2), methane (CH_4), nitrous oxide (N_2O), chlorofluorocarbons (CFCs) and ozone (O_3), are strongly associated with human activities. Among these anthropogenic GHGs, CO_2 is the most important one because of its abundance and long lifetime. The atmospheric concentration of CO_2 has so far increased by approximately 40% since the beginning of industrialization due primarily to the burning of fossil fuels and deforestation. Studies on ice cores extracted at Vostok Station (a Russian Antarctic research station) suggest that: (1) there is a high degree of correlation between the atmospheric concentration of CO_2 and the ambient mean temperature [Barnola et al., 1987]; (2) the present-day atmospheric concentration of CO_2, ~400 parts per million by volume, is apparently unprecedented over the last 420,000 years [Petit et al., 1999]. Indeed, similar trends of atmospheric CO_2 fluctuations are also observed from a more recent ice core study [Parrenin et al., 2007], in which 800,000 years of atmospheric CO_2 levels were extracted from ice cores. The elevated concentrations of CO_2 and other GHGs in the atmosphere have

resulted in an enhanced greenhouse effect which in turn has led to the increase in global temperature, known as global warming. Since the late 19th century, instrumental records show that the mean annual global temperature has risen up by 0.74±0.18^{o}C. The Intergovernmental Panel on Climate Change (IPCC) was established in 1988 by WMO and the United Nations Environment Programme (UNEP) to assess global climate change and its potential impacts on both human beings and nature. It's Fourth Assessment Report [IPCC, 2007] predicts that global temperatures could rise between 1.1^{o}C to 6.4^{o}C by the end of this century. Besides global warming, the enhanced greenhouse effect will also trigger a series of other feedbacks within the highly complex and interactive climate system, which as a whole are known as global climate change. For instance, several studies [e.g. Allen and Ingram, 2002] suggest that global total precipitation will increase by 1-3% per Kelvin increase in global mean temperature due to the enhanced evapotranspiration (ET). On the other hand, satellite observation data show that global mean precipitation has actually increased by a rate of ~7% per Kelvin of atmospheric warming over the past 20 years [Wentz et al., 2007]. A similar increasing rate of ~7% per Kelvin of surface warming is also observed in a high-resolution regional climate modelling study [d'Orgeville et al., 2014] over the Great Lakes basin. Many of the feedbacks are positive, and they have amplifying effects on climate change. For example, a warmer climate will result in more water vapor in the atmosphere, and a higher atmospheric water vapor concentration will further enhance the greenhouse effect.

The hydrologic cycle is one of the most important components of the climate system, and it consumes much of the solar energy incident upon earth. Even a minor change in climate may

impose significant impacts on the hydrologic cycle at various temporal and spatial scales, and hence water resources. Water supply is critical for many aspects of human well-being, and thus the potential changes in the access to fresh water represent a great concern for our society. A warmer global temperature will lead to a more intensified hydrologic cycle. According to Clausius–Clapeyron Equation, a well-established physical law, water holding capacity of the atmosphere will increase by about 7% per Kelvin of global warming [IPCC, 2007]. More moisture held in the atmosphere will lead to more frequent and intense storms which may cause flooding. On the other hand, even a small increase in temperature in a dry region may potentially cause further declines in water levels due to the greater loss of water through ET. In addition to the potential alterations in water quantity, future climate change may also have significant effects on water quality. Water quality may deteriorate by the elevated salinity due to greater water loss through higher ET, by the increased sediment loads due to more powerful streamflow which is a result of more intense precipitation, and by the altered chemical reaction kinetics because of warmer temperature [Whitehead et al., 2009]. Also, a warmer temperature may result in a lower level of dissolved oxygen (DO) and a higher level of biochemical oxygen demand (BOD) in water [Rehana and Mujumdar, 2011]. Unfortunately, decreased DO and increased BOD will lead to a serious challenge to the aquatic system.

Anticipating that human-induced climate change may have a significant impact on our already stressed water resources and fragile ecosystems, policy makers and water managers are faced with two critical questions. What are the plausible hydrologic responses to future climate change, and what kind of adaptive strategies can be implemented to mitigate any

potential negative impacts? Traditionally water managers use historical hydrologic and hydrogeologic data for short-term water resources planning and management. However, for long-term future adaptation planning, the validity of this conventional approach, which assumes stationarity, will be jeopardized under a changing future climate. A sound quantitative understanding of the evolution of surface and subsurface flow systems as influenced by a range of plausible future climate change scenarios is key to answering these questions.

1.2 Previous Studies

In recognition of the mounting evidence of climate change as well as the vital importance of water resources, a significant amount of research effort has been devoted to assess the plausible hydrologic impacts and to explore the potential adaptive strategies to mitigate such impacts at various spatial and temporal scales. Impact assessments have typically been carried out through conceptualization and examination of the relationships between future climate scenarios and water resources using hydrologic models. To the best of my knowledge, however, most hydrologic modelling studies in the literature that explore the impacts of climate change on water resources suffer from a combination of one or more of the following six deficiencies.

Deficiency 1: outputs from global climate models (GCMs), perhaps with a simple interpolation, are directly used to provide the forcing for hydrologic impact modelling studies at a regional or local scale without downscaling [e.g. Lofgren et al., 2002]. As the climate system is better understood, more sophisticated physics and parameterizations have been

incorporated into the GCMs. Meanwhile, current generation GCMs are now able to simulate the climate at a higher horizontal and vertical grid resolution thanks to the significant development in super computers over the last few decades. However, the spatial resolution of current GCMs is generally still too coarse for hydrologic impact studies at the regional scale which typically requires a spatial resolution of tens of kilometers. In addition, the land surface scheme used by GCMs is too simplistic and not realistic at the regional scale. For example, in a streamflow simulation study using the output of the third-generation GCM of the Canadian Centre for Climate Modelling and Analysis [Arora, 2001], only 4 out of 23 major rivers are accurately simulated within ±20% of the observed data. A statistical or dynamical downscaling that translates the climate signals from the coarse-resolution GCM outputs to a regional or local scale is typically required for hydrologic impact studies.

Deficiency 2: only one future greenhouse gas emissions scenario is considered [e.g. Pascal et al., 2009]. The simulation of future climate evolution requires an estimate of the future emission level of greenhouse gases and aerosols, and most GCM projections of future climate change are based on one of the IPCC SRES (Special Report on Emissions Scenarios) emissions scenarios [Nakicenovic and Swart, 2000]. Fundamentally these SRES emission scenarios are assumptions, rather than predictions, and they are developed on the basis of anticipated demographic, technological, social and economic development as well as other factors over the next century or so. The likelihood of these scenarios is essentially beyond the realm of natural science and thus cannot be quantified. The high degree of uncertainty embedded in IPCC SRES emissions scenarios is one of the two major uncertainties in projecting future climate change, and thus hydrologic impact studies based on just one

particular SRES scenario fail to provide meaningful recommendations for water managers or government policymakers. The evaluation of the sensitivity in hydrologic responses (e.g. change in stream discharge) to various SRES emission scenarios provides an alternative insight into the potential effect of future climate change.

Deficiency 3: only one climate model is used to obtain the future climate change projection [e.g. Sushama et al., 2006]. Another major uncertainty in predicting future climate evolution arises from climate models (including both GCM and RCM) which are only a simplified representation of the actual complex climate system. For example, simulation error can be partially attributed to oversimplified parameterization schemes due to inadequate understanding and/or computational constraints. Different models may use different spatial grid resolutions, initial conditions, parameterization schemes and parameter values, although the core governing equations may be similar or the same. As a result, although using identical forcings, simulation results from different models could be substantially different in many respects. It is commonly reported in the literature that hydrologic responses to climate change are more sensitive to climate models than to emissions scenarios [e.g. Kerkhoven and Gan, 2011; Choi et al., 2009; Minville et al., 2008]. Although skills of climate models in simulating present-day climate can be evaluated using observed data, better skills in present-day climate simulation do not automatically translate into more reliable future climate projections. At our current stage, the reliability assessment of future climate projections represents a daunting challenge because the consequence can only be directly verified decades from now, and the variation of climate signals between different climate models provides the most meaningful measure in this regard [Raisanen, 2006].

Deficiency 4: only hypothetical future climate change scenarios are used as the forcing to drive hydrologic models [e.g. Nemec and Schaake, 1982; Xu, 2000]. In this approach, future climate data are not obtained from the outputs of GCMs or RCMs. Instead, the future climate scenarios are generated by adding a hypothetical, frequently uniform, perturbation to the historical climatic data, and lacking local or regional variability in change. For example, future climate change scenarios have commonly hypothesized that the global mean temperature rises by 0.5-4^{o}C, and total precipitation changes by ±10-20% [Xu, 2000]. The use of hypothesized climate scenarios as the input for a hydrologic model is a common approach to investigate the potential effects of future climate change. The high popularity of this approach is mainly because: (1) there is considerably high degree of uncertainty in GCM projected future climate results, and this is particularly the case for the older generation GCMs; (2) there is a serious limitation (assuming stationarity) associated with the statistical technique for downscaling the coarse-scale GCM outputs to regional scales; (3) it is difficult for every researcher to have access to high-resolution RCM outputs given the excessive computational load of climate modelling. Although this approach provides the opportunity for sensitivity evaluation of the hydrologic responses to potential future climate change, it fails to quantitatively predict the imposed changes because the climate scenarios are not interconnected to SRES emission scenarios [Xu et al., 2005]. As our confidence in GCM simulation skills and RCM downscaling techniques gradually improves, more and more researchers adopt high-resolution RCM outputs as the forcing to drive hydrologic models. Today, hypothetical climate scenarios are still widely used in hydrologic impact studies, but they are mainly used during the initial research phase or for sensitivity analysis purpose only.

Deficiency 5: many impact studies fail to simulate both surface and subsurface flow using a physically-based, fully-integrated hydrologic model [e.g. Kerkhoven and Gan, 2011; Choi et al., 2009]. With adequate field data available for calibration, empirically-based models often perform as well as physically-based and spatially distributed models. However, a physically more realistic model may help reduce the uncertainty in simulation results under a changing climate [Minville et al., 2008], since the empirical relations derived from historical data may become invalid when the climate changes. The benefit of using a physically-based model becomes more significant when there is a lack of sufficient observed data. Groundwater accounts for about 30% of the total freshwater storage, and it is the main source of water in many places of the world. Both surface water and groundwater belong to the same hydrologic cycle, and the interaction between them is dynamic and active in many regions. For example, groundwater provides baseflow to feed streams and rivers, and watertable depth strongly influences the surface runoff generation during a rainfall event. Similarly, the watertable level may be largely controlled by surface water levels [Scibek et al., 2007]. Unfortunately, one of the two components is typically treated as a stationary boundary condition in an artificial manner in those uncoupled hydrologic modelling studies, and the exchange flux between the surface and the subsurface domain is computed independently without capturing the 'feedback' between them. Obviously, the stationary boundary condition will become more problematic under a changing climate, leading to an unreliable prediction of hydrologic responses to future climate change, because those “artificial” internal boundary conditions are subject to change under a different climate scenario. For example, streams are usually treated as a constant head boundary condition by a groundwater-only model, but this

stationary boundary condition will certainly be invalidated by changing stream levels induced by the future climate scenario. In contrast, a physically-based, fully-integrated hydrologic model, in which the aforementioned “artificial” stationary boundary condition no longer exists and both surface and subsurface flows are solved simultaneously at each time step as climate evolves, does not suffer from this serious weakness. Another major benefit of using a fully-integrated hydrologic model over an uncoupled model is the capability to estimate the groundwater recharge owing to the unique and robust feature that partitions the rainfall hitting ground into the three components: infiltration, surface runoff and ET. The rate of groundwater recharge is critical for the assessment of potential future climate change impacts on groundwater resources, because it represents the maximum amount of the available groundwater resource in a long-term average sense. In addition, sound groundwater simulation results (e.g. hydraulic head distribution) are largely contingent on an accurate estimate of groundwater recharge.

Deficiency 6: studies are frequently limited to a relatively small catchment or river basin [e.g. Goderniaux et al., 2009; Minville et al., 2008; Roosmalen et al., 2007]. Undoubtedly a small-scale simulation enjoys a few benefits in contrast to a larger scale simulation, such as higher resolution results, less computational demand, easier calibration, less input data requirement etc. However, the simulation results of a small-scale watershed are more vulnerable to the "boundary effect" than those of a larger scale domain. Taking the subsurface flow simulation of a small watershed as an example, the lateral boundary of the watershed is typically defined as a no-flow boundary, because groundwater drainage is generally assumed to coincide with the surface drainage systems [Spitz and Moreno, 1996].

However, in a continental-scale subsurface flow modelling study, Lemieux [2008] demonstrated that considerable regional or continental groundwater flow across the boundaries of many small-scale watersheds exists. Thus, ignorance of the non-negligible regional or continental flow will lead to biased simulation results. The "boundary effect" will become more significant in hydrologic impact studies when the climate changes over time. On the other hand, the "boundary effect" will be reduced to a minimum in large-scale simulations because the potential super-regional groundwater flow across small watershed boundaries is captured.

1.3 HydroGeoSphere

HydroGeoSphere, a physically-based, spatially-distributed, fully-integrated surface and subsurface flow and mass transport hydrologic model, is selected for hydrologic simulations in this study. Greater details regarding the comprehensive modelling capabilities of HydroGeoSphere are described in its user manual [Aquanty Inc., 2013]. An independent software review of HydroGeoSphere by Brunner and Simmons [2012] provides an informative coverage of model structure, main modelling capabilities, brief instructions for beginning users, and strengths/weaknesses in comparison to other commonly used hydrologic models. HydroGeoSphere can simulate a wide spectrum of hydrologic phenomena via either control-volume finite element [Forsyth, 1991] or finite difference approaches. Its simulation capabilities include 1D channel flow, 2D depth-averaged overland flow, actual ET, 3D variably-saturated groundwater flow, variable-density flow, 1D hydro-mechanical coupling, mean life expectancy (MLE) and solute transport with multiple species. With the added capability to simulate thermal energy transport, HydroGeoSphere can now

simulate snow accumulation/melting and soil freeze/thaw as well. Either the Newton-Raphson technique following Huyakorn and Pinder [1983] or the Picard iteration method can be used to solve non-linear problems, including surface flow, variably-saturated subsurface flow and variable-density flow problems. A unique feature of HydroGeoSphere is that the solutions of surface/subsurface flow and transport are simultaneously solved at each time step, giving complete water balance and solute budgets. This unique feature also gives HydroGeoSphere an edge in estimation of infiltration and groundwater recharge by partitioning the rainfall into three components (surface runoff, infiltration and AET) in a physically-based manner. Another noteworthy recent development of HydroGeoSphere is the multi-thread parallelization, which is immensely useful for simulating large and complex problems. HydroGeoSphere has been parallelized using the OpenMP approach for execution on Windows-based computers and on shared-memory supercomputers [Hwang et al., 2014]. So far, HydroGeoSphere has been successfully applied to many different types of problems at various scales, including: watershed studies, surface water/groundwater interactions, seawater intrusion, life time expectancy, glaciation, land subsidence, oil sand and mineral mine reclamation. To date, more than 40 modelling studies using HydroGeoSphere have been published in refereed journals in the literature.

In the subsurface domain, HydroGeoSphere simulates 3D variably-saturated groundwater flow using the following modified version of Richards' Equation:

$$-\nabla \cdot q + \sum \Gamma_{ex} \pm Q = \frac{\partial}{\partial t}\left(\theta_s S_w\right) \tag{1.1}$$

where q is the Darcy flux [LT^{-1}], Γ_{ex} is the volumetric fluid exchange rate [$L^3L^{-3}T^{-1}$] between subsurface domain and other domain types, Q [L^3T^{-1}] represents a source (positive) or a sink (negative) to the porous medium system, t represents the time [T], θ_s is the saturated water content [-] which is equal to the porosity and S_w is water saturation [-].

The Darcy flux q in Equation 1.1 is computed by:

$$q = -K \cdot k_r \nabla (\psi + z) \tag{1.2}$$

where K is the hydraulic conductivity tensor [LT^{-1}], k_r is the relative permeability of the medium [-], ψ is the pressure head [L] and z is the elevation head [L].

The hydraulic conductivity K in Equation 1.2 is a nine-component tensor. For the simplicity sake, it is defined here using its scalar form as:

$$K = \frac{\rho g}{\mu} k \tag{1.4}$$

where ρ is the water density [ML^{-3}], g is the gravitational acceleration [LT^{-2}], μ is the water molecular viscosity [$ML^{-1}T^{-1}$] and k is the intrinsic nine-component permeability tensor of the porous medium [L^2].

In HydroGeoSphere, the constitutive saturation-pressure relation is defined following van Genuchten [1980] by:

$$S_w = \begin{cases} S_{wr} + \left(1 + \left|\alpha\psi\right|^{\beta}\right)^{-\upsilon} & \text{for } \psi < 0 \\ 1 & \text{for } \psi \geq 0 \end{cases} \tag{1.5}$$

$$k_r = S_e^{(l_p)}\left[1-\left(1-S_e^{1/\upsilon}\right)^{\upsilon}\right]^2 \tag{1.6}$$

$$\upsilon = 1-\frac{1}{\beta} \tag{1.7}$$

$$S_e = (S_w - S_{wr})/(1-S_{wr}) \tag{1.8}$$

where S_{wr} is the residual water saturation [-], α is the inverse of the air-entry pressure [L^{-1}], β is the pore-size distribution index [-], S_e is the effective saturation [-] and l_p is the pore-connectivity parameter equal to 0.5 for most soils.

The right hand side (storage change) of Equation 1.1 can be approximated as:

$$\frac{\partial}{\partial t}(\theta_s S_w) \approx S_w S_s \frac{\partial \psi}{\partial t} + \theta_s \frac{\partial S_w}{\partial t} \tag{1.9}$$

where S_s is the specific storage coefficient of the porous medium [L^{-1}].

For the surface domain, 2D depth-averaged overland flow is computed in HydroGeoSphere using the following diffusion-wave equation which is an approximation to the full Saint Venant equation.

$$\frac{\partial}{\partial x}\left(d_o K_{ox}\frac{\partial h_o}{\partial x}\right) + \frac{\partial}{\partial y}\left(d_o K_{oy}\frac{\partial h_o}{\partial y}\right) + d_o \Gamma_o \pm Q_o = \frac{\partial \phi_o h_o}{\partial t} \tag{1.10}$$

where ϕ_o is the surface flow domain porosity [-], d_o is the flow depth [L], h_o [L] is the water surface elevation ($h_o = d_o + z$), K_{ox} and K_{oy} are surface conductance [LT^{-1}], Γ_o is the

volumetric fluid exchange rate [$L^3L^{-3}T^{-1}$] and Q_o is the volumetric flow rate per unit area representing external source or sinks [LT^{-1}]. A positive Γ_o represents fluid fluxes from the subsurface to the surface, and a negative exchange rate means fluid fluxes in the opposite direction.

Surface conductance K_{ox} and K_{oy} in Equation 1.10 are defined by the Manning Equation [Chow, 1959], an empirical equation solving uniform flow in open channels, as follows:

$$K_{ox} = \frac{d_o^{2/3}}{n_x} \frac{1}{\left[\partial h_o / \partial s\right]^{1/2}} \tag{1.11}$$

$$K_{oy} = \frac{d_o^{2/3}}{n_y} \frac{1}{\left[\partial h_o / \partial s\right]^{1/2}} \tag{1.12}$$

where n_x and n_y are Manning roughness coefficients [$L^{-1/3}T$] in x and y direction respectively and s is the horizontal distance along the maximum bed slope [L].

In HydroGeoSphere, the surface and subsurface flow equations are solved simultaneously in a fully-coupled manner. The exchange flux between the surface and subsurface domains is defined as:

$$d_o \Gamma_o = \frac{k_r K_z}{l_c} (h - h_o) \tag{1.13}$$

where k_r is the relative permeability for the exchange flux [-], K_z is the vertical saturated hydraulic conductivity of the underlying porous medium [LT^{-1}], h is the subsurface hydraulic head [L] and l_c is the coupling length [L]. When water flows from subsurface to surface, the

relative permeability term k_r used in Equation (1.13) has the same value as the one used for the underlying porous medium. When water flows from surface to subsurface, the relative permeability k_r is computed using the following equations:

$$k_r = \begin{cases} S_{exch}^{2(1-S_{exch})} & when\ d_o < H_s \\ 1 & when\ d_o > H_s \end{cases} \quad (1.14)$$

$$S_{exch} = \frac{d_o}{H_s} \quad (1.15)$$

where H_s is the total obstruction height [L].

1.4 Objectives

The main objective of this study is to assess the plausible impacts of future climate change on Canadian water resources through a continental-scale, physically-based and fully-integrated surface-subsurface flow modelling framework. This modelling framework is free of the aforementioned six common deficiencies that are frequently associated with other hydrologic impact studies reported in the literature. Other objectives of this study are described as follows:

- To demonstrate that a fully-coupled surface/subsurface flow simulation at the continental scale is possible. To the best of my knowledge, this is the largest scale (~10 million km^2 in area) hydrologic modelling study that fully couples surface and variably saturated subsurface flow.

- To evaluate the uncertainty/sensitivity in hydrologic responses to future climate change linked to different climate models and different SRES emissions scenarios respectively.

- To develop an operational method for reliable net precipitation estimation at the continental-scale using observed precipitation data in conjunction with high-resolution outputs from regional climate models. This may lead to a reliable estimation of actual evapotranspiration for the vast uninhabited areas in Northern Canada and the Alaska region.

1.5 Overall Modelling Approach

Overall, this modelling study consists of three major parts. In part one, a complex 3D hydrologic model is constructed. Construction of the hydrologic model involves building a 3D geology model, reliable model parameter estimation, appropriate boundary condition assignment, and a numerical discretization procedure.

During part two, present-day net precipitation is computed using observed total precipitation data in conjunction with high-resolution outputs from RCMs. Basically RCM data are used to compute the ratio of AET to total precipitation. The net precipitation data is used as the forcing to perform present-day steady-state hydrologic simulations. The hydrologic model is calibrated and validated against observed hydrologic data.

In part three, the future net precipitation is calculated based on multiple high-resolution RCM projections and corrected using present-day net precipitation data. To minimize the influence

of unrealistic RCM projections, a hybrid approach is used to determine the future net precipitation. Note that details regarding this hybrid approach are described in Chapter 5. The future net precipitation data are then used to drive the validated hydrologic model to predict the hydrologic responses to future climate projections. Sensitivities in the simulated results to various climate models and to different emission scenarios are also analyzed.

1.6 Thesis Organization

The thesis is organized into six chapters. Contents and objectives of each chapter are outlined below.

Chapter 2 describes the main characteristics the hydrologic model and explains how the model is constructed. The descriptions cover the model domain, the 3D geology model, model parameter values, numerical discretization, and boundary and initial conditions.

Chapter 3 contains descriptions of a global observed total precipitation dataset followed by approaches for GCM data downscaling and the motivation for choosing the dynamical approach in this study. Main characteristics of each climate model and their outputs as well as two IPCC emission scenarios are also summarized in this Chapter.

Chapter 4 firstly explains how the present-day net precipitation is calculated in this study, and secondly presents present-day steady-state hydrologic simulation results for comparison against observed streamflow and lake surface elevation data. The present-day hydrologic simulation serves for both calibration and verification purposes for the hydrologic model.

Chapter 5 describes the hybrid method for estimating the future net precipitation and then discusses the predicted long-term evolution of hydrologic responses to future climate scenarios. Sensitivity results based on four RCM outputs are also analyzed in this chapter.

Chapter 6 discusses the potential uncertainties and sensitivities in the simulation results. Limitations of this study, potential follow-up studies and an overall summary of this study are also presented in the end.

Chapter 2
Hydrologic Model Descriptions

2.1 Study Domain

As illustrated in Figure 2-1, the simulation domain of this study covers the Northern part of the North American continent, including most of Canada and part of the United States, with a total area of approximately 10 million square kilometers. To preserve area and minimize distortion, the Lambert Azimuthal Equal Area projection is utilized for this study. A radius of sphere of influence of 6,370,997 meters is used for this projection and the projection origin is located at 100 degrees West longitude and 45 degrees North latitude. The simulation domain is bounded on the West by the Pacific Ocean, on the North by the Arctic Ocean and Hudson Bay, and on the East by the Atlantic Ocean. On the interior Southern side, the domain boundary is delineated on the basis of super drainage basin dividing lines. As shown in Figure 2-1, the study area has a complex and wide-ranging terrain, with elevations ranging from tens of meters around Hudson Bay to two thousand meters or more along the Rocky Mountain range. The Rocky Mountain system acts as the continental divide, with water flowing into the Pacific Ocean in the west, into the Arctic Ocean and Hudson Bay in the north and central area, and into the Atlantic Ocean in the east. The Mackenzie, St. Lawrence, Yukon, Columbia, Fraser and Churchill are the major rivers within the study area in terms of length and mean annual stream discharge. In total, 20 representative gauging stations along the major rivers are selected for model calibration and validation purposes. Due to extensive glaciation/deglaciation, there are over two million surface water bodies distributed throughout the simulation domain. A large portion of the lakes are located within the

Canadian Shield region, where the terrain is relatively flat and low. The 10 largest lakes within the study domain by area are: Lake Superior, Lake Huron, Lake Michigan, Great Bear Lake, Great Slave Lake, Lake Erie, Lake Winnipeg, Lake Ontario, Lake Athabasca and Reindeer Lake. Figure 2-2 shows the major rivers, the 10 largest lakes in the simulation domain and the 20 selected gauging stations. Just like the terrain, the annual precipitation rate also varies vastly from region to region. Overall, the study domain is wet in the Western and Eastern coastal areas, and precipitation rates decrease gradually towards the central and Northern regions. The pacific coastal plains and the Western slope of the Rocky Mountains receive the greatest total precipitation, usually between 1000 and 2000 mm/year, and in contrast, the Northern and central regions receive as little as approximately 300 mm annual total precipitation.

2.2 Three-Dimensional Geology Model

Trustworthy hydrogeologic modelling simulation results not only rely on a robust numerical code, but also, perhaps to an even larger degree, depend on reliable model parameter values, e.g. hydraulic conductivities. A representative 3D geology model is the basis for reasonable parameter estimation; hence, it should be recognized that, because of the vast size of the study domain and the fact that subsurface geological data are unavailable in many areas, simplifications are essential. For example, local-scale hydrostratigraphic features such as individual aquifers and aquitards cannot be explicitly included. The simulation domain is therefore characterized using four major hydrogeological units: unconsolidated sediments, sedimentary rocks, basement rocks and permafrost. These four units predominantly control the groundwater flow at the continental scale. To construct a representative 3D geology

model, the 3D distribution of near-surface unconsolidated sediments is crucial because near-surface unconsolidated sediments often have relatively high permeabilities and they largely control the rates of groundwater recharge. However, at this moment, such data are only available for limited areas. At present, most existing continental-scale datasets are either mainly concerned with the shallow surficial soils derived from remote sensing data, or the bedrock geology. In addition, many existing maps were compiled inconsistently in terms of classifications, accuracy, formality and scales.

2.2.1 Thickness of Sediments

In light of the adversities discussed above, a commonly-used high-resolution (1 degree by 1 degree) global sediment thickness dataset [Laske and Masters, 1997] is utilized as the framework to construct the 3D geology model in this study. Based on seismic velocity and density data, the sediments are separated into three sub-layers in this dataset. Figure 2-3 exhibits the thickness of the first sub-layer and the total thickness of all three sub-layers. In this 3D geology model, the top sub-layer, which is up to 2,000 m thick, is used to define the unconsolidated sediments (see Figure 2-3a). Materials between the bottom of the first sub-layer and the bottom of the third sub-layer are classified as sedimentary rocks. Materials underlying the sedimentary rocks (deeper than the total sediment thickness in Figure 2-3b) are classified as basement rocks, which include igneous and metamorphic rocks. The top 50 meters of the basement rocks are classified as fractured basement rocks, since fractures commonly exist in shallow hard rocks. It is acknowledged that the differentiation between unconsolidated sediments and sedimentary rocks, which is based on seismic velocity and density data, will be subject to uncertainty. It is also acknowledged that the top sub-layer (up

to 2,000 m) of the global sediment thickness dataset, which is classified as unconsolidated sediments in this study, may actually include some sedimentary rocks. Nevertheless, the total thickness data of all sediments provided by this global dataset are believed to be reasonable.

2.2.2 Surficial Geology (Top 5.0 m)

It is generally true that the average hydraulic conductivity of the soil or rock decreases as the depth below ground surface increases. In addition, the interactions between surface water and groundwater are normally most vigorous in zones near the land surface. Therefore, well characterized surficial geological data are critical for hydrologic modelling. Ross et al. [2010] produced a gridded surficial geology dataset covering North America. Compilation of this dataset required a significant amount of effort to homogenize the differences among the numerous data sources. This dataset was compiled from a hydrologic perspective and is meant to represent the average hydraulic conductivity of a 5.0 m thick surficial layer. Depending on the location, the layer may include soils, rocks or a combination of them. For the sake of simplicity, the top surficial 5.0 m layer is classified into five zones spatially, and each zone is assigned a unique hydraulic conductivity value. Figure 2-4 exhibits the spatial distribution of the top 5.0 m surficial geological data across the study domain.

2.2.3 Permafrost

By definition, permafrost is a layer of ground, either soil or rock, that has been frozen continuously for at least two years or longer [Harris et al., 1988]. This designation is solely on the basis of temperature and has nothing to do with the intrinsic properties of the geological formations. Permafrost can only form and exist in a place where the mean annual

temperature is 0.0 ^{o}C or lower. In a permafrost region, the surficial layer that freezes in winter and thaws in summer is termed the "active layer". The hydraulic conductivity of permafrost formation is significantly lower than its fully liquid-water saturated hydraulic conductivity. When temperature drops below 0.0 ^{o}C, most of the pore water freezes. As the pore water freezes, liquid water saturation approaches zero, resulting in a significant decrease in relative permeability and hence hydraulic conductivity.

Permafrost plays an important role in continental-scale hydrology because of its low hydraulic conductivity and due to its vast extent in the study domain. Currently, the 2D permafrost distribution on the land surface based on field observation is available at the global scale [e.g. Brown et al., 1998]. However, except for some sporadically available borehole data, spatially-distributed permafrost thickness data are generally unavailable for most regions. To this end, a high-resolution (0.5 degree by 1.0 degree) present-day permafrost modelling output provided by Tarasov and Peltier [2007] is used to define the 3D permafrost distribution used in this study (see Figure 2-5). This model has a simulation domain covering the entirety of North America and it has been calibrated and validated against available bore-hole data. To avoid an abrupt change in hydraulic conductivity, which may lead to numerical difficulties in hydrogeological modelling, a transitional buffer zone is defined as a zone of discontinuous permafrost. The discontinuous zones are defined as the permafrost areas that are within 200 km distance from unfrozen ground. The remaining permafrost areas are then classified as the continuous permafrost zone. The transitional buffer zone is assigned a higher hydraulic conductivity than the continuous permafrost zone.

It is also assumed here that the zones of continuous and discontinuous permafrost remain static and are unaltered in the climate-change scenarios considered.

2.2.4 Final Product

The final 3D geology model forms when the three datasets above are merged together. When put together to form the final 3D geology model, the bedrock data go first, followed by the sediment thickness data, then the top 5.0 m surficial geological data and finally the permafrost data. In total, eleven hydrostratigraphic units are defined based mainly on their hydraulic properties and each unit is assumed to be statistically homogeneous, but not necessarily isotropic. Figure 2-6 shows the 3D geology model in plan and fence view. The flat bottom of the model domain is 500 m below sea level.

2.3 Model Parameter Estimation

In the subsurface domain, the permeability value of each geologic unit is assigned based on its physical properties with references to the literature in conjunction with trial-and-error calibration procedures. Parameter values for saturated hydraulic conductivity, total porosity and specific storage for the subsurface flow simulation are summarized in Table 2-1. Permeability estimation is generally challenging, because there is an extremely wide possible range, more than 14 orders of magnitude difference from one end of the spectrum to the other [Freeze and Cherry, 1979]. Most literature suggested permeability values are meant to be representative at a local-scale and few large-scale values are provided in the literature. As a general rule, effective permeability increases as the scale of the problem grows because of heterogeneities [e.g. Neuman, 1994]. This study involves continental-scale hydrologic

modelling, and thus the permeability values may appear to be higher than some of the literature suggested values for local regions. For example, a fully-saturated hydraulic conductivity of 1.0×10^{-11} m/s is used for the basement rocks in the Canadian Shield in a sub-regional scale hydrogeological modelling study [NWMO, 2012], but 1.0×10^{-7} m/s is used for the same rocks in this continental-scale modelling study in order to capture the effects of heterogeneities, such as fractures, in the large grid blocks.

The permeability of permafrost is especially difficult to estimate although it is normally viewed as an aquitard. There is little field data reported in the literature and almost all reported values are based on modelling exercises which are subject to a high degree of uncertainty. A talik is an unfrozen layer in permafrost regions and it may exist when there is a surface water body with a depth of 2.0 m or deeper [Harris et al., 1988]. Taliks will act like a conduit through the low-permeability permafrost layer, thus enhancing the effective bulk hydraulic conductivity of permafrost formations. However, due to the scale and resolution issues, most taliks are too small to be explicitly represented in this modelling study. As an alternative measure, a hydraulic conductivity that is somewhat comparable to the basement rocks is assigned to permafrost formations. Also due to the resolution issue, the current model does not include the active layer which is more permeable than the underlying permafrost layer. To implicitly take the active layer into account, a ratio of 10 between K_h and K_v (hydraulic conductivity in horizontal and vertical directions) is assigned to permafrost formations.

Values of van Genuchten parameters, Manning's roughness coefficients and surface/sub-subsurface coupling length are summarized in Table 2-2. In this work an identical van Genuchten parameter set is applied to the entire subsurface domain. This is adequate given that the hydrologic simulation is steady-state in nature and the targeted output variables such as surface water depth, streamflow, depth to water table and subsurface hydraulic head distribution are insensitive to these parameters at the continental scale. In the surface domain, commonly used Manning's roughness coefficients were initially assigned based on the land use/land cover (LULC) data. However, those values resulted in excessive surface water accumulation on the land surface. The unrealistic surface water depth results are likely due to the fact that a large number of sub-grid stream channels are not represented in the model due to the scale and resolution issues. After trial-and-error fitting procedure, a Manning's roughness coefficient of 0.001 ($s/m^{1/3}$) was chosen and this produces a more realistic surface water depth distribution. Note that sensitivity analyses showed that, except for surface water depth, steady-state streamflow and other simulation results are not sensitive to the Manning's roughness coefficient. A land coupling length of 1.0 m is chosen for this continental-scale modelling study. Sensitivity analyses suggest that a smaller land coupling coefficient does not produce much different results, but increases simulation time significantly.

2.4 Land Surface Elevation

Largely owing to the significant progress in remote sensing technology over the last few decades, there are now numerous digital elevation model (DEM) datasets that are available to the public from various governmental agencies. For hydrological modelling studies, choosing a reliable DEM is critically important, because topography predominantly controls the

surface hydrology. Thus, it is ideal to use a hydrologically corrected DEM for a hydrological modelling study. In this study, the land surface elevation of the 3D model is determined by a hydrologically-corrected DEM dataset - HYDRO1K [U.S. Geological Survey, 2000], and the model bottom is set flat, at a constant elevation of 500 meters below sea level. Shown in Figure 2-1 is the land surface elevation across North America based on HYDRO1K. In addition to elevation data, HYDRO1K also provides several other useful DEM-derived hydrological datasets, such as watershed boundaries, river networks, flow directions etc. It is important that these hydrological datasets are consistent with the DEM data. For example, a mismatch between the river network and the DEM data may result in alteration of simulated surface runoff. To obtain realistic surface water depth results for the major surface water bodies, ETOPO5 [NGDC, 1988], a global DEM without hydrologic correction, is used to assign the land surface elevation for the five Great Lakes, Great Bear Lake and Great Slave Lake. HYDRO1K has a spatial resolution of 1.0 km, and ETOPO5 has a resolution of 5-minute (~10 km). Note that the HYDRO1K dataset is hydrologically modified based on the natural flow systems and thus any artificial changes due to the construction of dams are not reflected in the DEM.

2.5 Numerical Discretization

The simulation domain is discretized into a 2D finite element triangular mesh using GRID-BUILDER which was developed at the University of Waterloo. GRID-BUILDER is a powerful triangular mesh generator and can be used as a pre-processor for HydroGeoSphere. The unstructured triangular mesh has various lateral dimensions, ranging from 3.0 to 30 km. The mesh is refined along hydrologically important features, such as stream lines and

boundaries of major watersheds and lakes. Vertically, the 3D finite element prism grid, derived from the 2D triangular mesh, has 15 elemental layers (16 nodal sheets) for the subsurface flow regime and one dual-node sheet coincident with the topmost subsurface grid layer for the surface flow regime. For the upper five meters of the subsurface domain, where the interaction between surface water and groundwater is most active, the vertical grid spacing is set to one meter and is spatially uniform for the entire study domain. The thickness of the underlying 10 layers gradually increases towards the bottom because groundwater flow dynamics decrease as depth increases. Figure 2-7 illustrates the cell volume of the 3D grid in both plan and fence view. Basically, cell volume is indicative of model resolution. Figure 2-8 shows a close-up view of the 3D grid in the Great Lakes region as an example of the unstructured mesh discretization. In total, the 3D model has 994,143 nodes and 1,809,696 elements.

2.6 Boundary Conditions

Boundary conditions are relatively simple in this modelling study thanks to the fully-integrated surface and subsurface flow model, HydroGeoSphere. Unlike many of the traditional hydrologic models, there are no arbitrary internal sinks or sources of water required to connect the surface water and groundwater flow regimes. In this work, the hydraulic head (total head) datum is set at the mean sea level (MSL), z = 0.0. For the subsurface flow regime, specified head (0.0 m) boundary conditions are applied to the coastal boundary nodes, assuming that the surrounding sea levels (z = 0.0 m) remain unchanged. Although global warming may result in up to a few centimeters rise in sea level over the next few decades, such an influence over the continental hydrology is expected to be negligible.

No-flow boundary conditions are assigned to the bottom and to the inland boundary nodes in the South of the study domain which also coincide with the super watershed boundaries. The elevation of the flat bottom of the 3D grid is 500 m below sea level. For most parts of the study domain, the geologic formation at the bottom is low-permeability basement rocks. Also, groundwater dynamics usually become weaker as the depth increases. Thus, it is reasonable to assume that there is negligible groundwater flow across the model bottom.

For the surface flow regime, a critical-depth boundary condition is assigned to the boundary nodes all around the domain, and spatially-distributed specified fluxes (net precipitation, present day or future time) are applied to the entire land surface. In this work, gridded net precipitation data are further interpolated from a resolution of tens of km to 10 km using the Natural Neighbor algorithm. The Natural Neighbor algorithm is an efficient spatial interpolation method, and it tends to provide smooth results. The interpolation process is performed using ESRI's popular ArcGIS for Desktop (version 9.3.1). Spatially-distributed net precipitation data are saved in ASCII Grid format which can be directly read by HydroGeoSphere. Basically, each surficial element is assigned a unique net precipitation value.

2.7 Initial Conditions

In this study, all numerical simulations are performed at steady-state. Thus, the choice of initial conditions for the hydrologic model are not a concern in terms of the accuracy of the simulation results since the steady-state results are only a function of the boundary conditions. However, initial conditions have a large influence on the computing time to

achieve steady-state results for non-linear problems. Obviously, the smaller the differences between the initial conditions (hydraulic head) and the final steady-state results, the faster will the model reach steady-state. Nevertheless, for most real-world hydrologic modelling simulations, it is very difficult to obtain an initial guess that is similar to the final steady-state conditions due to the high complexity of topography, geology, climate etc. To significantly speed up the continental-scale steady-state simulation, a two-step simulation approach was adopted in this study. Details of this efficient approach will not be described in detail here, since it is not directly related to the objectives of this study. During the first step, a simple initial condition of zero hydraulic head is applied uniformly to the entire domain. Then, the model is integrated to steady-state with a modified version of HydroGeoSphere, in which the entire subsurface regime is assumed fully saturated. Due to the substantially reduced non-linearity, the simulation speed is very much enhanced in the first step. Once steady-state is reached, the quasi-steady state results obtained in the first step are used as the initial conditions for the second step simulation, which entails the fully-coupled variably-saturated surface/subsurface system. In the end, this two-step approach significantly shortens the computational time to reach steady-state compared to the traditional one-step approach.

Table 2-1: Values for the fully-saturated hydraulic conductivity, total porosity and specific storage.

Hydrostratigraphic Unit	K_h (m/s)	K_h/K_v	n (-)	S_S (1/m)
Continuous permafrost	1.0×10^{-6}	10	0.05	1.0×10^{-7}
Discontinuous permafrost	1.0×10^{-5}	10	0.1	1.0×10^{-7}
Upper 5m Unit 5	5.0×10^{-2}	10	0.35	1.0×10^{-7}
Upper 5m Unit 4	1.5×10^{-2}	10	0.35	1.0×10^{-7}
Upper 5m Unit 3	5.0×10^{-3}	10	0.35	1.0×10^{-7}
Upper 5m Unit 2	1.5×10^{-3}	10	0.35	1.0×10^{-7}
Upper 5m Unit 1	5.0×10^{-4}	10	0.35	1.0×10^{-7}
Unconsolidated sediments	5.0×10^{-5}	10	0.3	1.0×10^{-7}
Sedimentary rocks	5.0×10^{-6}	10	0.05	1.0×10^{-7}
Fractured basement rocks	1.0×10^{-5}	1.0	0.1	1.0×10^{-7}
Basement rocks	1.0×10^{-7}	1.0	0.01	1.0×10^{-7}

Note: K_h and K_v are the hydraulic conductivity in the horizontal and vertical directions respectively; n is porosity and S_S is specific storage coefficient.

Table 2-2: Values for van Genuchten parameters, Manning roughness coefficient and coupling length.

van Genuchten Parameters		Residual water saturation	Manning's roughness coefficient	Coupling length
α (m^{-1})	β (-)	S_{wr} (-)	$n_{x,y}$ ($s/m^{1/3}$)	L_c (m)
1.9	6.0	0.18	0.001	1.0

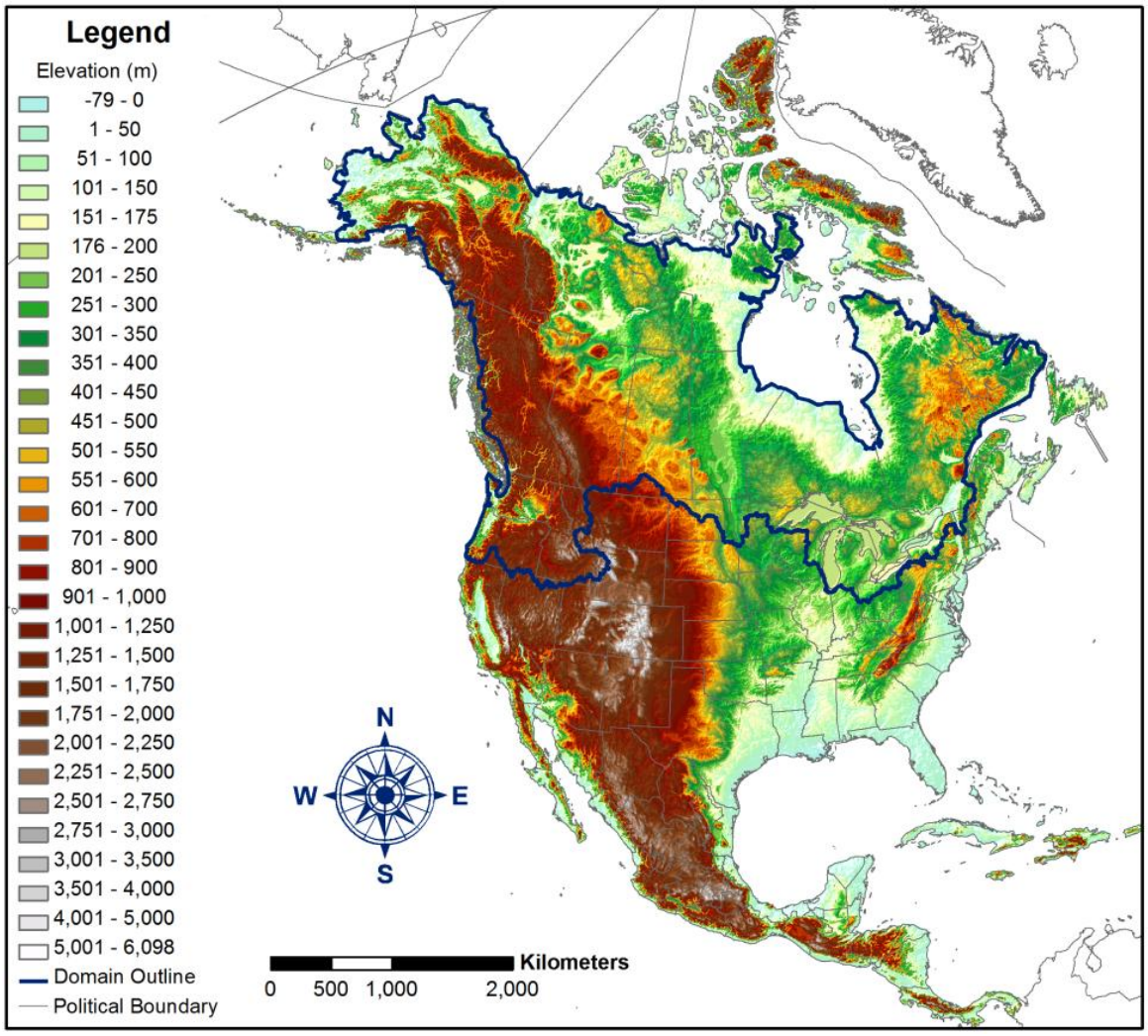

Figure 2-1: Geographical location of the study domain and the topography of North America. Elevation data is from HYDRO1K [U.S. Geological Survey, 2000]. The region within the blue line represents the model domain.

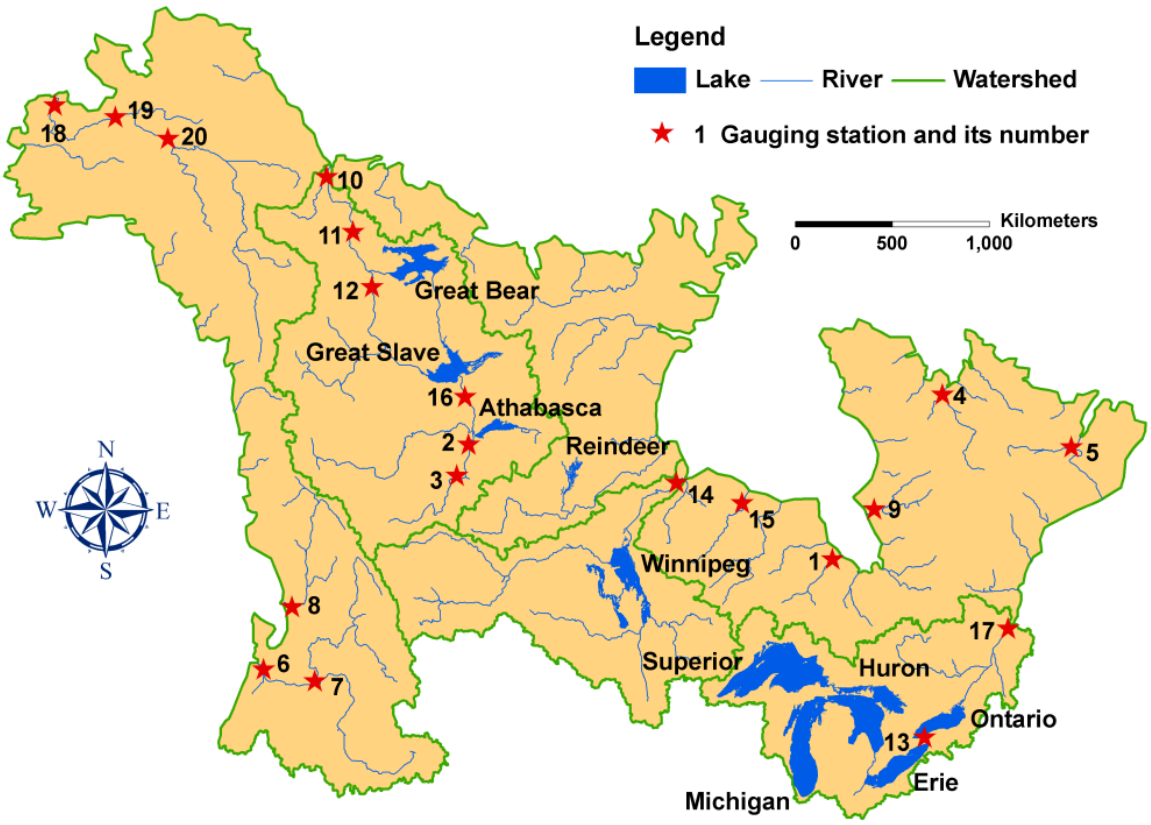

Figure 2-2: Super watersheds, major rivers, 10 largest lakes and 20 representative gauging stations selected for streamflow study within the simulation domain. Gauging station numbers are the same as those in Figure 4-3 and Figure 5-4.

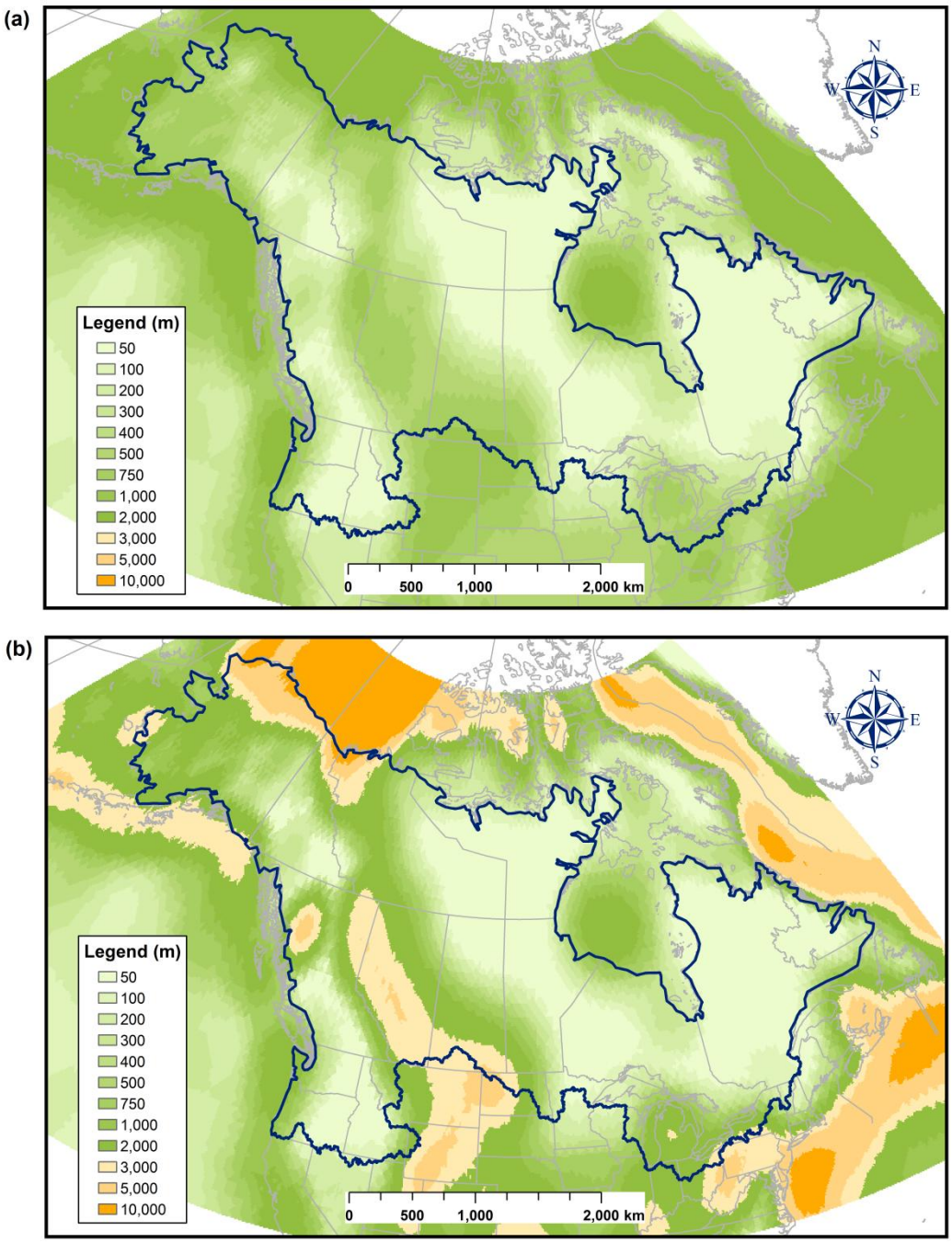

Figure 2-3: Thickness of sediments and sedimentary rocks. Maps are produced based on a global sediment thickness dataset [Laske and Masters, 1997]. (a) Thickness of unconsodidated sediments, up to 2,000 m; (b) Thickness of combined unconsodidated sediments and sedimentary rocks.

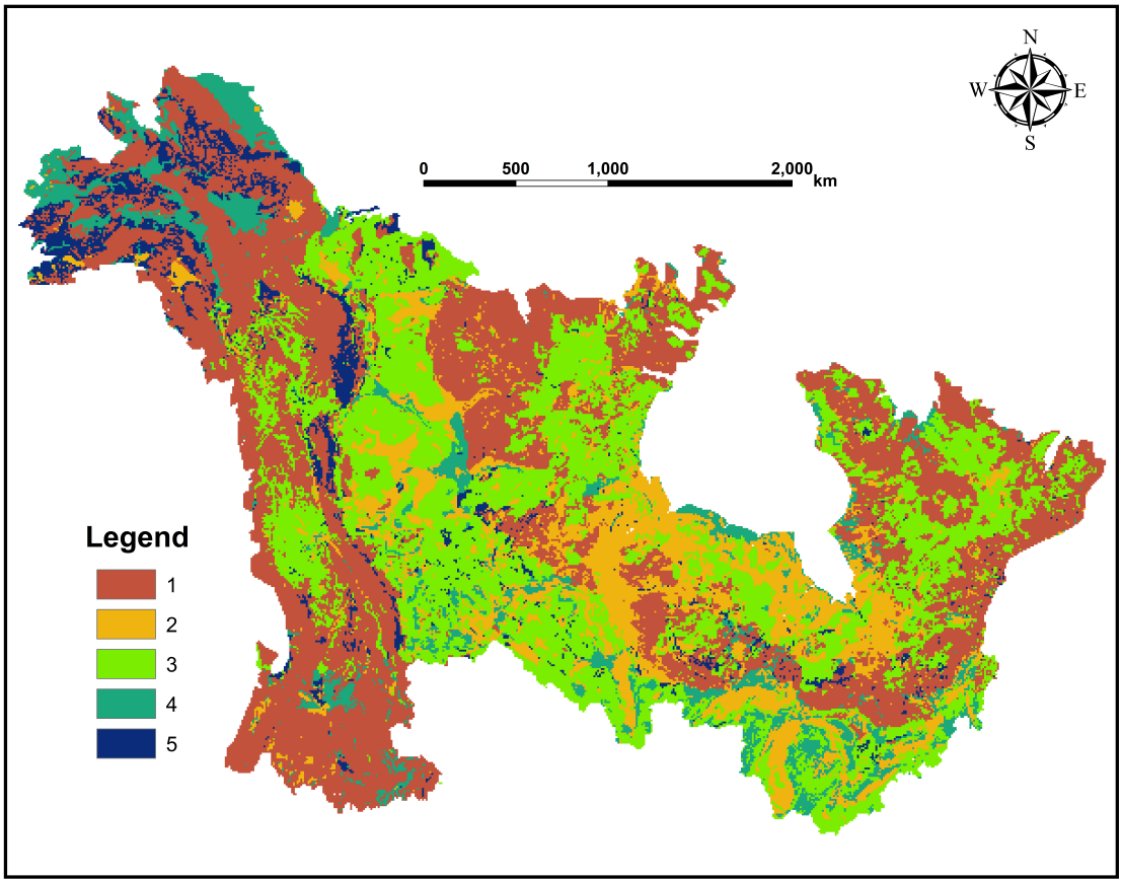

Figure 2-4: Top 5.0 m surficial geology across study domain. Unit classification is based on the hydraulic property of each formation, with Unit 1 having the lowest permeability and Unit 5 having the highest k. This map is produced based on Ross et al. [2010].

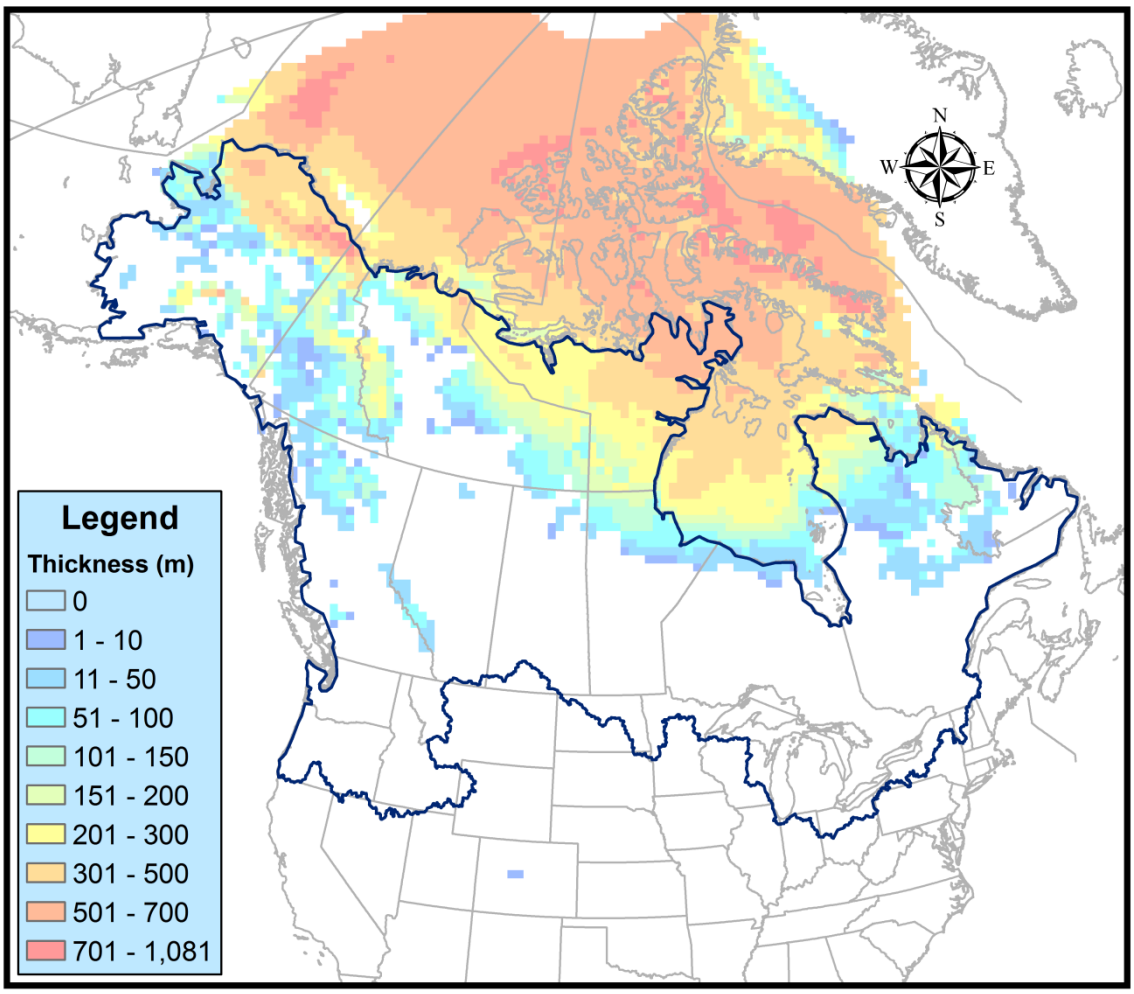

Figure 2-5: Simulated 3D distribution of present-day permafrost across North America by Tarasov and Peltier [2007].

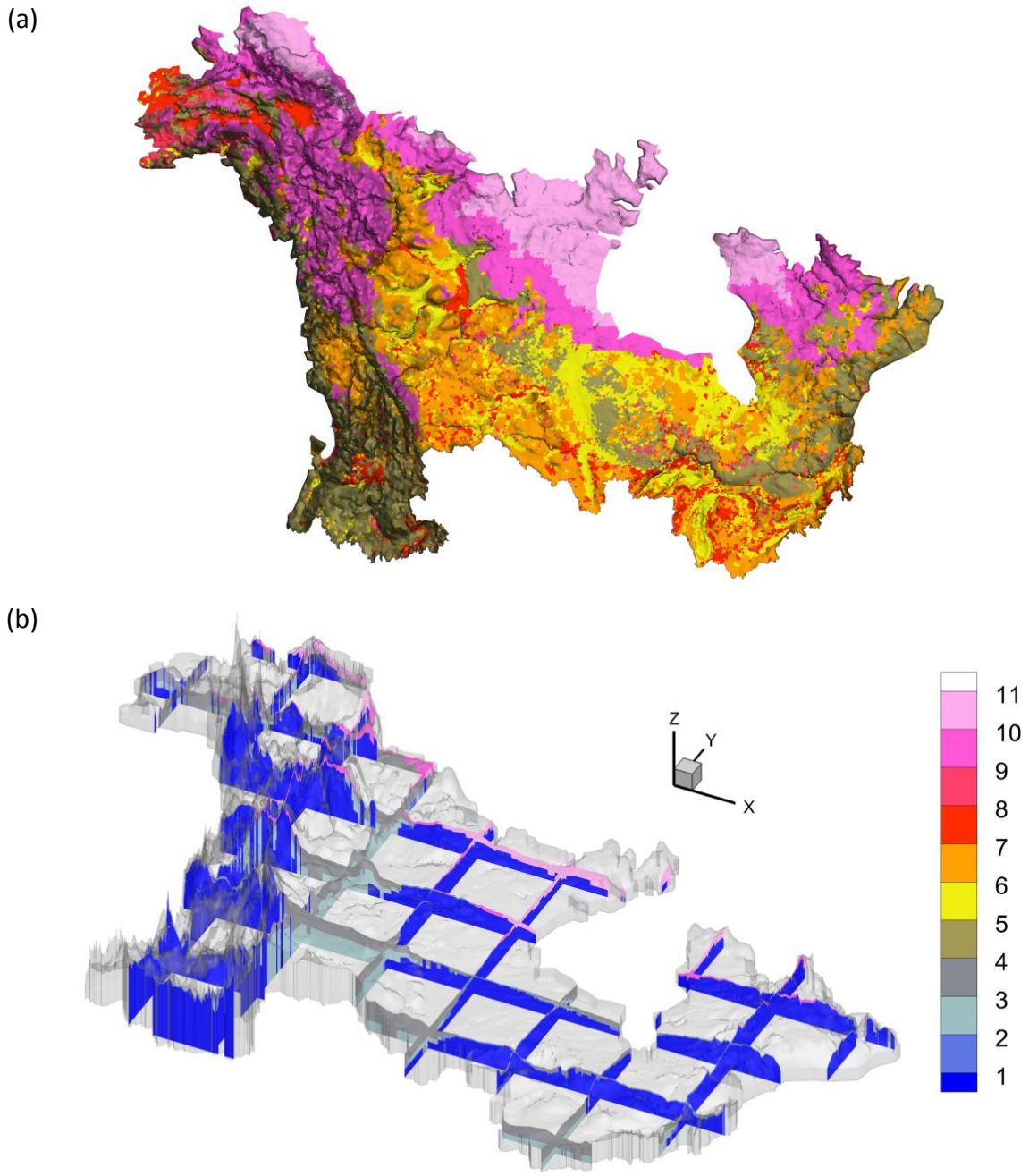

Figure 2-6: 3D Geology model in (a) plan view and (b) fence view. 1: basement rocks; 2: fractured basement rocks; 3: sedimentary rocks; 4: unconsolidated sediments; 5: upper 5 m unit 1; 6: upper 5 m unit 2; 7: upper 5 m unit 3; 8: upper 5 m unit 4; 9: upper 5 m unit 5; 10: discontinuous permafrost; 11: continuous permafrost.

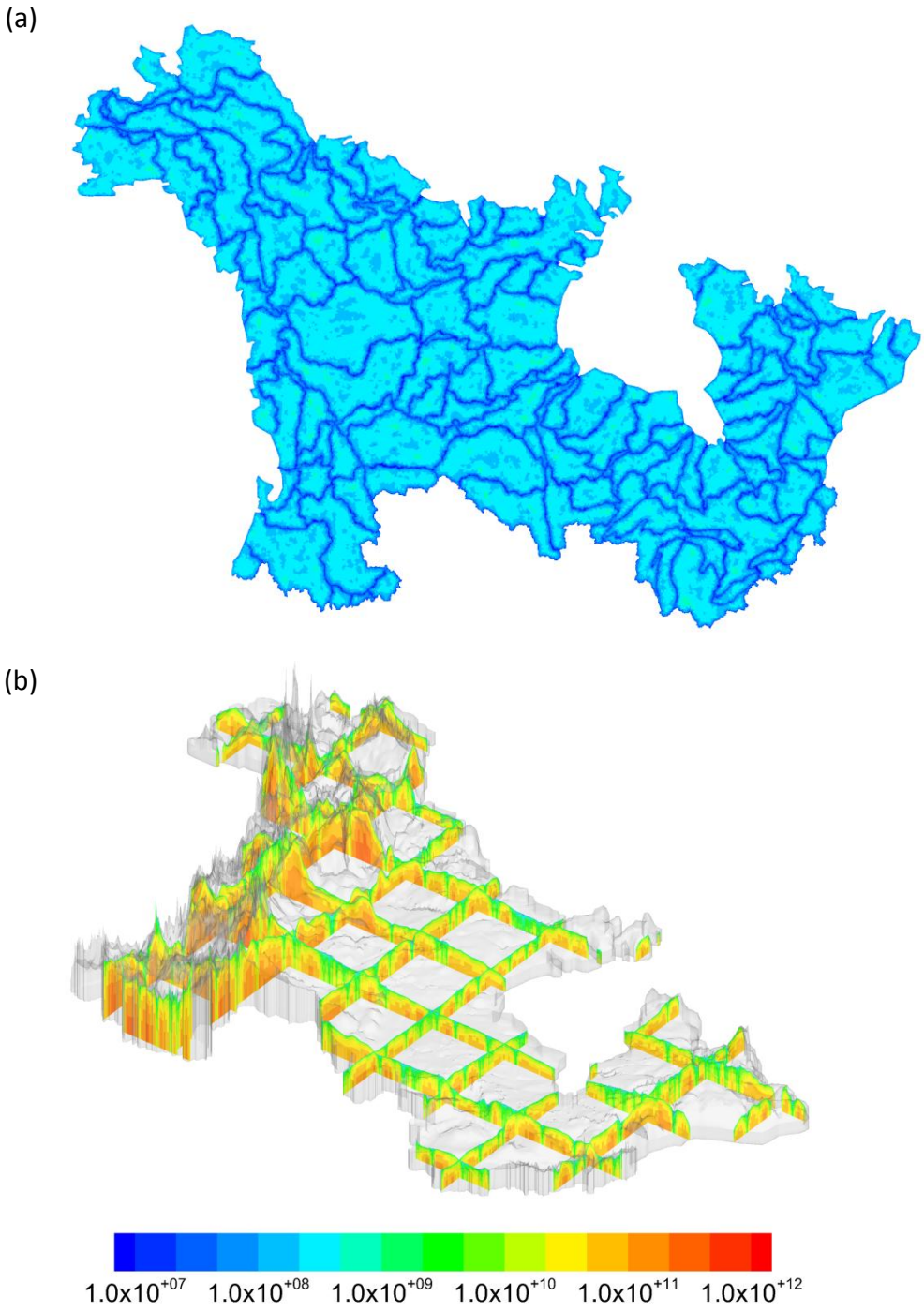

Figure 2-7: Cell volume (m^3) distribution of the 3D triangular prism grid in (a) plan view and (b) fence view. Cell volume is indicative of the elemental segment length and layer thickness.

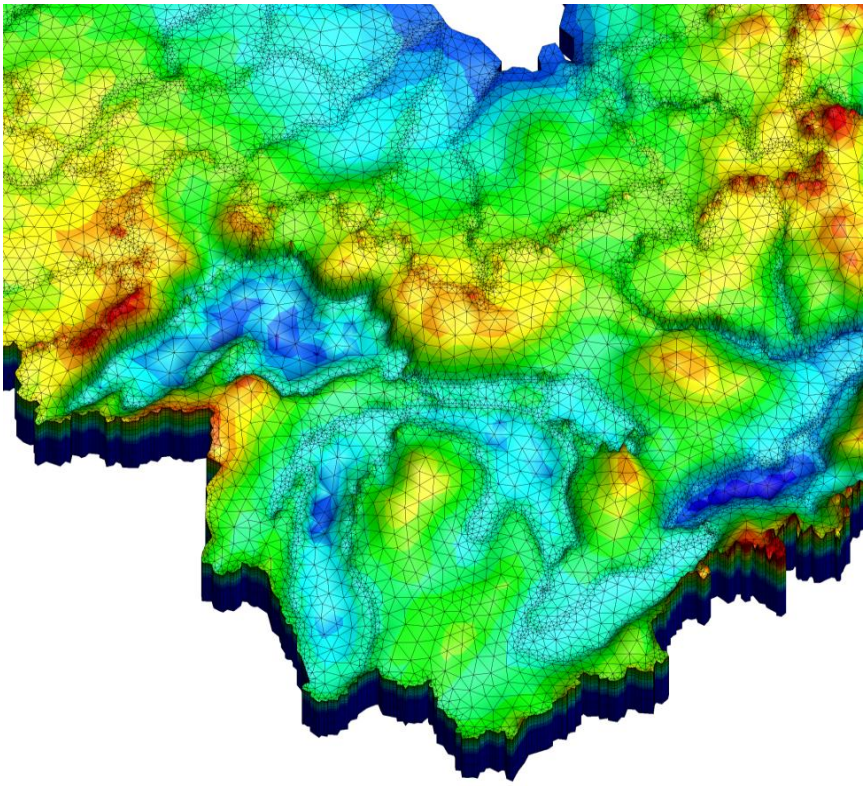

Figure 2-8: A close-up look at the 3D triangular prism grid along Great Lakes region. Red color represents high elevation and blue color represents low elevation.

Chapter 3
Climate Data

3.1 Observed Climate Data

Observed climate data are of vital importance for both hydrologic and climate modelling purposes. For example, observed precipitation data, perhaps in conjunction with other data, are often used as the forcing for hydrologic models. Meanwhile climate models require observed climate data for model tuning and model result corrections. Over the last century, which is a well-instrumented period, observed climate data have become increasingly abundant and reliable. However, the data availability is highly uneven, with the majority of them being collected from Europe and the United States. Primarily due to inclement weather conditions, a large portion of the vast study domain is uninhabited and few weather stations are located there. As a result, observed climate data are scarce for those uninhabited areas, and basically precipitation and temperature are the only two available observed meteorological datasets that cover the entire study domain.

3.1.1 Total Precipitation

A high-resolution (0.5 degree by 0.5 degree) and commonly used gridded global precipitation dataset - Terrestrial Precipitation: 1900-2008 Gridded Monthly Time Series (Version 2.01) is chosen for this study. It was developed by Matsuura and Willmott [2009a] at the Center for Climate Research (CCR) based at the University of Delaware, USA. This dataset provides monthly total precipitation (Pt) data that are compiled based on observed data collected from a large number of stations. Raw station data were obtained from multiple reputable sources,

including the Global Historical Climatology Network (GHCN), Environment Canada, the National Climatic Data Center (NCDC) under the National Oceanic and Atmosphere Administration (NOAA) and the National Center for Atmospheric Research (NCAR) to name a few. Station values were interpolated using a climatologically aided interpolation (CAI) method [Willmott and Robeson, 1995]. During data compilation, all station data were cross-validated station-by-station and cross-validation errors are provided for each grid point together with the monthly mean total precipitation data. Figure 3-1 shows the present-day (1961-2000) mean annual total precipitation (mm/year) across the study domain based on the CCR precipitation dataset. Note that the total precipitation data in this dataset include both the liquid (rain) and the solid (snow and ice) forms.

3.1.2 Temperature

The present-day (1961-2000) mean annual temperature distribution across the study domain is plotted in Figure 3-2. The temperature data are based on a high-resolution (0.5 degree by 0.5 degree) gridded global temperature dataset - Terrestrial Air Temperature: 1900-2008 Gridded Monthly Time Series (Version 2.01) which was also developed by Matsuura and Willmott [2009b] at the Center for Climate Research. Because the temperature data are only used for comparison purposes and are not directly used for this modelling study, details about this dataset are not described here.

3.2 IPCC SRES Emission Scenarios

Current future climate change assessments are based on a set of IPCC SRES scenarios [Nakicenovic and Swart, 2000], each of which makes a unique assumption of the emission

rate of greenhouse gases and aerosols during the twenty-first century. These emission scenarios were constructed by considering a number of underlying forces, including population growth, economy and technology development, energy system and LULC change. These underlying forces are highly uncertain, and thus, in total, 40 IPCC SRES emission scenarios were developed to address the uncertainty. Figure 3-3 exhibits the global CO_2 emissions for the 40 IPCC SRES scenarios during the 21st century relative to the actual CO_2 emissions in the 20th century, and each SRES scenario represents a possible image of future conditions. The IPCC SRES scenarios are designed for future climate projections and they can also be a useful tool to improve our understanding of the complex climate system through sensitivity analyses.

It is acknowledged that the IPCC Fifth Assessment Report (AR5) [IPCC, 2013] was constructed based on a new set of scenarios named Representative Concentration Pathways (RCPs) [van Vuuren et al., 2011]. The RCPs are a new set of four pathways: RCP8.5, RCP6, RCP4.5 and RCP2.6, and they have now replaced the SRES scenarios which were used in the last two IPCC reports, TAR and AR4. For clarity and consistency purpose, instead of RCPs, SRES will be used throughout this study.

It is ideal to have multiple future climate projections forced by different SRES scenarios to address the uncertainty associated with the emissions scenarios. However, due to high computational cost for the RCM and hydrologic simulations, only two IPCC SRES scenarios, A2 and A1B, are used in this study. For the A2 scenario, which is often referred as the "business-as-usual scenario", the major underlying theme is regionalization and continuous

global population growth. The A1B scenario assumes the global population peaks during the 2050s and then declines afterwards. It also assumes a future world of rapid economic growth with convergence among regions and a balanced energy source. As it is shown in Figure 3-3, A2 represents a mid-high emission scenario and A1B is a mid-range emission scenario.

3.3 Dynamical Downscaling

The new generation global climate models (GCMs) simulate the interactions between the atmosphere, ocean, cryosphere and the land surface. They are currently the best available modelling tools to predict the long-term responses of the climate system to gradually increased greenhouse gases at the global scale. Due to the substantially increased computing power in recent years, the grid resolution within GCMs has been improved from a few hundred to approximately 100 kilometers. The grid resolution of GCM data has increased from T21 (~500 km) (First Assessment Report (FAR)) in 1990, to T106 (~110 km) (Fourth Assessment Report (AR4)) in 2007. However, numerous studies [Grotch and MacCracken, 1991; Xu, 1999; Xu, 2005] have demonstrated that the original GCM outputs are not suitable for impact studies at the regional scale. One of the main reasons for this unsuitability is the typically very coarse horizontal resolution of the GCM data. Impact studies typically require climate data with a spatial resolution of tens of kilometers or finer. Another important reason attributing to the unsuitability of GCM outputs for impact studies is their parameterization schemes [Giorgi and Mearns, 1991]. Parameterization is a commonly used approach that is based on semi-empirical relationships to approximate the bulk effects of the physical processes occurring at scales that are too small to be directly represented, are too complex or are poorly understood. All parameterization schemes introduce errors to some degree, and a

more detailed parameterization scheme that may yield acceptable results for a particular model may not yield suitable results when applied in a different model. The parameterization schemes used by most current generation GCMs are meant to be representative over scales of hundreds of kilometers. That is to say, original GCM outputs may not be suitable for regional impact assessment studies even if the GCM grid resolution has somehow been refined to the level of a few tens of kilometers.

To overcome this obstacle, different types of downscaling methods have been developed to transfer the climatic information from the coarse-scale GCM outputs to regional or local scales. Statistical and dynamical downscaling are currently the two predominantly used approaches for downscaling GCM data, although some other simple methods (interpolation or delta approach) have been used [Fowler, et al., 2007]. Each method has its own advantages and limitations. Statistical downscaling requires two steps. Statistical relationships between the GCM projections and local variables are established using observed historical climatic data during the first step. The statistical relationships are then used to transform the GCM projections to regional or local scales in the second step. The dynamical downscaling method involves running a high resolution RCM on a sub-domain of interest driven by the GCM outputs or reanalysis data along its lateral boundaries. With access to super computers becoming more readily available, the regional climate modelling approach has become increasingly popular for downscaling GCM data.

The statistical approach is computationally efficient, and this approach is able to downscale the GCM output to the station-scale level given sufficient historical climate data. However,

statistical downscaling requires long series of reliable historical data for calibration. In addition, this approach has a serious weakness in that a stationary relationship between the climate system projection (predictand) and the historical data (predictor) is assumed under a changing climate [Fowler et al., 2007]. The dynamical downscaling approach does not suffer from this shortcoming because the "feedback effects" will be captured by the RCMs. Also, RCMs simulate the regional climate system in an equivalently physically consistent way as their parent GCMs. Moreover, RCMs include more physics of the atmospheric system compared to their driving GCMs in terms of orographic precipitation, extreme weather events and climate variability [Fowler et al., 2007]. These improvements are sometimes referred as the "added value" provided by RCMs. Nevertheless, dynamical downscaling is computationally demanding and sometimes bias-correction and/or further downscaling is still required for the RCM output. Primarily due to the lack of long-term historical observed climate data covering the entire study domain, and the other benefits listed above, the RCM approach is chosen here to downscale GCM outputs employed in this study.

3.4 Main Characteristics of Global Climate Models

Outputs obtained with three leading GCMs are used to provide boundary conditions for the RCM simulations. The three GCMs are the Community Climate System Model version 3 (CCSM3), the Canadian Global Climate Model version 3 (CGCM3) and the Hadley Centre Coupled Model version 3 (HadCM3). CCSM3 [Collins et al., 2006] is a community model and it has been developed by a group of institutions led by NCAR (National Center for Atmospheric Research). CGCM3 [Flato and Boer, 2001] is a Canadian GCM developed by CCCma (Canadian Centre for Climate modelling and analysis). Basically CGCM3 is an

upgraded version of CGCM2 [Flato and Boer, 2001] with a much improved atmospheric component AGCM3 (Generation Atmospheric General Circulation Model version 3) [McFarlane et al., 2005]. HadCM3 [Gordon et al., 2000] is an UK version of GCM developed by the United Kingdom Meteorological Office (UKMO) Hadley Centre. Major characteristics of these three GCMs are summarized in Table 3-1.

3.5 Main Characteristics of Regional Climate Models

In this study, the downscaling of GCM outputs is performed using three state-of-the-art RCMs, namely the Canadian Regional Climate Model version 4.2.1 (CRCM), the Hadley Centre Regional Model version 3 (HRM or HadRM3) and the Weather Research and Forecasting model version 3.2.1 (WRF). Major characteristics of these three RCMs are summarized in Table 3-2 and Figure 3-4 shows the three RCM model domains relative to this study domain and North America. Brief descriptions of these three RCMs are as follows.

3.5.1 CRCM

The CRCM [e.g. Music and Caya, 2007] is a regional climate model developed in Canada by the Université du Québec à Montréal (UQAM) together with the CCCma. It uses a dynamical kernel that is based on the fully-elastic nonhydrostatic Euler equations solved by a non-centered semi-implicit and semi-Lagrangian approach. When projected in a stereo-graphic projection method, CRCM's horizontal grid appears to be uniform. A state-of-the-art land surface scheme – Canadian LAnd Surface Scheme version 2.7 (CLASS 2.7) [Verseghy, 1991; Verseghy et al., 1993] is used in CRCM to compute the heat and moisture fluxes across the interface between the land surface and the atmosphere. Due to the fact that large

surface water bodies have a considerable influence on regional climate systems, a simple "mixed layer" lake sub-model is coupled to CRCM to simulate the surface water temperature and the ice cover for the Laurentian Great Lakes [Goyette et al., 2000]. In this work, CRCM is used to downscale CGCM3 global data under the IPCC SRES A2 scenario.

3.5.2 HRM

HRM [Jones et al., 2004] is the UKMO Hadley Centre's regional climate model, version 3. In HRM, an Arakawa B grid [Arakawa and Lamb, 1977] is used for horizontal domain discretization. HRM uses a rotated pole projection and it has approximately uniform grid box area throughout the simulation domain. A timestep of 300 seconds is used in HRM to ensure numerical stability because of the fine grid resolution. HRM adopts the UKMO unified forecast and climate model as its atmospheric component which is based on a hydrostatic version of the full primitive equations. The land surface scheme used in HRM is the UK Met Office Surface Exchange Scheme version 2.2 (MOSES 2.2) [Cox et al., 1999]. To the best of my knowledge, HRM does not currently include an explicit lake component. In this study, HadCM3 global data under the IPCC SRES A2 scenario are used to drive the HRM model.

3.5.3 WRF

WRF is the next generation mesoscale community model designed for both atmospheric research and weather forecasting purposes and it has several different versions. The version selected for this study is the Advanced Research WRF (ARW), version 3.2.1 [(Skamarock et al., 2007]. WRF was originally developed as a community model by NCAR, NOAA (National Oceanic and Atmospheric Administration) and several other institutions /

universities. WRF uses a lambert conformal conic projection for its horizontal grid coordinates which is centered at 50 ^{o}N and 100 ^{o}W. The Noah land surface model [Chen and Dudhia, 2001] is used by WRF for its land surface scheme. The original WRF model does not contain a lake component. To bridge the gap, Gula and Peltier [2012] added a freshwater lake model – FLake [Mironov, 2008; Mironov et al., 2010] to WRF to handle large lakes in the simulation domain. Initially FLake model was coupled offline to the Noah land surface scheme in version 3.2.1, and it can be used as a fully-coupled (online) component by a newer version of WRF, e.g. version 3.4 [d'Orgeville et al., 2014] and version 3.4.1 [Erler et al., 2015]. In all three cases, offline or online, the FLake model helps produce more realistic simulation results. In this study, WRF is used to downscale two CCSM3 global outputs. One is under the IPCC SRES A2 scenario and the other is under the A1B scenario.

3.6 Descriptions of RCM Outputs

In total, four high-resolution RCM outputs are used in this study and detailed attributes of each RCM output are summarized in Table 3-3. Based on these four RCM outputs, 11 long-term climate datasets are derived and used to drive the HydroGeoSphere model. For clarity purpose, details of these datasets are tabulated in Table 3-4.

CRCM (A2) data are obtained from the Canadian Centre for Climate Modelling and Analysis [Music and Caya, 2007]. The CRCM dataset provides 40-year historical record covering the period from 1961 to 2000, and 100-year climate projections covering the period from 2001 to 2100. Its future data coverage period is the longest among the three RCM datasets. As shown

in Figure 3-4, the CRCM data have a complete coverage over the study domain. The CRCM data used in this work have a grid resolution of 45 km true at 60 ^{o}N.

HRM (A2) data are acquired from the North American Regional Climate Change Assessment Program (NARCCAP) [Mearns et al., 2007]. HRM dataset offers a 30-year historical coverage from 1971 to 2000 and a 30-year future coverage from 2041 to 2070. It has a grid resolution of 50 km. As illustrated in Figure 3-4, the HRM data do not cover the entire study domain, excluding a small less important area in the North-West part of the study domain. In this regard, extrapolation is applied for the small area without data coverage. HRM has the shortest historical data coverage (only 30 years) and it also has the smallest model domain among these three RCMs.

The WRF (both A2 and A1B) data were provided by Gula and Peltier [2012]. The WRF data have the highest grid resolution of 30 km among these three RCMs. This dataset provides 40-year historical data covering the period from 1961 to 2000, and a 30-year climate projection covering the period from 2041 to 2070. As shown in Figure 3-4, the WRF data also have a complete coverage over the study domain. Note that WRF is the only RCM that offers future climate data under both IPCC SRES A2 and A1B scenarios.

It was intended to include a few more RCM outputs in this work to analyze the uncertainties associated with the climate model structures and formulations. For example, the international program NARCCAP provides multiple high-resolution RCM projections which are all under the SRES A2 scenario. Although this program is primarily for the North American region, unfortunately, none of its RCM outputs cover the entire study domain. As a matter of fact,

the HRM model domain is the largest among them and a significant portion of the study domain in the Northwest will have no data coverage if outputs from the other RCMs are used. Because excessive data extrapolation may be necessary, this could introduce serious bias to the hydrologic modelling results. Thus, only one RCM output (HRM driven by HadCM3) from the NARCCAP program is selected for use in this study.

3.6.1 Present-day Results of P, AET and T

Figure 3-5 exhibits the present-day (1971-2000) mean annual total precipitation (mm/yr), the mean annual actual evapotranspiration (AET) (mm/yr) and the mean annual temperature (Celsius) simulated by the three RCMs. For the sake of consistency, historical data for the period 1961 to 1970 from the CRCM and WRF models are not used in this case. The comparison between the RCM simulated and the observed present-day precipitation data (see Figure 3-1) demonstrates that all three RCMs have good skills for reproducing the present-day precipitation data. They share a high degree of similarity, wet in the West and East coastal areas and dry in the central and Northern regions.

As mentioned at the beginning of this chapter, there is no reliable actual ET data available that cover the entire study domain. Therefore, the skills of each RCM for simulating present-day AET cannot be accurately evaluated here. All three present-day AET results exhibit some similar overall spatial patterns. For example, AET is high in the St. Lawrence River Basin and the SW portion of the study domain, and AET gradually decreases towards the North. Also, compared to the precipitation data, AET appears to be more similar to the temperature data in terms of the overall spatial trend. Among the three RCM AET results,

more similarities are observed between the CRCM and the WRF outputs. Compared to the CRCM and WRF results, the HRM simulated AET is generally higher in the central and Northern areas. Perhaps more importantly, Figure 3-5 shows that the HRM simulated AET over the Great Lakes appears to be even lower than that of the nearby land surface. This result appears to be counter-intuitive and questionable, although there is no observed AET data available for verifying the accuracy of the simulated AET results. Higher AET over large surface water bodies is generally anticipated than over adjacent vegetated land [Zhang et al., 2010].

For the temperature data comparison, all three RCM models show comparable patterns compared to the observed dataset (see Figure 3-2). However, the WRF simulated results appear to match the observed data somewhat better than the other RCM results. WRF seems to produce more regional variations in the mountainous regions compared to the other two RCMs almost certainly because of its high spatial resolution. In general, temperatures decrease from South to North, with the isotherms tilting a bit from NW to SE. Note that there is no mean temperature provided in the HRM dataset and the mean daily high and low temperatures are used to compute the mean annual temperature. The bias of using this method is expected to be insignificant over a long time period.

3.6.2 Predicted Changes in P, ET and T during the 21st Century

The RCM projected changes in the mean annual total precipitation (mm/yr) over the 21st century are exhibited in Figure 3-6. Among the six 30-year-period mean projections, four are for the mid-21st century (2041-2070) with the other two (both under A2 scenario provided by

CRCM) being for the early (2011-2040) and late (2071-2100) 21st century. Three of the four 2041-2070 projections are forced by the A2 scenario and only one WRF projection is under the A1B scenario. According to the three CRCM projections, which are illustrated on the left column in Figure 3-6, the total precipitation will gradually increase over the 21st century for the most part of the study domain except for some of the SW and central areas. CRCM predicts a modest decrease (1-30 mm/yr) in parts of the SW and central regions during 2011-2040. As time moves forward, areas receiving less total precipitation gradually shrink and almost the entire domain will receive more precipitation by 2041-2070 and later based on the CRCM predictions. A comparison among the four 2041-2070 projections indicates that the three A2 outputs exhibit noticeable differences, although they preserve some commonality in overall patterns. For example, all three A2 2041-2070 projections show that the total precipitation may increase from a few 10s up to 300 mm/yr by 2041-2070 for the vast Northern areas. Compared to the other two A2 2041-2070 outputs, WRF (A2) 2041-2070 predicts a larger area receiving less total precipitation in the Southern and Central regions. On the other hand, based on the HRM (A2) 2041-2070 projection, the total precipitation is likely to increase over most of the study domain. A comparison between the WRF (A2) 2041-2070 and WRF (A1B) 2041-2070 outputs reveals that the A1B scenario predicts smaller areas receiving less total precipitation in the central region. Other than this difference, these two WRF outputs share similar characteristics concerning predictions of total precipitation during 2041-2070 in other regions of the study domain.

Shown in Figure 3-7 are the RCM predicted changes in the mean annual actual evapotranspiration (AET) during the 21st century. The three CRCM (A2) projections (the left

column in Figure 3-7) illustrate the trend and evolution of AET over the next 90 years. According to the CRCM projections, AET is likely to steadily increase by 1~30 mm/yr during the early 21st century to 30~100 mm/yr for most of the study domain. For the entire 21st century, only a small portion of the study domain is predicted by CRCM to decline in AET, and these limited areas are mainly located in the Western coastal areas and the Prairie region. In addition, a similar spatial pattern that the AET gradually increases towards South is observed among the three CRCM (A2) projections. A comparison between the four projections for 2041-2070 shows that HRM (A2) forecasts a smaller increase in AET than the other three projections and that HRM (A2) is the only projection forecasting a decrease in AET along the Rocky Mountains. Results also reveal that these four projections all forecast an increase in AET for most of the study domain, with the highest AET increase occurring over the Great Lakes. As can be seen, the predicted changes in AET based on the two WRF (A2 and A1B) projections are similar in terms overall patterns, but WRF (A2) forecasts a smaller increase in the Prairie region. A much larger area of land in the vicinity of the Great Lakes is predicted to have a decrease in AET by 2041-2070 by the two WRF projections than by the other projections. Although the large difference in AET responses to climate change between land and the Great Lakes are exhibited by the results for all four 2041-2070 RCM projections, it is obvious that the actual shapes of the five Great Lakes are best reflected in the two WRF projections. This fact strongly suggests that the lake effect on regional climate system has been better captured by WRF than the other two RCMs and this may be due to the higher grid resolution in WRF outputs and/or the sophisticated fresh-water lake model –

FLake that has been off-line coupled to WRF to include the presence/absence of lake ice during the winter months.

The RCM predicted changes in the mean annual temperature (Celsius) are illustrated in Figure 3-8. The three CRCM (A2) projections clearly show that mean annual temperatures will steadily increase over the entire study domain during the 21st century. CRCM predicts mean annual temperatures to increase by about 1~2 ^{o}C by 2011-2040 and increase 3~5 ^{o}C by 2071-2100 over most of the domain. Compared to the change in total precipitation and AET data, the predicted mean annual temperature data exhibit more similarity among the RCMs and the IPCC SRES scenarios for the period of 2041-2070. In all four 2041-2070 cases, the mean annual temperature is predicted to increase for the entire study domain, ranging from 1-2 to 4.5 ^{o}C. Based on these six RCM projections, it appears that the mean annual temperature may increase more rapidly in the Northern and SE regions. Relatively, CRCM (A2) 2041-2070 predicts only a modest temperature increase in the Northern regions compared to the other three 2041-2070 projections. It is somewhat surprising to observe the high degree of similarity between the two WRF projections because they are forced by different SRES scenarios. Perhaps the similarity can be explained by an examination of Figure 3-3, which reveals that the total CO_2 emissions by the 2050s are not much different between the A2 and A1B scenarios.

Table 3-1: Major characteristics of three GCMs used in this study. Table is adapted from Randel [2007].

	CCSM3	CGCM3	HadCM3
Country	USA	Canada	UK
Atmosphere Top	2.2 hPa	1.0 hPa	5.0 hPa
Atmosphere Vertical level	26	31	19
Atmosphere Resolution	1.4×1.4^{o}	1.9×1.9^{o}	2.5×3.75^{o}
Ocean Resolution	$0.3 - 1.0^{o}$	0.9×1.4^{o}	1.25×1.25^{o}
Ocean Vertical level	40	29	20
Sea Ice	Rheology, leads	Rheology, leads	Free drifts, leads
Coupling / Adjustments	No adjustments	Heat, fresh water	No adjustments
Land Surface	Layers, canopy, routing	Layers, canopy, routing	Layers, canopy, routing

Table 3-2: Major characteristics of the three RCMs used in this study. This table is adapted from NARCCAP (http://www.narccap.ucar.edu/data/rcm-haracteristics.html).

	CRCM	HRM	WRF
Dynamical Core	Non-hydrostatic, Compressible	Hydrostatic, Compressible	Non-hydrostatic, Compressible
Lateral Boundary Treatment	9 points	4 points	15 grid points
Land Surface Scheme	CLASS	MOSES	NOAH
Thermal / Water Layers	3/3	4/4	4/4
Vegetation Types	21 classes	53 classes	24 classes
Boundary Layer	Local K, gradient Richardson number formulation	First order turbulent mixing	Yonsei Univ. (YSU) planetary boundary layer (PBL) scheme
Explicit Moist Physics	Removal of super-saturation	Prognostic cloud liquid and ice; liquid potential T	Prognostic cloud liquid and ice, rain, snow
Cumulus Parameterization	Mass Flux	Mass Flux, including downdraft	Kain- Fritsch2 mass flux
# Vertical Levels in Atmosphere	29	19	28
Type of Vertical Coordinate	Gal-Chen scaled-height	Hybrid terrain following & pressure	Terrain following
Sponge Zone Depth (# grid pts)	10	8	10.5
Length of Timestep	900 Seconds	300 Seconds	150 seconds
Spectral Nudging	Yes	No	No
Longwave Radiation Scheme	Morcrette [1984]	PRECIS	CAM3
Shortwave Radiation Scheme	Fouquart and Bonnel [1980]	PRECIS	CAM3
Aerosol Representation	Non-uniform	Non-uniform	Uniform
Grid Size	182 x 174	171 x 146	290 x 200

Table 3-3: Attributes of each RCM output used in this study.

	CRCM	HRM	WRF
Grid Resolution (km)	45	50	30
Driving GCM	CGCM3	HadCM3	CCSM3
IPCC SRES A1B	×	×	✓
IPCC SRES A2	✓	✓	✓
Historical Period	1961-2000	1971-2000	1961-2000
Future Period	2001-2100	2041-2070	2041-2070

Table 3-4: Summaries of the attributes and data application purposes about the climate datasets used in this study which are derived from the RCM outputs described in Table 3-3. The datasets are the mean values of the entire data period indicated in the table.

Dataset Derived from RCM Outputs	RCM	SRES Scenario	Data Period	Application Purpose
CRCM 1961-2000	CRCM	20C3M*	1961-2000	Used for present-day net precipitation estimation
WRF 1961-2000	WRF	20C3M	1961-2000	
CRCM 1971-2000	CRCM	20C3M	1971-2000	Used as the control for future net precipitation estimation
HRM 1971-2000	HRM	20C3M	1971-2000	
WRF 1971-2000	WRF	20C3M	1971-2000	
CRCM (A2) 2011-2040	CRCM	A2	2011-2040	Used for future net precipitation estimation
CRCM (A2) 2041-2070	CRCM	A2	2041-2070	
CRCM (A2) 2071-2100	CRCM	A2	2071-2100	
HRM (A2) 2041-2070	HRM	A2	2041-2070	
WRF (A2) 2041-2070	WRF	A2	2041-2070	
WRF (A1B) 2041-2070	WRF	A1B	2041-2070	

*20C3M is an IPCC scenario following observed GHG concentrations through the 20th century.

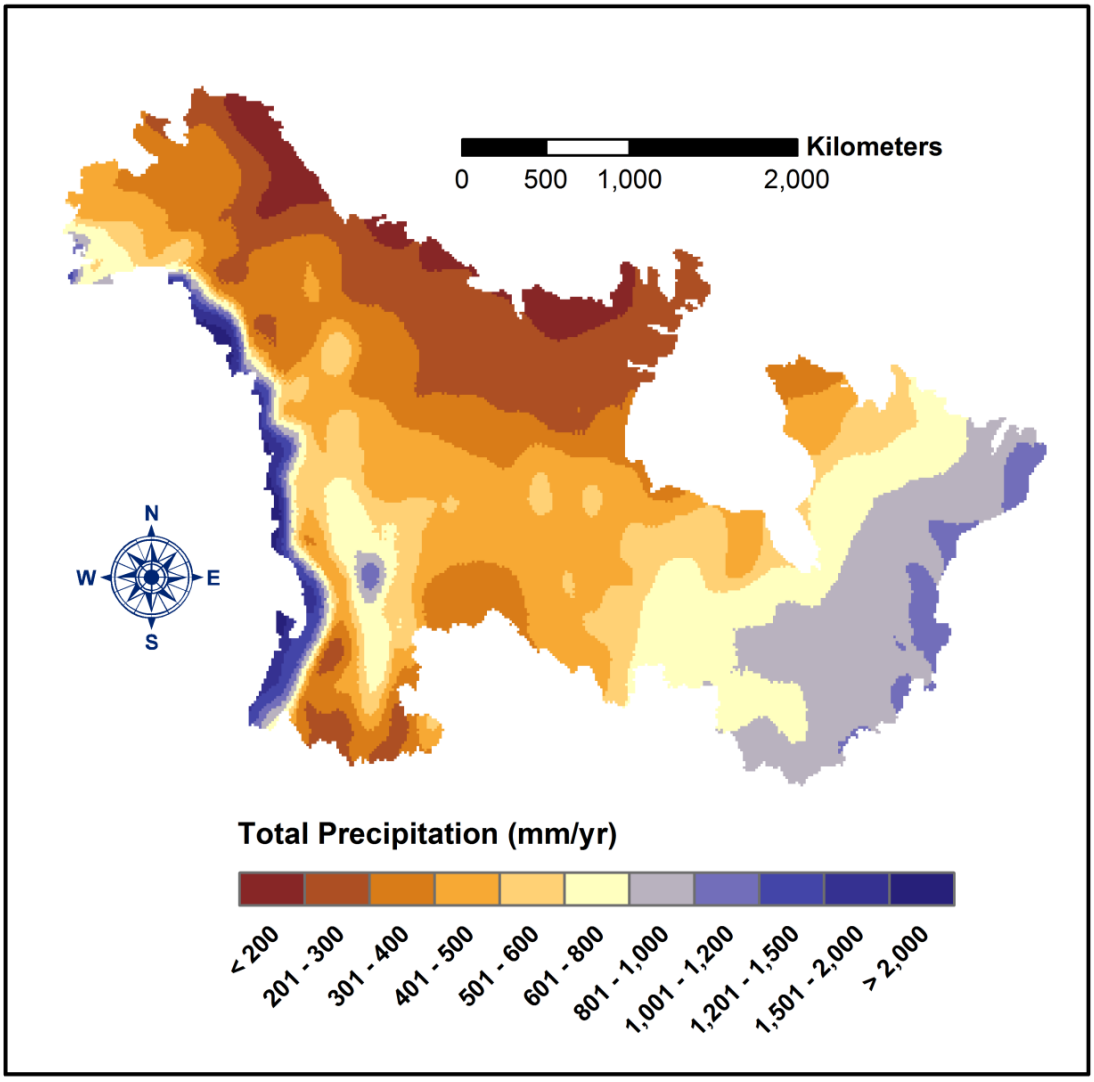

Figure 3-1: Observed present-day (1960-2000) mean annual total precipitation (mm/year) across the study domain. The plotting is based on a 0.5 degree by 0.5 degree gridded global dataset compiled by Matsuura and Willmott (2009a).

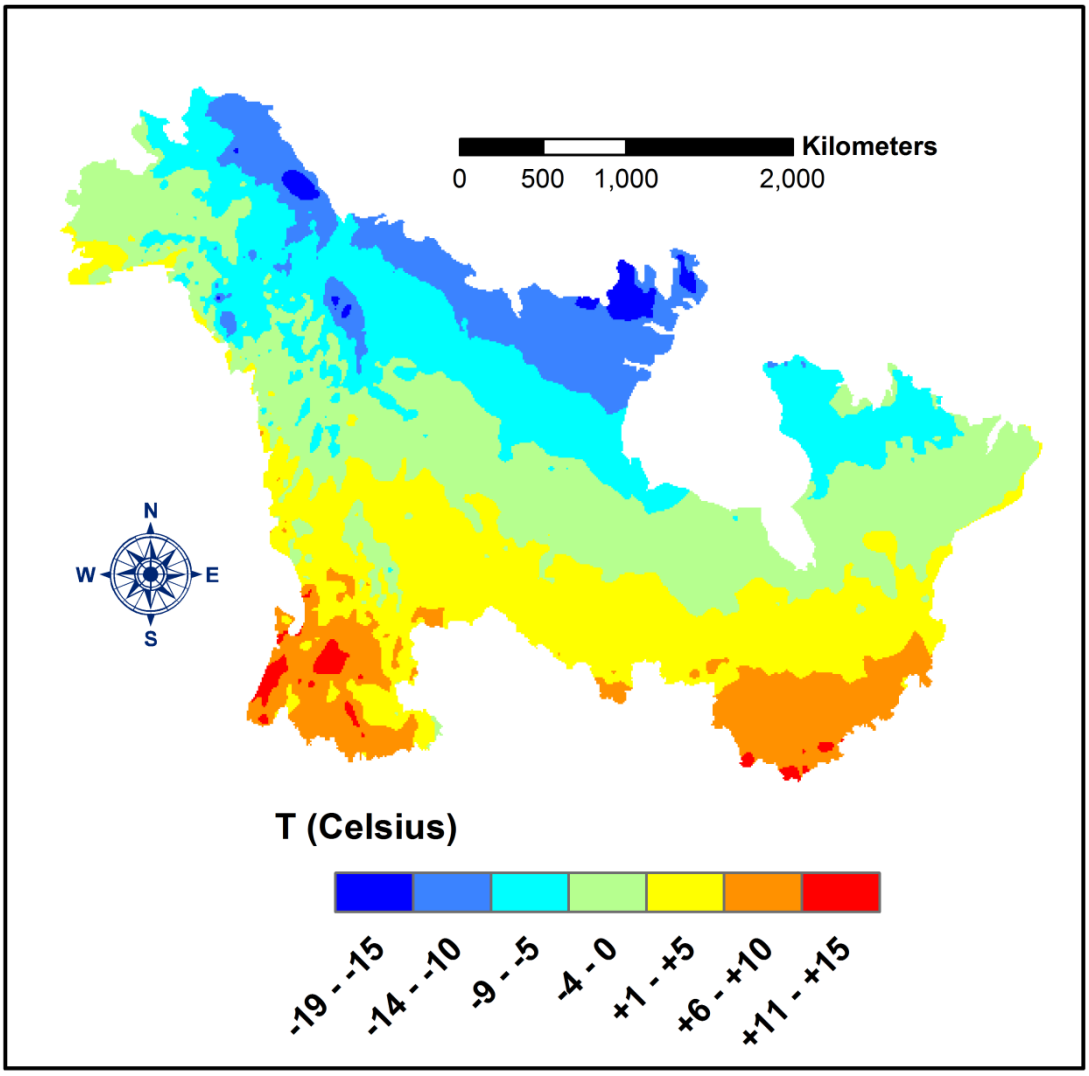

Figure 3-2: Observed present-day (1961-2000) mean annual air temperature (Celsius) across the study domain. The plotting is based on a 0.5 degree by 0.5 degree gridded global dataset compiled by Matsuura and Willmott (2009b).

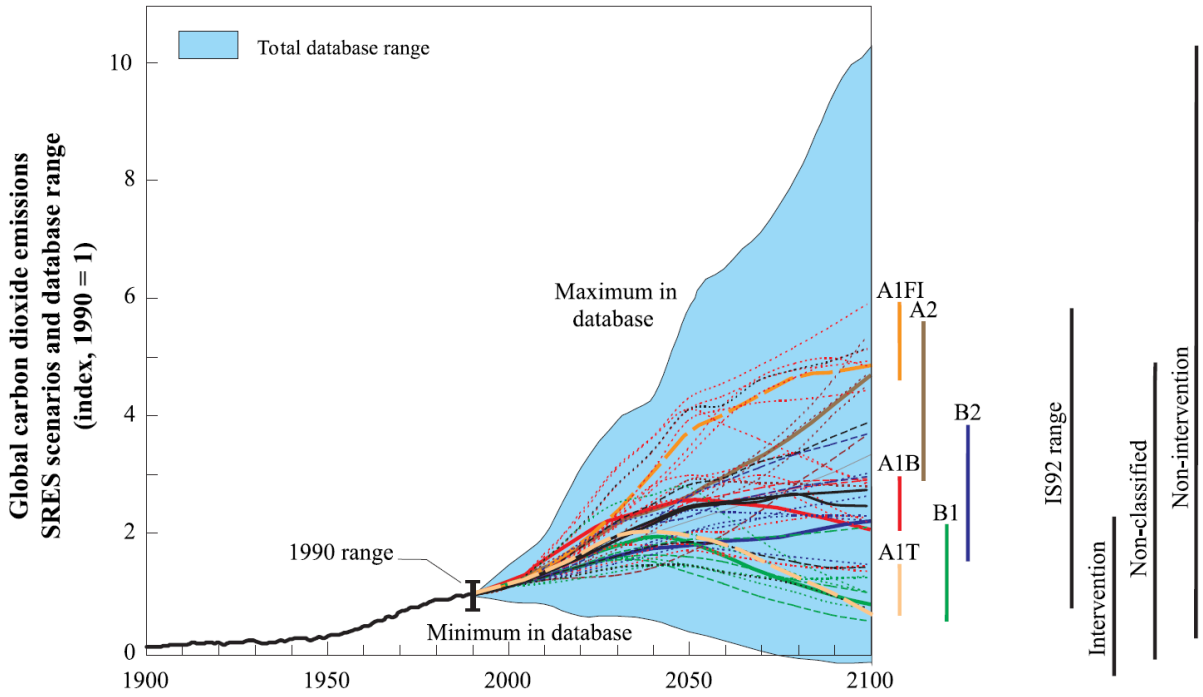

Figure 3-3: Global carbon dioxide emissions due to energy and industry from 1900 to 1990 and for the 40 SRES scenarios from 1990 to 2100. Data are shown as an index (1990 = 1). The dashed time-paths represent the individual SRES scenarios and the blue-shaded area illustrates the total SRES database range. This figure is after the IPCC Emission Scenario Special Report.

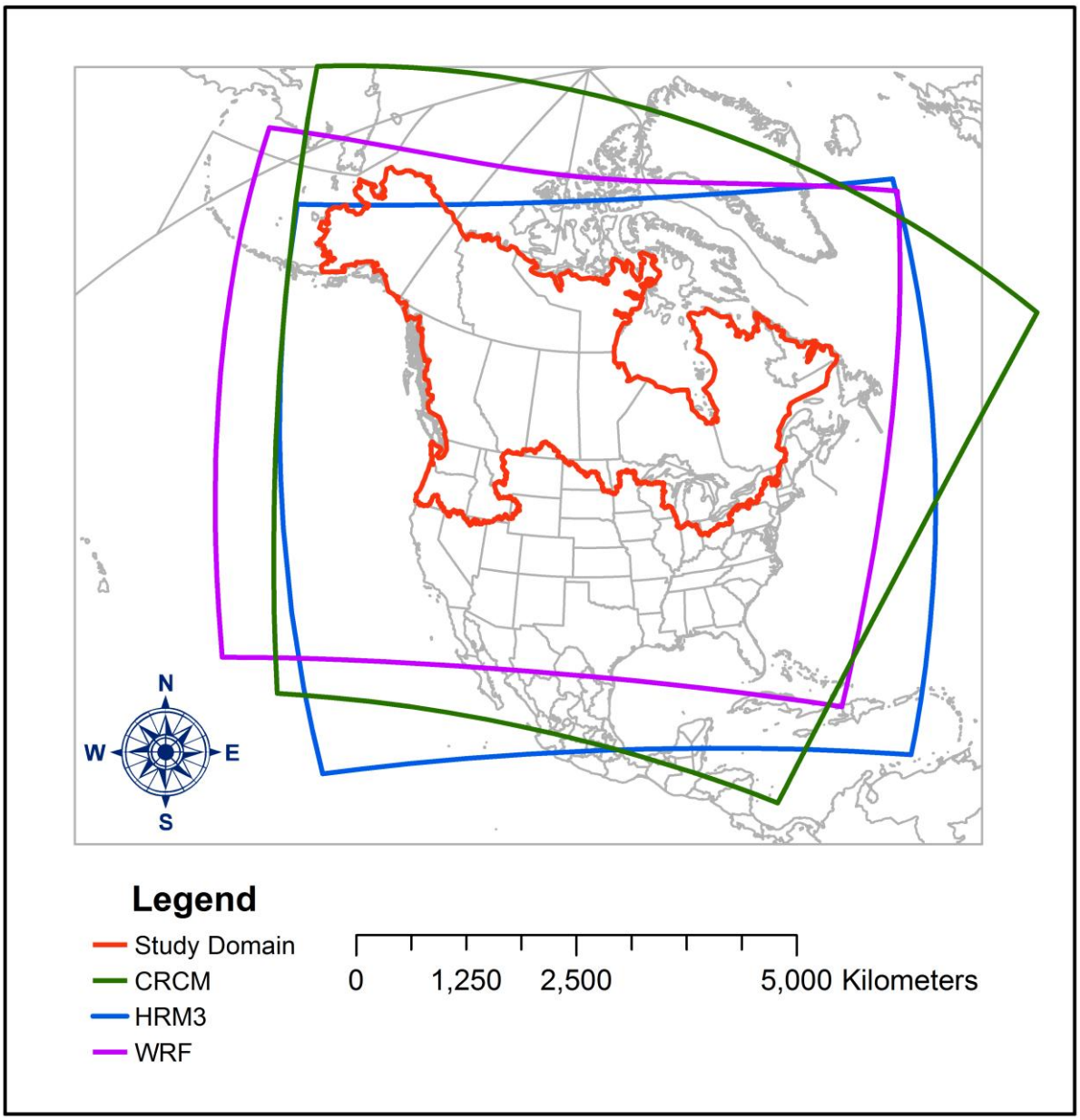

Figure 3-4: Model domains for the three RCMs (CRCM, HRM and WRF) relative to study domain and North America.

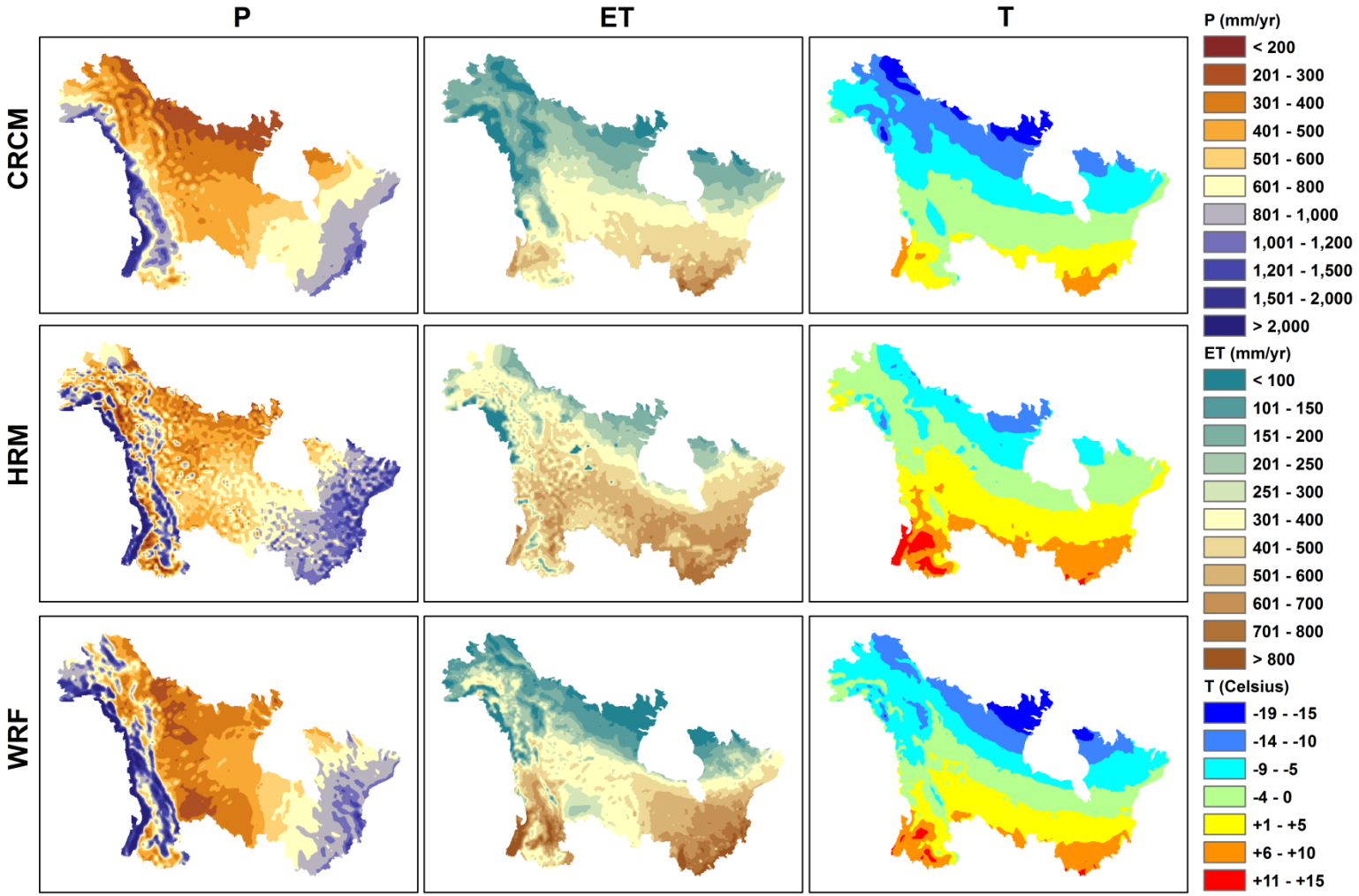

Figure 3-5: Simulated present-day (1971-2000) mean annual total precipitation (mm/year), mean annual actual evapotranspiration (mm/year), and mean annual temperature (Celsius) by three RCMs (CRCM, HRM and WRF).

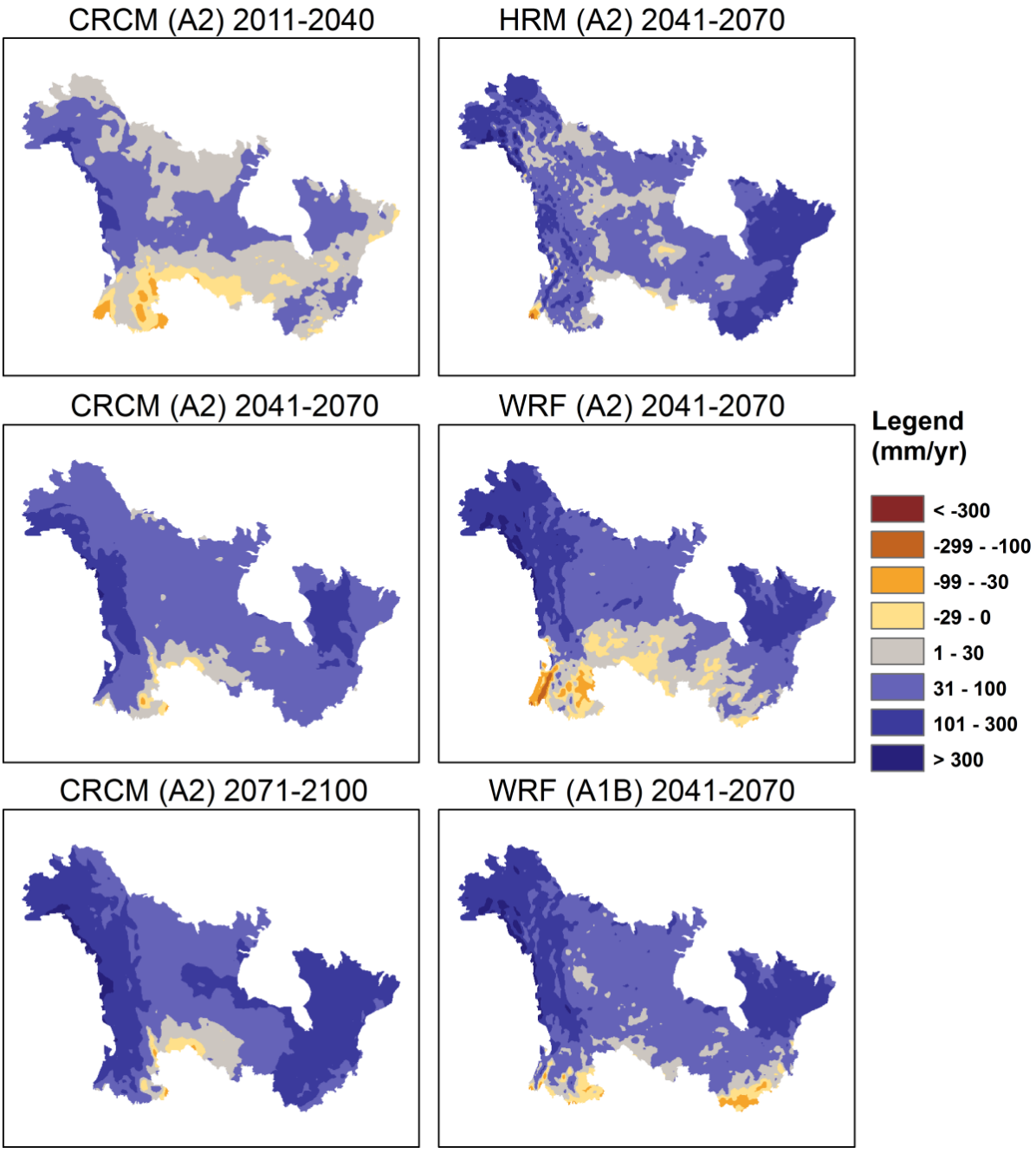

Figure 3-6: RCM predicted changes in mean annual total precipitation (mm/year). A positive change means an increase and a negative change represents a decrease.

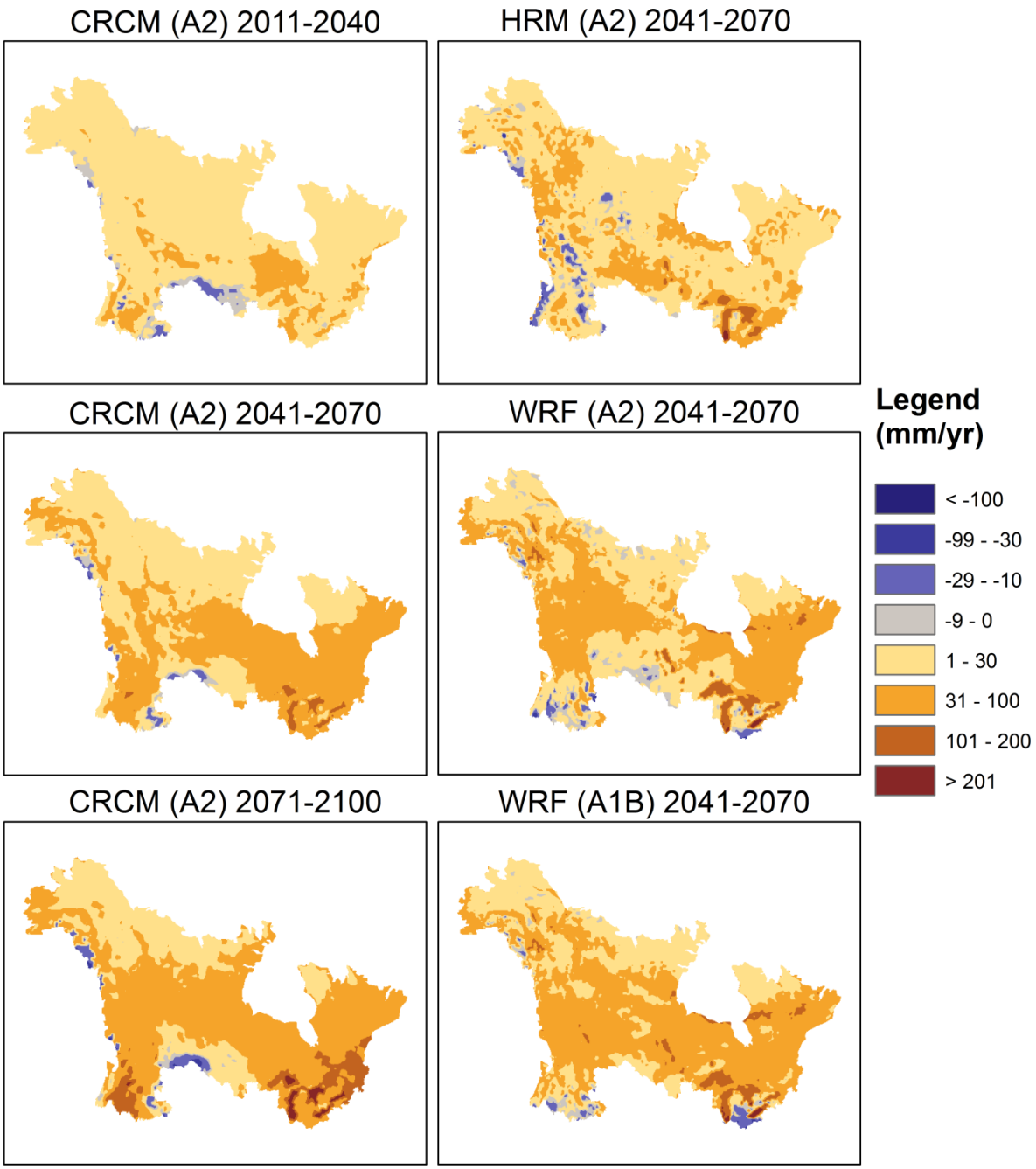

Figure 3-7: RCM predicted changes in mean annual actual evapotranspiration (mm/year). A positive change means an increase and a negative change represents a decrease.

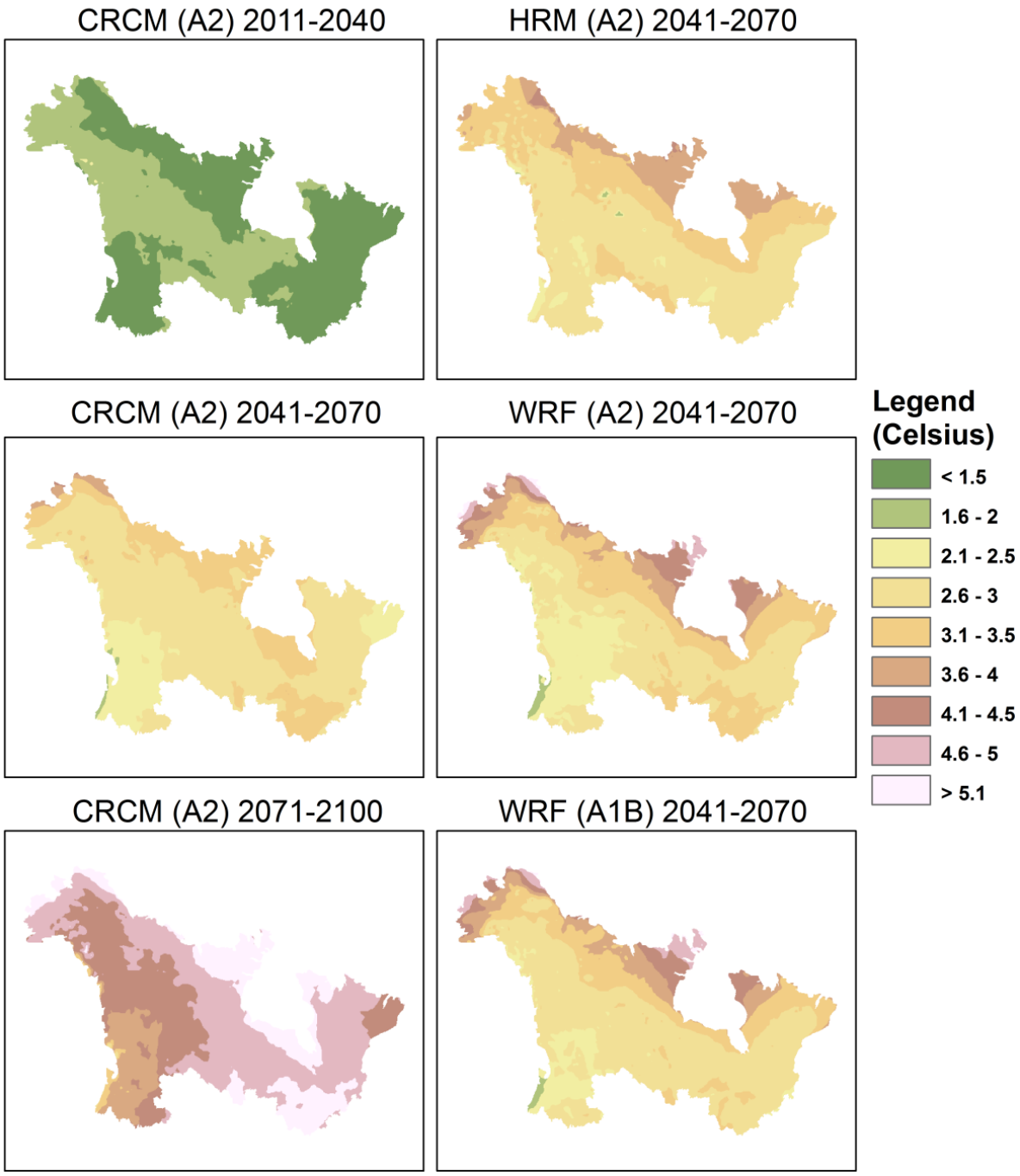

Figure 3-8: RCM predicted changes in mean annual temperature (Celsius). Positive changes indicate an increase.

Chapter 4
Present-day Steady-State Hydrologic Simulation

4.1 Present-day Net Precipitation

Net precipitation (Pn) equals the total precipitation (Pt) minus the actual evapotranspiration (AET) when the changes in water stored as soil moisture, surface water bodies and snow packs on the ground etc. becomes negligible over a long time period, e.g. 10 years or longer.

$$Pn = Pt - AET \tag{4.1}$$

The net precipitation is hydrologically important because it essentially represents the maximum available renewable water for water budget analyses. In this study, the net precipitation is used as the forcing to drive the hydrologic (HydroGeoSphere) model. HydroGeoSphere is capable of directly simulating ET processes and computing the AET if it is provided with potential evapotranspiration (PET) and precipitation data. However, reliable PET data across the entire domain is difficult to obtain due to the lack of high-resolution long-term historical climate data such as humidity, radiation, wind speed etc. Data become particularly scarce for most of the vast Northern Canada and Alaska regions. To counter this, high-resolution RCM-simulated present-day climate outputs in conjunction with observed total precipitation data are used to estimate the present-day net precipitation used in this study. It may be worth noting that turning off the ET calculations in HydroGeoSphere also reduces the already high computational burden. It is well-known that there are generally considerable differences between the GCM/RCM simulated present-day climate simulations and the observed data. For example, precipitation is one of the least reliable GCM/RCM

outputs mainly because of the inadequate understanding of the detailed physical processes controlling the short-term variations [Bazzaz and Sombroek, 1996]. Thus, the original RCM outputs are not directly used here for net precipitation estimation in this work according to Equation (4.1). Instead, the RCM data are utilized to estimate the ratio of AET to Pt at each grid point. To a certain degree, the rate of AET is correlated with the rate of Pt, because the rate of precipitation has a direct influence on the atmospheric humidity and surficial soil moisture which strongly controls the rate of AET. It is believed that the ratio of AET to Pt is more reliable than the original GCM/RCM outputs because some of the inherent bias may be cancelled out. With the ratios calculated, the present-day net precipitation is determined according to Equation (4.2) using an observed total precipitation dataset [Matsuura and Willmott, 2009].

$$Pn_{present} = Pt_{observed} \times \left(1.0 - \frac{AET_{RCM}}{Pt_{RCM}} \right) \tag{4.2}$$

where $Pn_{present}$ is the present-day net precipitation, the subscript *RCM* denotes RCM simulated values and the subscript *observed* denotes observed values.

All variables used in Equation (4.2) are present-day (1961-2000) mean annual values. To keep net precipitation values meaningful (between the total precipitation and zero), ratios of AET to Pt are adjusted within the range of 1.0 and 0.0. Average values of the CRCM and WRF outputs are used to compute the ratios of AET to Pt in Equation (4.2), and the calibration procedure shows that the arithmetic mean ratios of these two RCM outputs give slightly better streamflow simulation results compared to observed data. The improved

simulation results may be because some of the bias due to model structural differences is cancelled out during the averaging process. Although results calculated with this method are inevitably subject to some bias, which are mainly associated with the current climate models, it is certainly a step forward compared to the method that assumes net precipitation accounts for a uniform percentage, i.e. 50%, of total precipitation across the study domain.

Shown in Figure 4-1 is the present-day mean annual net precipitation data (mm/yr) computed using the method described above. As demonstrated in the figure, there is a large variation in the net precipitation among different regions. The Western coastal areas receive the highest net precipitation, over 1000 mm/yr, and the central to Northern regions of the study domain are the driest, receiving only a few tens to 200 mm/yr net precipitation. As a byproduct of the calculation of the net precipitation data, the present-day mean annual AET data are presented in Figure 4-2. The AET data are very difficult to estimate and thus this dataset may have high potential for application in the agricultural, hydrologic and climatic fields.

4.2 Observed Hydrologic Data

Observed hydrologic data are critical for hydrologic modelling because they are needed for both model calibration and validation. Streamflow and lake surface elevation data are the only available observed hydrologic data at the continental scale for this study domain. Although watertable depth and hydraulic head data are sporadically available mainly along inhabited areas, these data are of little utility for calibration or validation purposes because of scale and resolution issues. Moreover, watertable data are contained in individual provincial

datasets that in general have not been thoroughly reviewed for quality control/quality assurance purposes, and are not freely available.

4.2.1 Streamflow Data

A global monthly streamflow dataset obtained from the Global Runoff Data Centre (GRDC) [2011] is used for model performance evaluation in this study. The long-term mean monthly streamflow dataset includes more than 3,000 gauging stations within drainage basins larger than 2.5 square kilometres and have at least 10 years of data record. In total 20 representative gauging stations along the major rivers are selected for model calibration and validation. The locations of the 20 gauging stations are shown in Figure 2-2. Detailed information for these stations is summarized in Table 4-1. Note that, except for the La Grande and Caniapiscau Rivers, all measured streamflow data are representative averages for the entire historical period (1961-2000). For these two rivers, their observed streamflow data are compiled based on data collected prior to the year 1980 when a dam interfering with the natural flow system was constructed.

4.2.2 Lake Surface Elevation Data

Observed mean annual lake surface elevation data are also used for calibration and validation purposes in this study. In total, the 10 largest lakes within the study domain were selected. Their locations are shown in Figure 2-2 and their observed mean annual surface elevations are summarized in Table 4-2. The Great Lakes data are obtained from the U.S. Environmental Protection Agency (US EPA) and surface elevation data for the other lakes were obtained from Statistics Canada.

4.3 Results and Discussions

4.3.1 Surface Flow Results

All results presented in this section are for a steady-state hydrologic simulation representing average conditions over the historical period (1961-2000) driven by the spatially-distributed mean annual net precipitation described in the previous section. Figure 4-3 shows the simulated mean annual streamflow results for the 20 representative major rivers against the observed data. Overall, the simulated streamflow results match very well with the GRDC observed data. Of the 20 gauging stations, 14 of the simulated flows are within ±10% of the observed data and five are within ±10~25%. The Fraser River is the only exception, being overestimated by 31%. The simulated surface elevation data for the 10 largest lakes are provided in Figure 4-4. It can be seen that the discrepancy between the simulated and measured data is negligible. Figure 4-5 presents the pattern of surface drainage networks simulated by HydroGeoSphere and surface water depth distribution across the domain. A comparison between Figure 4-5 and Figure 2-2 suggests that the steady-state hydrologic simulation results, especially for the major rivers and lakes, mimic the actual surface drainage networks reasonably well. However, there are some small areas of artificial ponding in regions where the mesh is too coarse, especially in the mountainous areas. It is believed that the number of artificially ponded depressions would be significantly reduced in a simulation that has a higher grid resolution.

The infiltration/exfiltration results simulated by HydroGeoSphere, as defined by the exchange flux across the land surface and subsurface, are presented in Figure 4-6a, together

with the infiltration results calculated by CCSM3 [Collins et al., 2006] as an example of the infiltration estimated by a climate model (Figure 4-6b). As illustrated in Figure 4-6a, the pattern of interactions between the surface and subsurface flow regimes is highly complex, with the total recharge area being much larger than the total discharge area. The simulated results show that the infiltration rate is generally comparable to the prescribed net precipitation and that the exfiltration, which occurs mostly along the streams and surface water bodies, is higher than the net precipitation. The total infiltration across the entire land surface is calculated to equal 1872 km^3/year which, at steady state, approximates the total recharge to the water table. Overall, the HydroGeoSphere simulated infiltration and exfiltration results are in good agreement with our general understanding of the interactions between surface water and groundwater. For example, the rivers and lowland areas are primarily fed by groundwater, and groundwater is discharging near-shore into the major lakes. On the other hand, for the CCSM3 results displayed in Figure 4-6b, water only flows from the surface water regime into the subsurface and no groundwater discharges to the surface water regime across the entire domain. In my view, this is a serious deficiency borne by most current-generation climate models. This deficiency is indeed attributed to the oversimplified 1D infiltration package in the land-surface module used by climate models. A physically more realistic representation of subsurface flow including the deeper groundwater system in climate models will help make the representation of the terrestrial hydrologic cycle more complete [Kite et al., 1994] and improve the computation of energy exchange between land and the atmosphere [Maxwell and Kollet, 2008] in climate modelling.

4.3.2 Subsurface Flow Results

The high-resolution (1 km) steady-state depth to water table distribution across the domain is shown in Figure 4-7. The results are derived from the HydroGeoSphere calculated watertable elevation data in conjunction with the high-resolution HYDRO1K DEM. The depth to the water table data shown in Figure 4-7 was computed as the simulated watertable elevation subtracted from the high-resolution HYDRO1K DEM representing the land surface elevation, with negative values being set to zero. Overall, Figure 4-7 reflects the trend and pattern of watertable depths across the study domain: it is deep in the mountainous areas in the west and shallow in the Canadian Shield and Hudson Bay lowland regions.

Figure 4-8 exhibits the simulated steady-state near-surface hydraulic head distribution across the study domain. It can be seen that the heads are high along the Rocky Mountains and are low around Hudson Bay and the major surface water bodies. To demonstrate the 3D aspects of the subsurface flow system, two vertical cross-sectional profiles are plotted for two hydrologically and geographically representative regions, one across the Rocky Mountains (A-A') and the other passing through the Great Lakes region (B-B'). The locations of these two profiles are shown in Figure 4-8. Shown in Figure 4-9 is the steady-state hydraulic head distribution as well as a 2D flow net across the Rocky Mountains. As illustrated in Figure 4-9, the Rocky Mountains are acting as a natural water divide, with no groundwater flowing across the Rocky Mountains. It is also demonstrated by the 2D flow net that groundwater is discharging to rivers (Fraser River in this case) in mountainous areas. Similarly, the steady-state hydraulic head distribution along Great Lakes region is shown in Figure 4-10. As illustrated by the 2D flow net, water flows from high-elevation regions to low-elevation

regions and the lakes receive discharge from the groundwater regime. In general, these results demonstrate that the hydrologic model captures the overall subsurface flow patterns and the interactions between the surface water and groundwater regimes.

4.3.3 Water Budget Analysis for the Great Lakes

The Laurentian Great Lakes are a series of inter-connected lakes, which include Superior, Michigan, Huron, Erie and Ontario (see Figure 4-11), comprising the largest fresh-water hydrologic system in the world. The Great Lakes contain approximately 21% the world's (or ~84% of North America's) total surface fresh water resources. In addition, the Great Lakes are economically and socially important to both Canada and the United States. Except for Lake Michigan, which solely belongs to the USA, all other four lakes are shared by both Canada and the USA. Because of the hydrologic, economic and social importance, the Great Lakes are selected for water budget analysis as a representative example in this study.

Over a long period of time, when the change in lake water storage becomes negligible, the water balance equation for a lake can be defined as:

$$Pn + I + R + G = O \tag{4.3}$$

where Pn is the net precipitation over the lake area, I is the channel inflow from the upstream basin, R is the basin surface runoff to the lake, G is the net direct groundwater discharge to the lake, and O is the total outflow from the lake. Net basin supply (NBS) represents the net amount of water entering or exiting a lake from its drainage basin, and it is frequently used for a lake water budget analysis. Mathematically NBS is defined as:

$$NBS = Pn + R + G \tag{4.4}$$

With the substitution of Equation (4.4), Equation (4.3) can be written as:

$$NBS = O - I \tag{4.5}$$

As it is shown in Figure 4-11, Superior and Michigan are the two upstream lakes that receive zero inter-basin channel inflow. Lake Superior drains into Lake Huron through St. Marys River. Technically Lake Michigan is connected to Lake Huron and these two lakes share the same lake surface elevation. Lake Huron receives the outflow from both Lake Superior and Lake Michigan. The outflow of Lake Huron drains into Lake Erie through St. Clair River, and the outflow from Lake Erie flows to Lake Ontario through Niagara River. Note that Lake St. Clair is counted as part of Lake Erie for water budget analysis purpose.

In this study, three water budget components: total outflow, net groundwater discharge and on-lake net precipitation are firstly determined for each of the five Great Lakes. Using these three components, the remaining water budget components are computed according to Equations 4.3 – 4.5, and the results of all components are summarized in Table 4-3. As can be seen, the NBS is of the same order of magnitude for all five Great Lakes, with Lake Huron being the highest. Results also show that all five Great Lakes receive water from the subsurface regime. Simulation results reveal that the net direct groundwater discharge component accounts for about 13% or more of the NBS for the Great Lakes, with Lake Superior being the highest, 26%. This indicates that the contribution from net direct groundwater discharge is not negligible in a water budget analysis, and it should not be

ignored. As expected, Lake Superior receives the highest volume of on-lake net precipitation among the five, accounting for 36% of its NBS. For the other four lakes, ~20% of their NBS is from the on-lake net precipitation component. Approximately 38% of the NBS is from the basin overland runoff for Lake Superior, and the percentage increases to around two thirds for other four lakes. As expected, the inter-basin channel inflow and the total outflow increase from the upstream lakes (Superior and Michigan) to the downstream lakes (Huron, Erie and Ontario).

Except for Lake Michigan, the simulated outflows of all Great Lakes are compared to the streamflows measured at nearby gauging stations, and the data match reasonably well. Specifically, the simulated outflows of Lakes Superior, Huron, Erie and Ontario are 64%, 81%, 89% and 89% respectively of the measured streamflows collected at nearby gauging stations [Hunter and Croley, 1993]. Note that there is no observed streamflow data available for the outflow from Lake Michigan to Lake Huron. The underestimation of Lake Superior outflow could be due to the fact that the sub-basin boundaries are not refined in the HydroGeoSphere model which is evident in Figure 2-8. The component of net groundwater discharge is often unavailable because it is typically difficult to quantify over the entire lake area in practice. For the Great Lakes, Lake Michigan is the only one that has an estimate of relatively high confidence [Neff and Nicholas, 2005], and it is estimated to be around 2.4×10^{9} m^3/yr, approximately 56% of the HydroGeoSphere simulated value. On the basis of the above discussion as well as the reasonable agreements between the present-day simulation results and the observed data for other parts of the study domain, the water budget component results presented here is believed to be overall sensible.

4.3.4 Comments on Transient Annual Cycle Simulations

Steady-state hydrologic simulations lack the capacity to capture the effects of seasonal trends and extreme events, although the results provide useful information on the average long-term behaviour of the hydrologic system. It is acknowledged that a transient simulation, such as an annual cycle simulation, can provide much more powerful insights into the hydrologic impact of climate change. Thus, attempts were made to perform transient annual cycle for the period of 1961-2000 (present-day). In the attempted transient annual cycle simulation, 12 mean monthly net precipitation datasets based on CRCM outputs were used to drive the HydroGeoSphere model with linear temporal interpolation. Simulated hydrograph results were compared to observed data. Unfortunately, but not surprisingly, the simulated transient results overall did not provide a good match with the observed data, and thus the annual cycle results are not presented in this thesis. The unsuccessful annual cycle simulation could be due to a combination of the following reasons: (1) the grid resolution of the hydrologic model and/or the RCM is too coarse; (2) the parameter values used in the steady-state hydrologic model are inappropriate for a transient simulation; and (3) the RCM does not have a good skill for simulating accumulation and melt of snow/ice.

Table 4-1: Information on streamflow gauging stations used in this study.

ID *	Name **	GRDC Station Number	Latitude (degree)	Longitude (degree)	Years of Data	Measured Mean Annual Streamflow (m^3s^{-1})
1	Albany	4214520	51.3306	-83.8389	42	980
2	Athabasca1	4208871	58.2000	-111.3900	14	750
3	Athabasca2	4208730	56.7806	-111.4000	51	625
4	Caniapiscau	4214040	57.4300	-69.2500	46	1,291
5	Churchill(NL)	4244500	53.2478	-60.7892	59	1,745
6	Columbia1	4115201	46.1815	-123.1840	41	6,523
7	Columbia2	4115200	45.6073	-121.1734	132	5,372
8	Fraser	4207900	49.3806	-121.4514	95	2,703
9	La Grande	4214770	53.7300	-78.5700	21	1,690
10	Mackenzie1	4208025	67.4583	-133.7447	37	9,187
11	Mackenzie2	4208150	65.2739	-126.8442	65	8,539
12	Mackenzie3	4208005	61.8686	-121.3569	71	6,880
13	Niagara Falls	4236010	43.1569	-79.0472	146	5,862
14	Nelson	4213711	56.3975	-94.3694	21	3,200
15	Severn	4214440	55.3750	-88.3250	25	631
16	Slave	4208400	59.8722	-111.5833	87	3,384
17	St. Lawrence	4243151	45.4150	-73.6236	52	8,492
18	Yukon1	4103200	61.9337	-162.8829	34	6,467
19	Yukon2	4103300	64.3271	-158.7219	11	6,239
20	Yukon3	4103450	64.7405	-155.4919	29	4,488

* ID used in this study (see Figure 2-2).

** Names used in this study (see Figure 4-2 and Figure 5-2).

Table 4-2: Observed mean annual surface elevations of 10 largest lakes in study domain.

10 Largest Lakes in Study Domain	Mean Annual Surface Elevation (m)
Athabasca*	213
Erie**	173
Great Bear*	156
Great Slave*	156
Huron**	176
Michigan**	176
Ontario**	74
Reindeer*	337
Superior**	183
Winnipeg*	217

* Data are from Statistics Canada (http://www.statcan.gc.ca/tables-tableaux/sum-som/l01/cst01/phys05-eng.htm).

** Data are from U.S. Environmental Protection Agency (US EPA) (http://www.epa.gov/glnpo/atlas/gl-fact1.html).

Table 4-3: Present-day (1961-2000) simulated mean annual water budget components for the Great Lakes.

Water Budget Component		Superior	Michigan	Huron	Erie	Ontario
Total Outflow	(m^3/yr)	4.29E+10	2.81E+10	1.33E+11	1.63E+11	1.94E+11
Net Basin Supply (NBS)	(m^3/yr)	4.29E+10	2.81E+10	6.16E+10	3.00E+10	3.15E+10
Net Direct Groundwater Discharge to the Lake	(m^3/yr)	1.13E+10	4.28E+09	7.76E+09	4.32E+09	5.03E+09
	As of NBS (%)	26%	15%	13%	14%	16%
On-lake Net Precipitation	(m^3/yr)	1.53E+10	6.00E+09	1.33E+10	5.74E+09	5.69E+09
	As of NBS (%)	36%	21%	22%	19%	18%
Basin Overland Runoff	(m^3/yr)	1.63E+10	1.79E+10	4.05E+10	1.99E+10	2.08E+10
	As of NBS (%)	38%	63%	66%	66%	66%
Inter-basin Channel Inflow	(m^3/yr)	0	0	7.10E+10	1.33E+11	1.63E+11
	As of Outflow (%)	0%	0%	54%	82%	84%

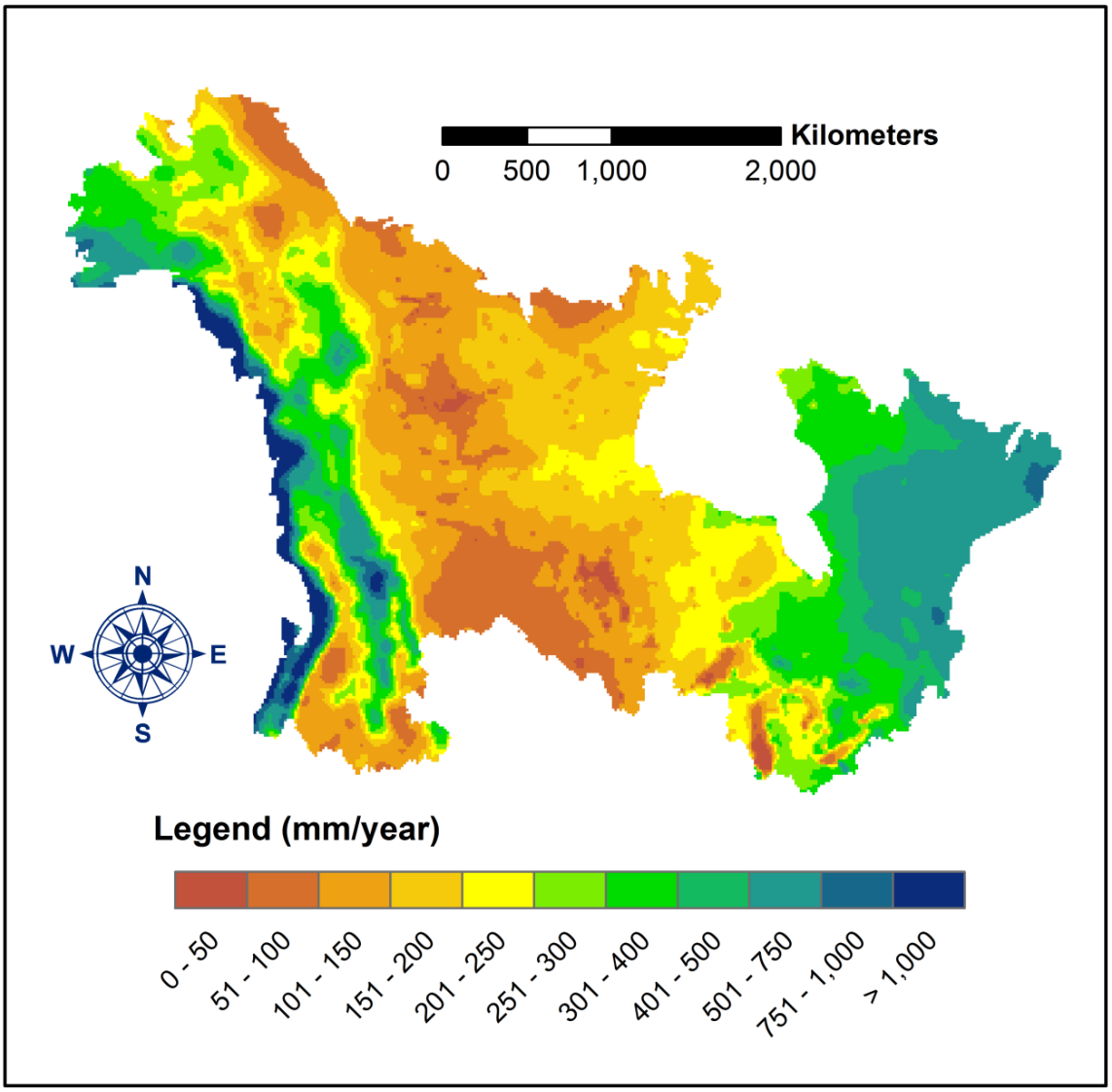

Figure 4-1: Present-day (1961-2000) mean annual net precipitation patterns (mm/year) across the study domain.

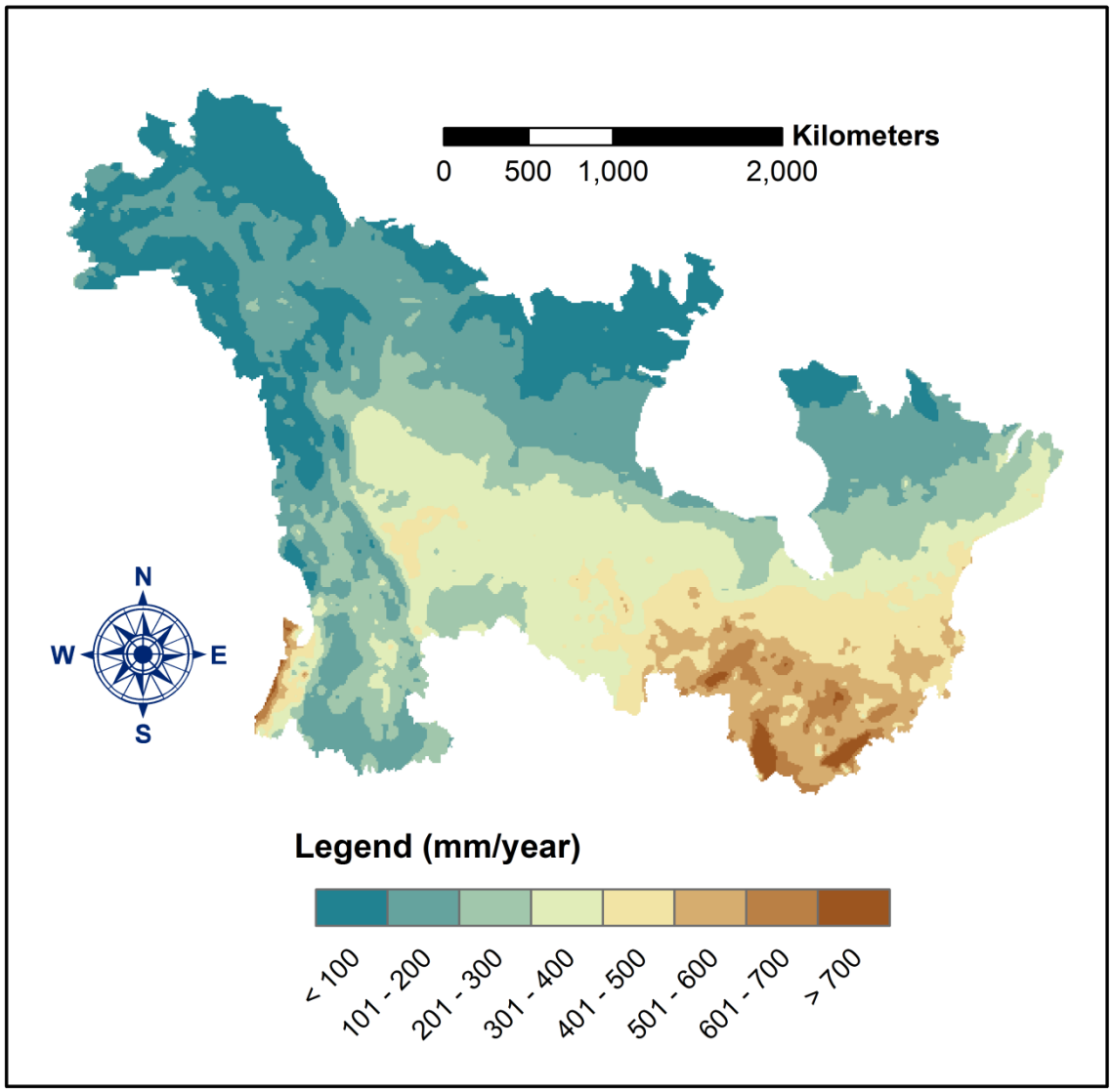

Figure 4-2: Present-day (1961-2000) mean annual actual evapotranspiration (mm/year) across the study domain.

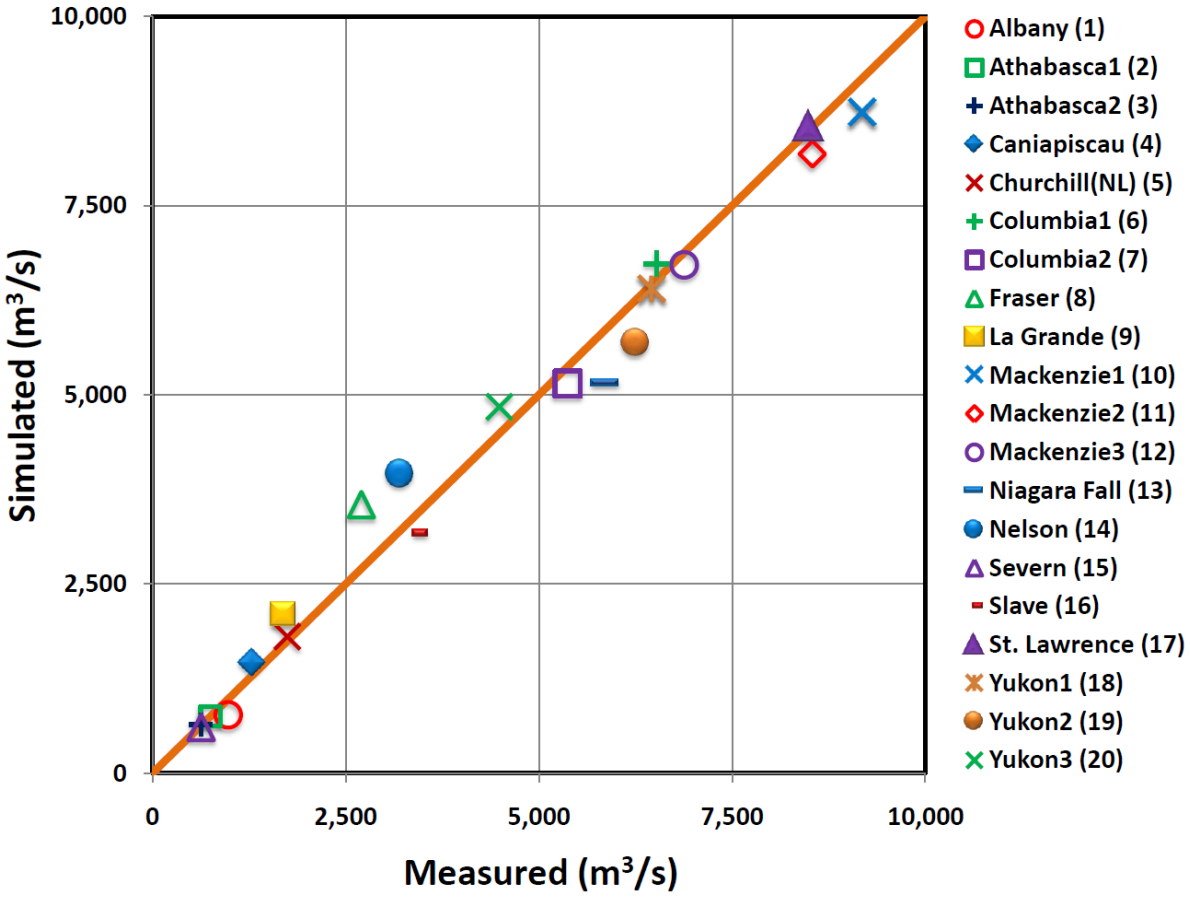

Figure 4-3: HydroGeoSphere simulated and observed present-day (1961-2000) mean annual streamflow for the major rivers in the study domain. Locations of the gauging stations can be found in Figure 2-2 according to the numbers in parentheses.

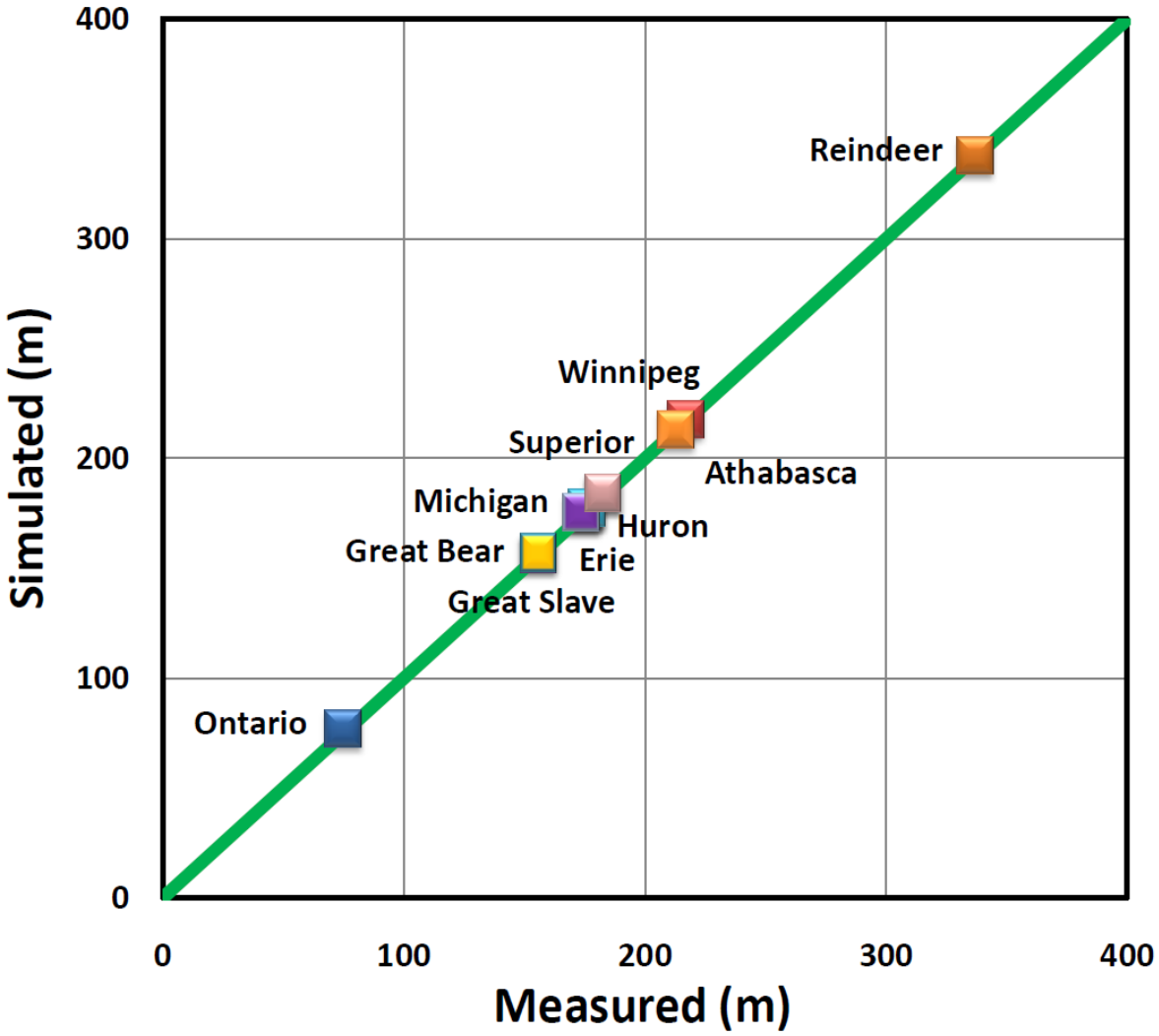

Figure 4-4: HydroGeoSphere simulated and observed present-day (1961-2000) mean annual lake surface elevations for the 10 largest lakes in the study domain. See Figure 2-2 for the location of each lake.

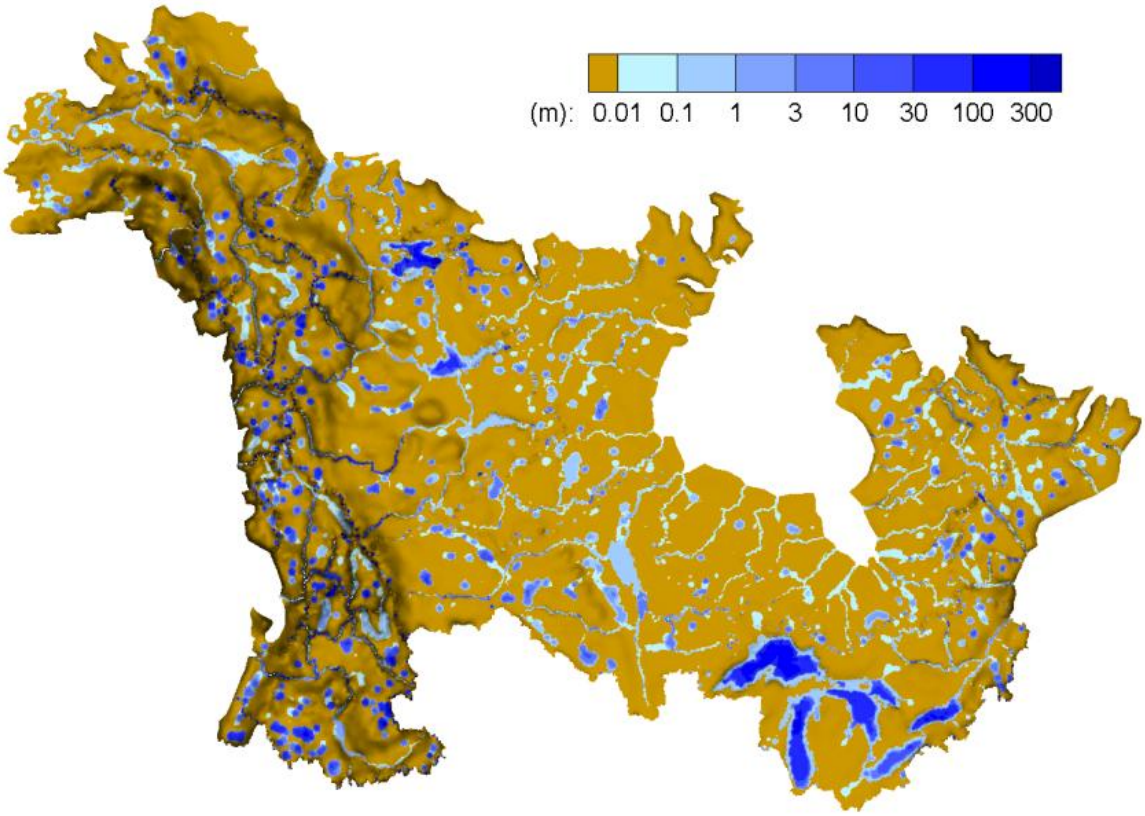

Figure 4-5: HydroGeoSphere simulated present-day (1961-2000) surface water drainage patterns and mean annual surface water depth distribution across the study domain.

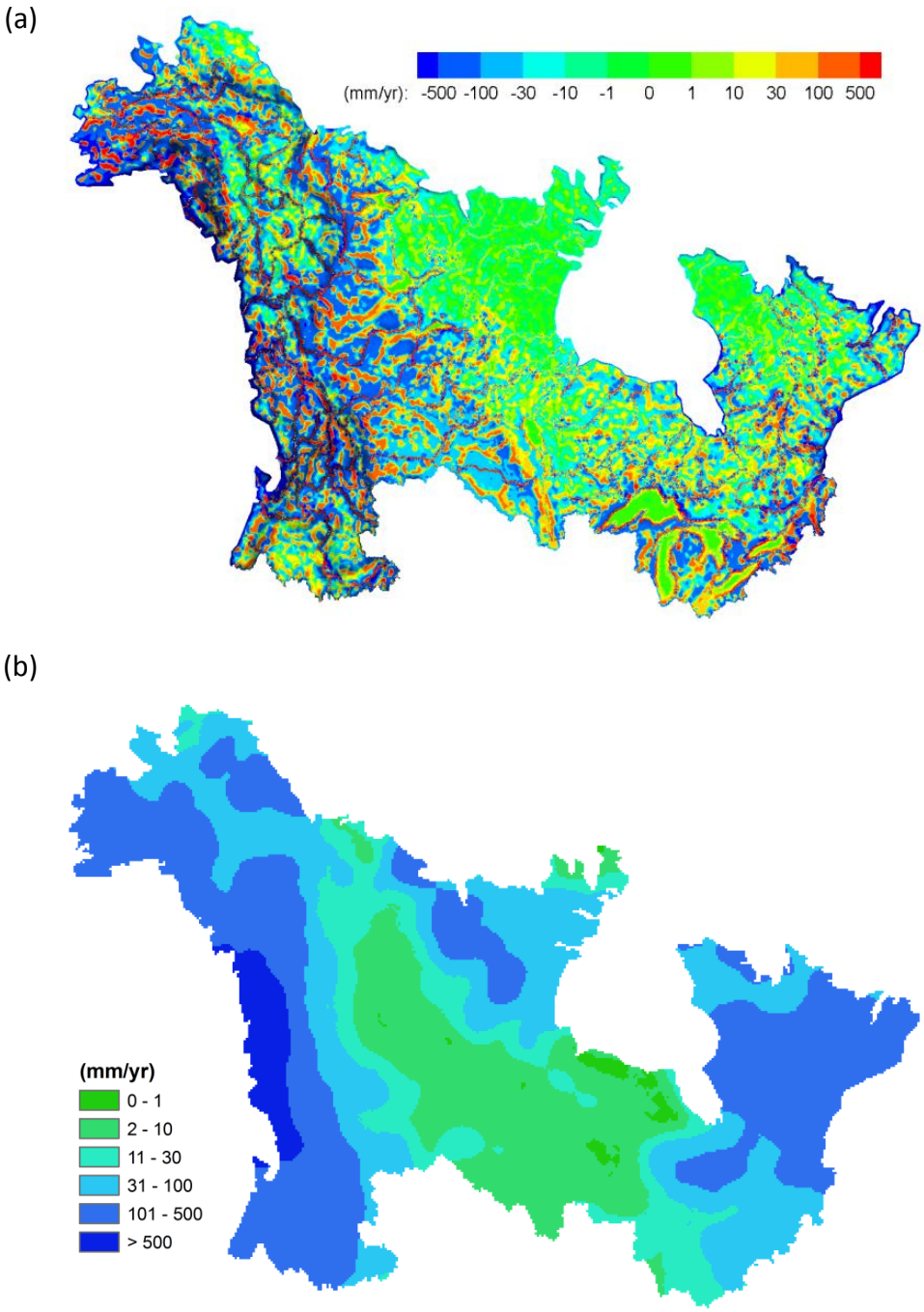

Figure 4-6: An inter-comparison of present-day (1961-2000) mean annual infiltration / exfiltration results (mm/year) across the study domain between HydroGeoSphere and CCSM3. (a) HydroGeoSphere computed infiltration (negative) / exfiltration (positive) results. (b) CCSM3 computed infiltration results.

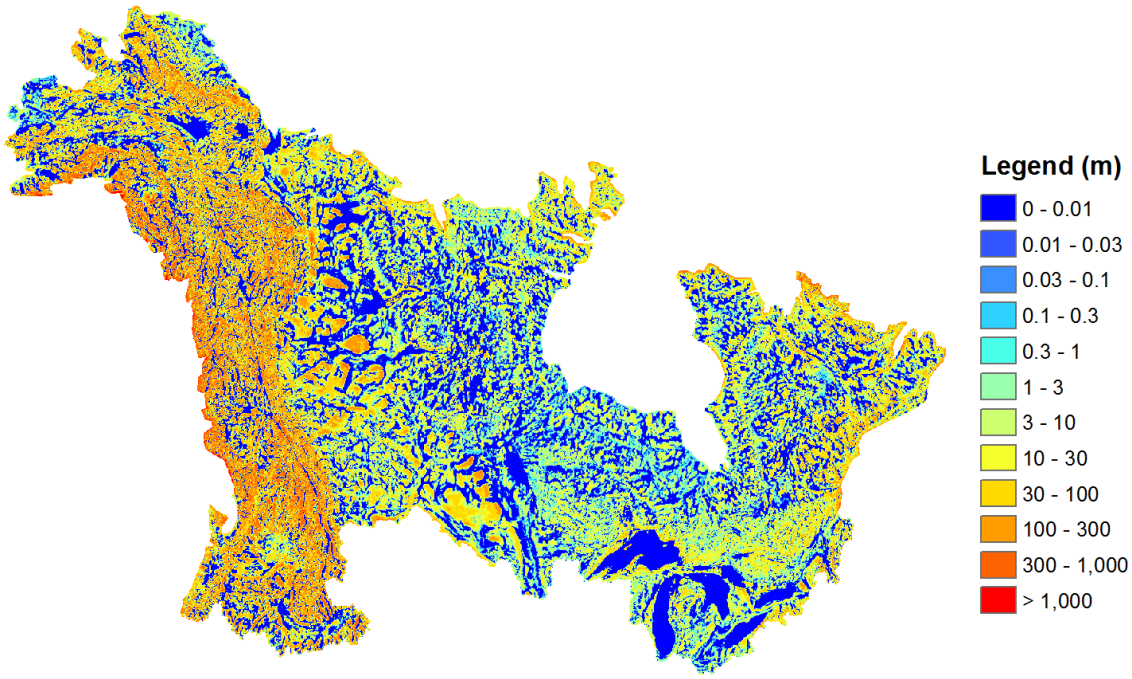

Figure 4-7: Present-day (1961-2000) mean annual depth to water table across the study domain. This map is produced using HydroGeoSphere computed watertable elevation data in conjunction with high resolution land surface elevation data.

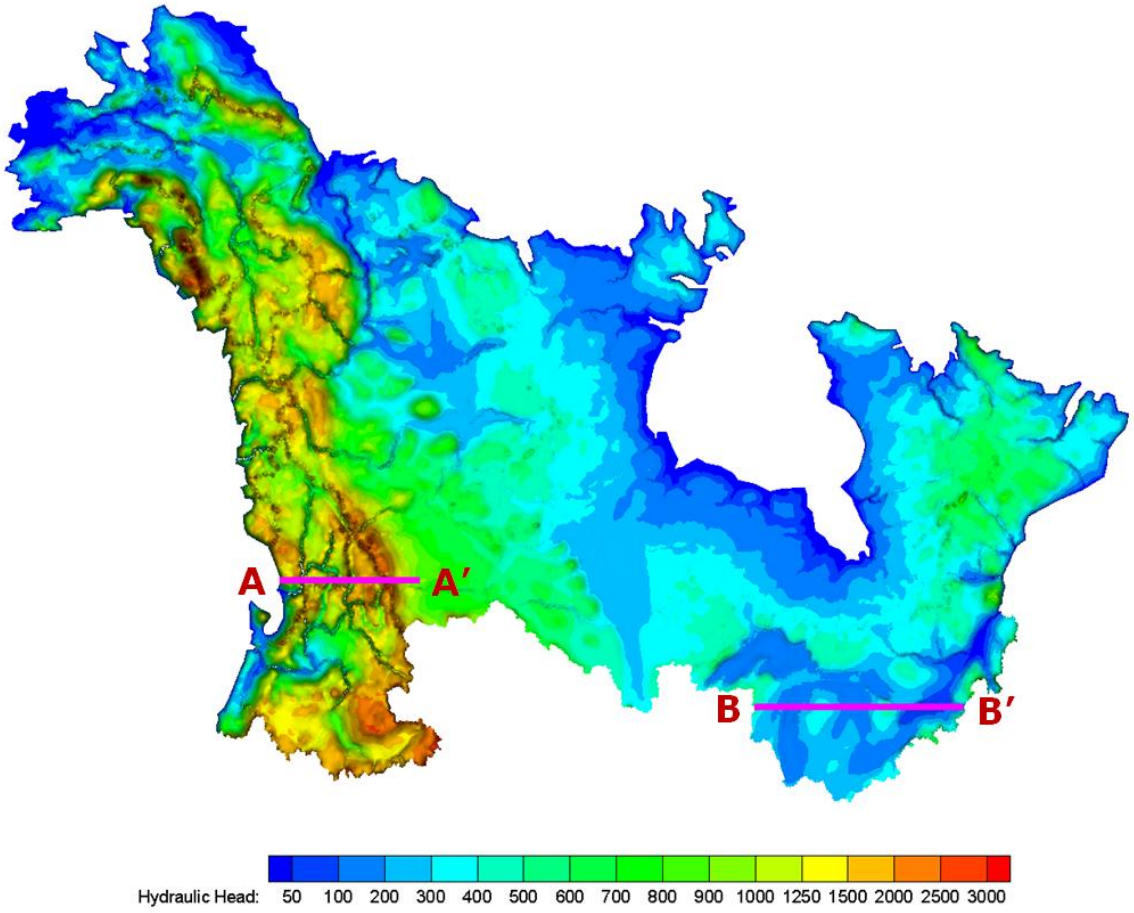

Figure 4-8: HydroGeoSphere simulated present-day (1961-2000) mean annual hydraulic head distribution on the land surface (m). A-A' and B-B' are two cross-sectional profiles shown in Figure 4-9 and Figure 4-10.

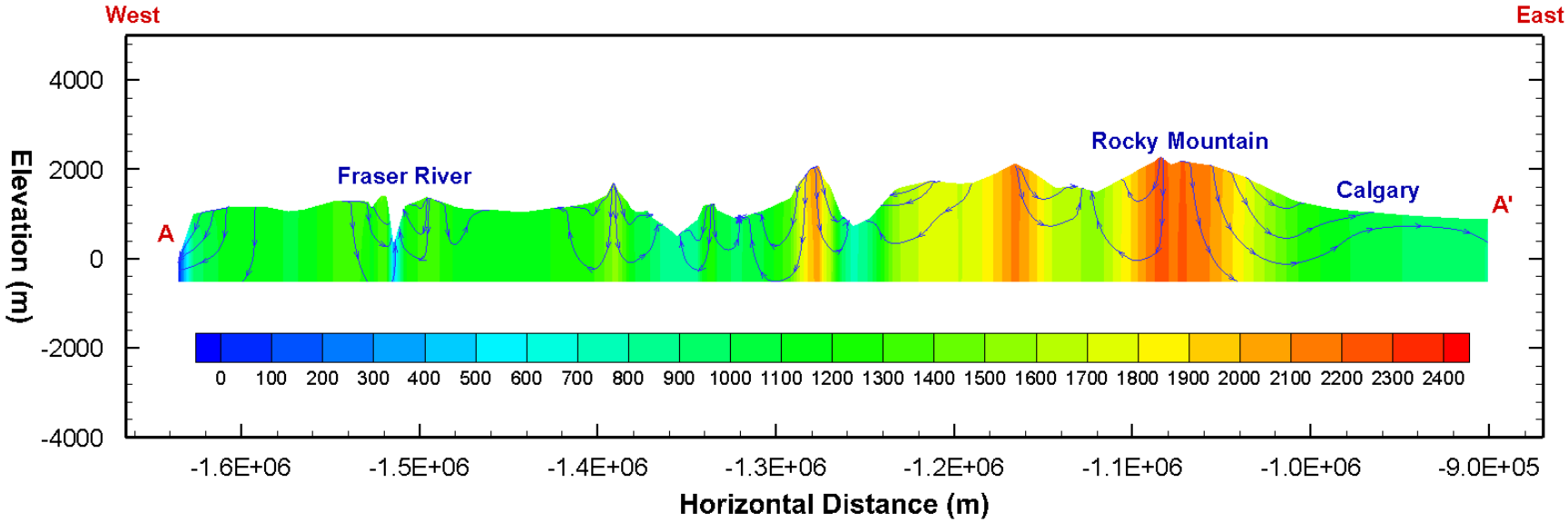

Figure 4-9: A cross-sectional view of the present-day (1961-2000) mean annual hydraulic head distribution (m) and quasi-2D flow net across the Rocky Mountain area (see Figure 4-8 for the location of A-A'). Vertical scale is exaggerated 25 times.

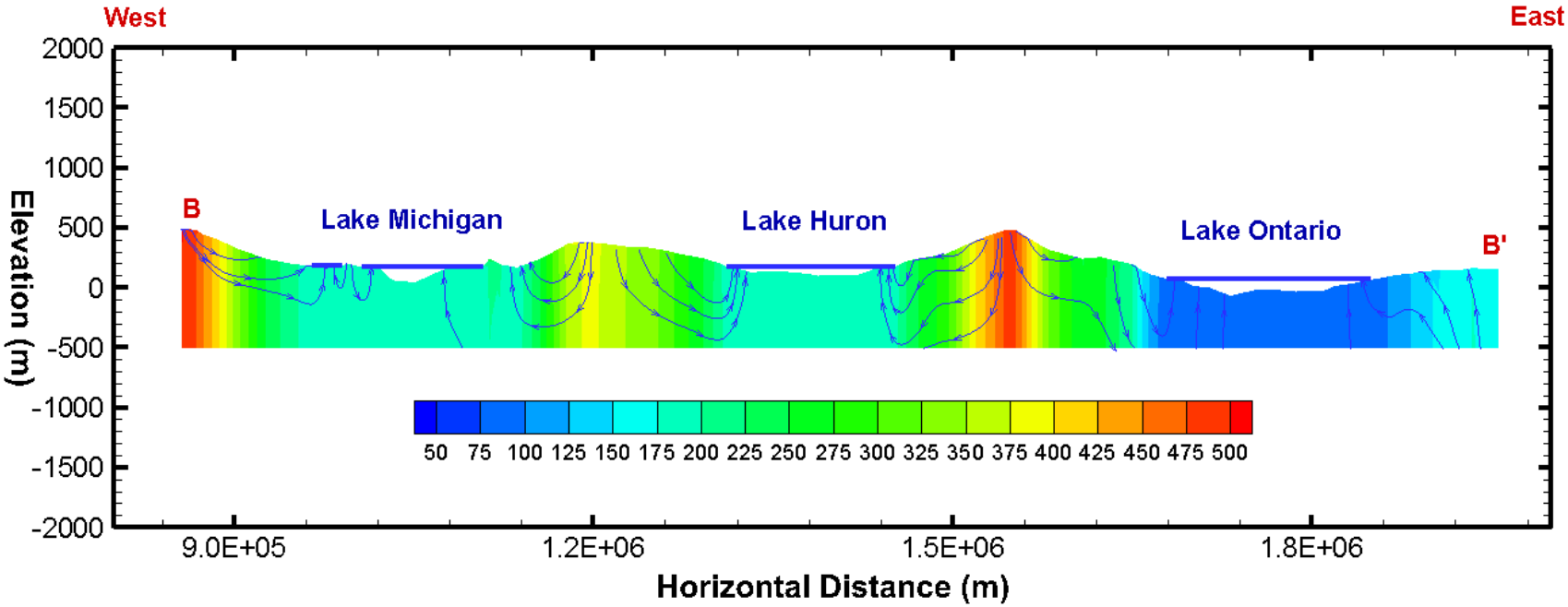

Figure 4-10: A cross-sectional view of the present-day (1961-2000) mean annual hydraulic head distribution (m) and quasi-2D flow net across the Great Lakes area (see Figure 4-8 for the location of B-B'). Vertical scale is exaggerated 50 times.

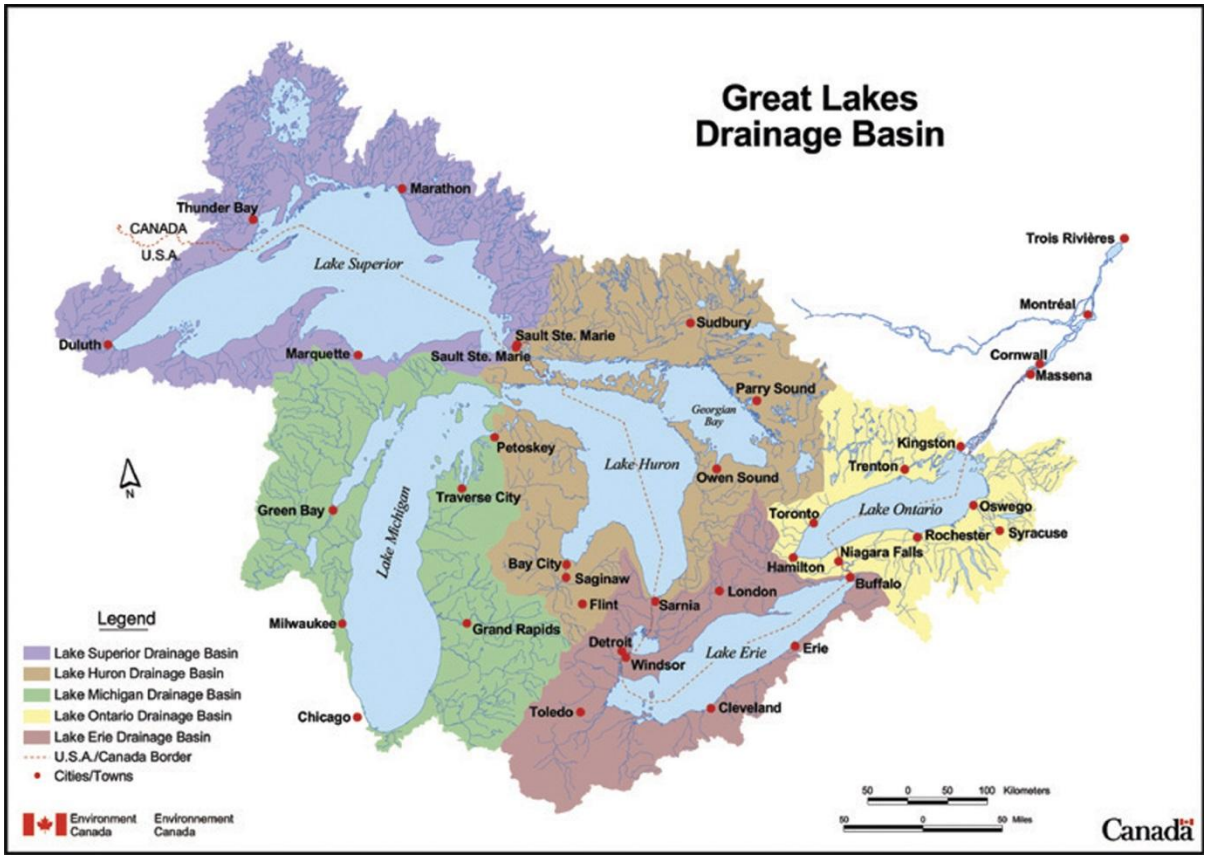

Figure 4-11: Laurentian Great Lakes and their drainage basins. This map is from Environment Canada (https://www.ec.gc.ca/grandslacs-greatlakes/).

Chapter 5
Hydrologic Impacts of Future Climate Change

5.1 Key Assumptions and Their Justifications

It is well known that topography has a profound impact on hydrology, both on the surface and the subsurface. Topography may change markedly over a long time period, e.g. tens of thousands of years, due to post-glacial rebound (also known as glacial isostatic adjustment). For example, a portion of the study domain is currently experiencing post-glacial rebound at a rate of between -5 to 13 mm/year. In other words, in the extreme case, the land surface elevation in some areas within the study domain may change up to 1.3 meter over next 100 years or so. However, such a change is not expected to have a significant influence on continental-scale hydrology. Topography may also change due to erosion or deposition, but such changes are expected to be only local and insignificant within a time period of 100 years. Thus, in this study, the land surface elevation is assumed to remain unchanged for the next 100 years.

Hydraulic conductivity is another highly influential parameter for both surface and subsurface hydrology. In general, the intrinsic permeabilities of geological formations are not expected to change substantially over a time period of 100 years, although some changes may occur at a local scale due to processes such as cementation or natural fracturing. There is, however, one possible exception to this because the effective hydraulic conductivity of permafrost may change if the climate warms significantly over the next century. In a continental-scale paleo-hydrogeologic modelling study, Lemieux et al. [2008] demonstrated

that permafrost has an immense impact on continental-scale hydrology due to its vast extent and its low hydraulic conductivity. As most climate models project the mean annual temperature will rise up to a few degrees Celsius for areas covered by permafrost by the end of this century, the spatial extent of permafrost may diminish to some degree. Most changes are likely to occur along the edges and on the land surface. It may be worth noting that the thaw of permafrost will result in a significant amount of originally frozen organic matter melting. The thawing organic materials will begin to decay and release greenhouse gases to the atmosphere. This process could lead to a global warming amplification or feedback loop. Unfortunately, projection data for the evolution of the permafrost distribution in three dimensions over the next century, to the best of my knowledge, is not available. On the basis of the above discussion, hydraulic conductivities of all geological formations, including permafrost, are assumed to be constant for the next century.

Manning's roughness coefficients, whose values describing the resistance for overland flow are in part determined by the LULC data, and are also important hydrologic parameters for transient surface runoff simulations. Values may be subject to change should land cover (e.g. vegetation) change under a changing climate. However, numerical tests performed in this work have shown that the steady-state surface and subsurface flow results were not sensitive to the choice of values for Manning's roughness coefficients. In addition, as mentioned in Chapter 3, only one value is used for the entire study domain because of the coarse resolution grid and the lack of sensitivity to this parameter for steady-state calculations. Thus, Manning's roughness coefficient is assumed unchanged for the future projections made in this study.

Global mean sea level (GMSL) rise, which is induced mainly by the thermal expansion of sea water and by the melting of land ice sheets, will undoubtedly have a profound effect on low-elevation coastal areas and islands [IPCC, 2007]. Instrumented records show that the GMSL has risen at a rate of ~3.1 mm/yr since the early 1990's and that it has risen about 3.4±0.4 mm each year between 1993 and 2009 [Nerem et al., 2010]. However, sea level change is not anticipated to have a major impact on the continental-scale hydrology under discussion here considering the predicted rate of rise. Therefore, a constant prescribed hydraulic head of 0.0 m for the coastal boundary condition is assumed for both present-day and future-time simulations.

In summary, except for net precipitation, all parameters / boundary conditions input to the hydrologic model are assumed static for modelling the hydrologic responses to future climate change in this study.

5.2 Future-Time Net Precipitation

The original meteorological outputs of climate models are not recommended for direct application as the inputs for hydrologic impact studies [Jones et al., 2004], because there is considerable discrepancy between GCM/RCM simulated present-day climate and observed data. A delta change factor approach is commonly used to adjust the meteorological projections because the differences between future and present-day simulations provided by a climate model are believed to be more reliable than the original climate model outputs [e.g. van Roosmalen et al., 2007]. This argument has an underlying assumption that the inherent model bias will be partially cancelled out in the difference values between the future and the

present. The classic delta change approach computes a delta change factor, *R*, which is the ratio between a variable, such as precipitation *P*, in the future and from a historical simulation. For example:

$$R = \frac{P_{future}}{P_{present}} \tag{5.1}$$

This factor *R* is then applied to the present-day observed data, transforming the observed data set into time series that are representative of the future climate. However, the classic method may introduce a significant amount of bias for estimating the future-time net precipitation, because the delta change factor may become unrealistically large when the net precipitation during the control period (which is a denominator in the equation) approaches 0.0 for very dry areas. To overcome this problem, a hybrid approach is used for estimating the future-time net precipitation and it is described as follows.

In this study, to account for the inter-annual variability, the mean annual net precipitation of the three 30-year time periods (2011-2040, 2041-2070 and 2071-2100) are used to assess the future climate impact. Mean annual values for the historical 30-year time period (1971-2000) are used as the control to compute the differences between present-day and future-time climate. Future-time mean annual net precipitation is determined according to Equations 5.2 to 5.4.

$$Pn_{control} = Pt_{control} - AET_{control} \tag{5.2a}$$

$$Pn_{future} = Pt_{future} - AET_{future} \tag{5.2b}$$

$$R = \min\left\{2.0, \max\left[0.5, \left(\frac{Pn_{future} - Pn_{control}}{\left|Pn_{control}\right|} + 1\right)\right]\right\} \tag{5.3}$$

$$Pn_{final} = \begin{cases} Pn_{actual} \times R & \text{if } Pn_{control} \geq 100 \text{ mm/year} \\ \max\left\{\left(Pn_{actual} + Pn_{future} - Pn_{control}\right), 0\right\} & \text{if } Pn_{control} < 100 \text{ mm/year} \end{cases} \tag{5.4}$$

where *Pn* is net precipitation, *Pt* is total precipitation, *AET* is actual evapotranspiration, *R* is the delta change factor for net precipitation, the subscript *future* represents one of the future periods (2011-2040, 2041-2070 or 2071-2100), *control* represents the control period (1971-2000), Pn_{actual} is the present-day net precipitation that is calibrated and used for the present-day (1961-2000) hydrologic simulations described in the previous Chapter, and Pn_{final} represents the final future-time net precipitation that will be used for the future hydrologic impact simulations. Note that except for Pn_{actual} and Pn_{final}, all other variables in the four equations presented above are derived directly from the original RCM outputs. Also, all variables are expressed as mean annual values. In step one, the net precipitation of the control period and future time are calculated according to Equation 5.2a and 5.2b, respectively. A delta change factor *R* is then computed using Equation 5.3. The delta change factor *R* is restricted to values between 0.5 and 2.0, in order to screen out unrealistic results. It is believed that the relative change (ratio) method is more reliable and meaningful than the absolute change when the net precipitation during the control period is sufficiently large. On the other hand, when the net precipitation during the control period approaches zero, the absolute change is believed to be more reliable than the relative change. In this work, the relative change approach is chosen when the net precipitation of the control period is equal or

greater than 100 mm/yr, and otherwise the absolute difference approach is selected. The final value of future-time net precipitation is determined according to Equation 5.4.

Figure 5-1 presents six RCM-predicted changes in the mean annual net precipitation, adjusted as described above, relative to the control period (1971-2000). Three changes for the three different future periods, namely CRCM (A2) 2011-2040, CRCM (A2) 2041-2070 and CRCM (A2) 2071-2100, were obtained using CRCM under the SRES A2 scenario. The other three projections are for the Mid-21st century (2041-2070) based on HRM (A2) 2041-2000, WRF (A2) 2041-2000 and WRF (A1B) 2041-2000 outputs. The three CRCM-based results are an indication of the long-term trend in the net precipitation over the study domain. For the Northern part of the study domain, the net precipitation is likely to keep increasing during the 21st century. In the vicinity of the Great Lakes region, the signal is mixed, projecting an increase on land but a decrease over lakes. Among the four projections for the period of 2041-2070, HRM (A2) is the wettest projection, and WRF (A2) is the driest. Once again, perhaps due to the similar total CO_2 emissions by Mid-21st century between the A2 and A1B scenarios (see Figure 3-3), the net precipitation changes based on the WRF (A2) and WRF (A1B) projections are similar.

5.3 Results and Discussions

After calibration against the available observed hydrologic information using the corrected present-day (1961-2000) net precipitation data (results are described in previous Chapter), the HydroGeoSphere model was employed to predict the potential hydrologic responses to future climate change using the adjusted future-time net precipitation data as the forcing. In

this work, the assessment of the hydrologic impact of climate change was performed using the HydroGeoSphere model for the six different climate forcing scenarios (see Figure 5-1). The hydrologic responses represent steady-state conditions during each of the three 30-year periods into which the 21st century is divided.

5.3.1 Evolution of Hydrologic Responses to Three Incremental CRCM Projections during the 21st Century

The evolution of hydrologic responses to future climates was first assessed using the adjusted CRCM projections which cover the entire 21st century. The HydroGeoSphere model was integrated to steady-state using each of the three 30-year CRCM forcings. Figure 5-2 presents the long-term evolution of streamflows for 20 representative gauging stations along major rivers over the next 90 years. Relative changes in streamflow for each gauging station for the early, mid and late 21st century are also exhibited in Figure 5-4. The results indicate that many rivers, especially those in the NW regions, are likely to have a steady increase in streamflow over the 21st century. Among them, the Yukon River is predicted to have the highest increase in streamflow, close to 40% by the end of the 21st century. Streamflow for the St. Lawrence, Columbia, Albany and Severn rivers is expected remain more or less the same as present-day (±10%) over the next 90 years. For most rivers, the trend is clear over the entire 21st century. As time progresses, the range in percentile changes in streamflow at these gauging stations becomes larger.

Presented in Figure 5-3 is the predicted evolution of the mean annual surface elevation of the 10 largest lakes in study domain based on the CRCM projections. Changes in the surface

water depths for the entire study domain are also shown in Figure 5-5. According to the simulation results, lake surface elevations are likely to rise gradually over the 21st century for the Great Bear, Great Slave, Athabasca and Reindeer lakes which are located in the northern half of the study domain. It appears that the further north the lakes are located, the higher is the increase in lake surface elevation. The Great Bear Lake is predicted to experience an increase of as much as ~7.0 cm in lake surface elevation by the late 21st century. For the Great Lakes and Lake Winnipeg, a modest decrease in the lake surface level is forecast by 2011-2040. As time moves forward to 2041-2070, the surface level of these six lakes is predicted to rise slightly, but still remain below the present-day level. By 2071-2100, except for Lake Superior, all other lakes are predicted to have higher surface elevations compared to present-day levels.

The predicted evolution of the changes in watertable elevations (m) and groundwater recharge rates (mm/yr) based on the CRCM projections over the 21st century are presented in Figure 5-7 and Figure 5-8. According to the simulation results, watertable elevation may rise along the mountainous area in the West, where the watertable depth is currently deep, from a few meters up to more than 100 m. However, for most of the central and Eastern parts of the study domain where the water table is close to the ground surface, the water table is predicted to remain essentially unchanged over the 21st century. Results for the changes in groundwater recharge rates, which are presented in Figure 5-8, show similarities to the watertable results in overall pattern. The areas where the watertable elevations increase tend to overlap with the areas predicted to receive more groundwater recharge, as expected. Similarly, regions predicted to have little change in watertable elevations are also predicted to have little change

in recharge in the future. According to the simulation results, it appears that groundwater is less sensitive to climate change than the surface water regime in large-scale context, but this may not be the case locally.

5.3.2 Hydrologic Responses to Various RCM Projections by 2041-2070

5.3.2.1 Impacts on Streamflow and Surface Water Depth

Note that all simulation results and data discussed in this sub-section are based on RCM projections for the period 2041-2070. Results for the predicted percentage change in mean annual streamflow for the 20 selected river gauging stations for the 2041-2070 are presented in Figure 5-4. In general, predicted changes in streamflow based on the four RCM forecasts share both some similarities and some differences, although the streamflows at most of the gauging stations are predicted to increase. According to HRM's forecast, streamflow at all 20 gauging stations are predicted to increase, but those based on the other three RCM projections are mixed. WRF-based (both A2 and A1B scenarios) predictions are more diverse than those based on CRCM and HRM projections. All RCM projections forecast streamflow for the Yukon, Mackenzie, Fraser, La Grande, Caniapiscau, Churchill (NL) and Slave Rivers to increase by 2041-2070. The exception is for the HRM-based simulation which forecasts an increase in streamflow for the St. Lawrence River. The WRF (A2) scenario is the only RCM projection that forecasts a decrease in streamflow for the Columbia and Athabasca Rivers. Note that the Athabasca River streamflow projection results (a decrease) based on the WRF (A2) output in this study are upheld by a high-resolution (10 km) regional climate modelling study [Erler et al., 2015] using WRF V3.4.1.

Figure 5-5 shows the absolute changes in surface-water depths across the domain. As illustrated in Figure 5-5, the changes in surface water depths are negligible for most of the study domain except for the lakes and rivers. All four RCM projections for 2041-2070 produce an increase in surface-water depths over the Northern half of the simulation domain, but signals are mixed for the Southern half. The HRM-based (A2) results predict that four of the five Great Lakes may experience an increase in water depth, but the other three RCM outputs forecast a decrease in water depth, from a couple of cm to up to 10 cm, for all the five Great Lakes.

Exhibited in Figure 5-6 are predicted changes in lake surface elevation for the 10 largest lakes within the study domain by 2041-2070 based on the four RCM projections. The figure reveals that the changes in lake surface elevation for the lakes located in the North are generally similar among the simulations based on these four RCM projections. However, the predicted changes in lake level for the Great Lakes by the HRM projection are very different than those based on the other three forcings. In particular, the differences are drastic if compared to the two WRF projections. HRM output forecasts a rise in lake surface elevation for all the Great Lakes, ranging from 4.0 to 8.6 cm, except for Lake Superior with a decline of 0.5 cm. On the other hand, the remaining three RCM outputs all project a decline in the lake level for all of the five Great Lakes. In particular, based on the two WRF (A2 and A1B) projections, the lake levels of the Great Lakes are expected to decrease 4.0-10.0 cm by 2041-2070. Compared to the two WRF projections, the CRCM projection forecasts only a modest decline of 1.0-2.0 cm in lake surface elevation for the Great Lakes. The substantial different results of the changes in lake level between the HRM and the other three RCM-based

simulations may be explained by the projected changes in net precipitation shown in Figure 5-1. As can be seen, two WRF outputs forecast a significant decrease in net precipitation by 2041-2070 for the most part of the Great Lakes Basin, with only a small portion of land between the Great Lakes receiving more net precipitation. However, HRM projects a smaller area receiving less net precipitation and a larger area receiving more net precipitation compared to the WRF projections. The CRCM-based changes in net precipitation for the Great Lakes region are in between the HRM and the two WRF projections. The causes for the drastically different predictions of lake surface level changes for the Great Lakes based on different RCM projections will be further discussed in the following water budget analysis.

5.3.2.2 Impacts on Water Budget Components for the Great Lakes

A detailed breakdown analysis of the change in each water budget component for the Great Lakes is performed in this study. Predicted changes in each water budget component for the Great Lakes by 2041-2070 based on four RCM projections are summarized in Table 5-1.

CRCM (A2) 2041-2070 Projection:

Based on the CRCM (A2) projection, both the total outflow and the NBS of the Great Lakes are predicted to decrease 3-6% by 2041-2070. The inter-basin channel inflow is predicted to decrease 3-4% for the three downstream Great Lakes that receive channel inflow from the upstream lakes. The net direct groundwater discharge is predicted to decrease no more than 3% for all Great Lakes, with Lake Ontario predicted to essentially remain unchanged. Net groundwater discharge contributes approximately 10% of the NBS change. The predicted

changes in basin runoff are within ±3% of the present-day values for the Great Lakes by 2041-2070, and Lake Huron is the only lake that is predicted to receive more basin runoff. Except for Lake Superior, changes in basin runoff have a significant influence on the NBS change. According to the results, changes in basin runoff account for 22-39% of the NBS change for Lakes Michigan, Ontario and Erie, but it accounts for -70% of the NBS change for Lake Huron. Based on the CRCM projection, on-lake net precipitation is predicted to have the largest percentile change among all water budget components, decreasing between 8% (Superior) and 19% (Michigan). Relatively, the change in on-lake net precipitation is also the largest contributor for the NBS change based on CRCM (A2) projection.

HRM (A2) 2041-2070 Projection:

Similar to the results for lake level changes, the HRM projection also forecasts significant changes in the total outflow for the Great Lakes except for Lake Superior by 2041-2070. The total outflow is predicted to decrease by about 1% for Lake Superior, and it is predicted to increase between 13% (Huron) and 26% (Michigan) for the other four Great Lakes. The inter-basin channel inflow is forecasted to increase between 9% (Huron) and 14% (Ontario) for the three downstream Great Lakes. Similar to the results for the changes in total outflow, the NBS is projected to decrease by about 1% for Lake Superior, but increase between 17% (Huron) and 26% (Michigan) for the other four Great Lakes. The predicted changes in net direct groundwater discharge are within ±5%, with Lake Superior being the only one expected to receive less contribution (-2%) from groundwater discharge by 2041-2070. Groundwater discharge accounts for 36% of the NBS change for Lake Superior, but less than

5% for the other four lakes. As for the on-lake net precipitation component, Lake Superior is the only one predicted to have a decrease of 14%, and the other four are predicted to have an increase of between 7% (Huron) and 21% (Ontario) by 2041-2070. On-lake net precipitation appears to be the dominant component contributing to the NBS change for Lake Superior, 340%, but it only contributes between 8% (Huron) and 20% (Ontario) to the NBS change for the other four Great Lakes, less than the basin runoff component's contribution. Based on the HRM projection, all Great Lakes are predicted to receive 10-32% more basin runoff. Lake Superior is predicted to receive 10% more basin runoff, although it is forecasted to have a decrease in lake surface elevation and NBS. For the other four Great Lakes, basin runoff appears to be the dominant contributor for the NBS change, accounting for between 76% (Ontario) and 91% (Huron) of the NBS change.

WRF (A2) 2041-2070 Projection:

The WRF (A2) projection forecasts a decrease of between 11% (Michigan) and 24% (Superior) in total outflow for the Great Lakes. Similar percentile changes of between 14% (Ontario) and 19% (Huron) in inter-basin channel inflow are predicted for the three downstream Great Lakes. NBS is also predicted to decrease for all five Great Lakes, with Lake Superior having the largest percentile decrease of 24% and Lake Erie having the smallest decrease of 5%. The net direct groundwater discharge is predicted to decrease between 1% (Ontario) and 7% (Superior) for all Great Lakes according to the WRF (A2) projection, and it accounts for between 2% (Ontario) and 9% (Erie) of the NBS change. On-lake net precipitation is projected to significantly decrease for the Great Lakes by 2041-2070,

ranging from 27% (Ontario) to 61% (Michigan). Results show that changes in on-lake net precipitation account for between 65% (Ontario) and 119% (Erie) of the NBS change. Signs (increase or decrease) for the predicted changes in basin runoff are mixed for the Great Lakes, with Lakes Superior, Huron and Ontario having a decrease and Lakes Michigan and Erie having an increase. The percentile changes in basin runoff are predicted to be between -10% (Superior) and 3% (Michigan) by 2041-2070. Basin runoff is estimated to contribute between -27% (Erie) and 33% (Ontario) of the NBS change.

WRF (A1B) 2041-2070 Projection:

The predicted changes in water budget components for the Great Lakes are overall similar between the two WRF (A1B and A2) projections, despite some differences. One of the main differences lies in the predicted change in basin runoff for Lake Erie. The WRF (A1B) projection forecasts a decrease of 15%, but an increase of 2% is predicted based on the WRF (A2) projection. As a result, the NBS of Lake Erie is predicted to decrease by 18% based on the A1B projection but only 5% based on the A2 projection. The other two main differences are from the Lake Superior results. Based on the A1B projection, the basin runoff is predicted to decrease by about 1%, but it may decrease by ~10% if based on the A2 forcing. Also, the net direct groundwater discharge is forecasted to remain essentially unchanged for Lake Superior according the A1B projection, but the A2 projection forecasts a decrease of 7% in net direct groundwater discharge.

Summary of All Four RCM Projections:

In all four cases, the predicted changes in lake level are strongly correlated to the changes in total outflow, and the strong correlation is generally expected for open-basin lakes. Results of all four cases show that the changes in net groundwater discharge are usually less significant, in terms of both percentage change and absolute change, compared to the changes in basin runoff and on-lake net precipitation. The changes in net groundwater discharge generally account for less than 10% of the NBS change. However, it should be particularly noted that the predicted changes in net groundwater discharge consistently bear the same sign as the changes in NBS for all Great Lakes based on all four projections. Results also reveal that the percentage changes in total outflow are similar to the changes in NBS and inter-basin channel inflow (if applicable) in an average sense among the four projections. Except for the HRM case, the changes in on-lake net precipitation appear to be the primary water budget component dictating the changes in NBS for the Great Lakes. For the HRM case, basin runoff seems to be the main contributor to the changes in NBS.

Overall, as noted for the results of changes in lake levels, the predicted changes in water budget components are also drastically different between the HRM and the two WRF projections. Frequently, HRM-based predictions have a different sign than that of the WRF-based predictions. The CRCM-based projections generally carry the same signs as the predictions based on the two WRF projections, although predicted changes based on the WRF outputs are often larger in magnitude than the CRCM-based results. The HRM-based predictions, e.g. an increase in on-lake net precipitation for four of the five Great Lakes by 2041-2070, appear to be counter-intuitive and questionable, given the fact that HRM does not

explicitly couple a lake model to capture the strong lake effect on regional climate over the Great Lakes region.

5.3.2.3 Impacts on Watertable Depth and Groundwater Recharge

Results for predicted absolute changes in watertable elevation by 2041-2070 are presented in Figure 5-7. In general, watertable elevations remains relatively unchanged, within ±1.0 cm, for the regions surrounding Hudson Bay, but more significant changes in watertable elevations, mainly ranging from ±0.3 m to ±30 m, are expected in the Prairie, Rocky Mountain and Alaska regions. Based on the outputs from CRCM (A2), WRF (A2) and WRF (A1B), the watertable elevation is projected to decrease from tens of centimeters to a few meters for most of the Prairie region. On the other hand, the HRM (A2) output leads to an increase in watertable elevations in general for the Prairie region. Results for absolute changes in the rate of groundwater recharge based on four RCM projections for the period 2041-2070 are presented in Figure 5-8. In general, changes in the rate of groundwater recharge are strongly correlated with the changes in the watertable elevations. Regions with a rising (or declining) water table usually have an increase (or decrease) in groundwater recharge as well. Changes in the rate of groundwater recharge are also highly correlated with the depth to the water table. Regions with a shallow (or deep) water table generally experience smaller (or larger) changes in recharge.

5.3.3 Sensitivity/Uncertainty Analysis

The standard deviations of the percentage change in streamflow, the absolute change in surface-water depth and watertable elevation obtained from the various RCM projections are

summarized in Table 5-2. Overall, the inter-model deviations are more significant than the inter-scenario deviations. Among the three projections performed under the A2 scenario, the CRCM scenario has the highest degree of agreement with the WRF (A2) case, and the predictions based on the HRM output are least similar to those based on the WRF (A2) output. These results indicate that the hydrologic responses to future climate change are more sensitive to the choice of climate model than to the differences between the various emission scenarios. However, it should be emphasized that the difference between the SRES A2 and A1B scenarios is relatively minor during the first half of the 21st century although the differences gradually increase towards the late 21st century. Thus, the inter-scenario deviation may be underestimated in this study. It is acknowledged that standard deviation analyses are ideally performed based on a large number of samples. Unfortunately, due to data availability limitations, only four RCM projections are available for use in this study. Thus, the conclusions drawn from the standard deviation analyses that are based on these four cases are subject to some uncertainty. A more reliable conclusion on the sensitivity/uncertainty of hydrologic responses to climate change will eventually be drawn when more RCM projections become available.

Table 5-1: Predicted changes in water budget components for the Great Lakes by 2041-2070 based on four RCM future projections. (a) CRCM (A2); (b) HRM (A2); (c) WRF (A2) and (d) WRF (A1B).

(a) CRCM (A2)

Changes in Water Budget Components		Superior	Michigan	Huron	Erie	Ontario
Change in lake surface elevation	Absolute (cm)	-0.95	-2.10	-1.90	-1.01	-1.88
Change in total outflow	Relative (%)	-3%	-6%	-3%	-3%	-3%
	Absolute (m^3/yr)	-1.25E+09	-1.66E+09	-4.10E+09	-5.40E+09	-6.52E+09
Change in inter-basin channel inflow	Relative (%)	N/A	N/A	-4%	-3%	-3%
	Absolute (m^3/yr)	N/A	N/A	-2.91E+09	-4.10E+09	-5.40E+09
	As of outflow change (%)	N/A	N/A	71%	76%	83%
Change in net basin supply (NBS)	Relative (%)	-3%	-6%	-2%	-4%	-4%
	Absolute (m^3/yr)	-1.25E+09	-1.66E+09	-1.19E+09	-1.30E+09	-1.12E+09
	As of outflow change (%)	100%	100%	29%	24%	17%
Change in net direct GW discharge	Relative (%)	-1%	-3%	-1%	-3%	0%
	Absolute (m^3/yr)	-1.36E+08	-1.49E+08	-7.10E+07	-1.39E+08	8.00E+04
	As of NBS change (%)	11%	9%	6%	11%	0%
Change in on-lake net precipitation	Relative (%)	-8%	-19%	-15%	-11%	-13%
	Absolute (m^3/yr)	-1.16E+09	-1.14E+09	-1.95E+09	-6.54E+08	-7.63E+08
	As of NBS change (%)	93%	69%	164%	50%	68%
Change in basin runoff	Relative (%)	0%	-2%	2%	-3%	-2%
	Absolute (m^3/yr)	4.57E+07	-3.70E+08	8.31E+08	-5.05E+08	-3.58E+08
	As of NBS change (%)	-4%	22%	-70%	39%	32%

(b) HRM (A2)

Changes in Water Budget Components		Superior	Michigan	Huron	Erie	Ontario
Change in lake surface elevation	Absolute (cm)	-0.46	8.60	7.85	4.06	7.96
Change in total outflow	Relative (%)	-1%	26%	13%	14%	15%
	Absolute (m^3/yr)	-6.17E+08	7.19E+09	1.73E+10	2.32E+10	2.92E+10
Change in inter-basin channel inflow	Relative (%)	N/A	N/A	9%	13%	14%
	Absolute (m^3/yr)	N/A	N/A	6.57E+09	1.73E+10	2.32E+10
	As of outflow change (%)	N/A	N/A	38%	75%	79%
Change in net basin supply (NBS)	Relative (%)	-1%	26%	17%	20%	19%
	Absolute (m^3/yr)	-6.17E+08	7.19E+09	1.07E+10	5.91E+09	6.01E+09
	As of outflow change (%)	100%	100%	62%	25%	21%
Change in net direct GW discharge	Relative (%)	-2%	5%	1%	0%	5%
	Absolute (m^3/yr)	-2.20E+08	1.96E+08	4.41E+07	1.16E+07	2.32E+08
	As of NBS change (%)	36%	3%	0%	0%	4%
Change in on-lake net precipitation	Relative (%)	-14%	20%	7%	20%	21%
	Absolute (m^3/yr)	-2.10E+09	1.21E+09	8.74E+08	1.15E+09	1.19E+09
	As of NBS change (%)	340%	17%	8%	19%	20%
Change in basin runoff	Relative (%)	10%	32%	24%	24%	22%
	Absolute (m^3/yr)	1.70E+09	5.78E+09	9.80E+09	4.75E+09	4.59E+09
	As of NBS change (%)	-276%	80%	91%	80%	76%

(c) WRF (A2)

Changes in Water Budget Components		Superior	Michigan	Huron	Erie	Ontario
Change in lake surface elevation	Absolute (cm)	-8.21	-9.03	-9.80	-4.14	-7.34
Change in total outflow	Relative (%)	-24%	-11%	-16%	-14%	-13%
	Absolute (m^3/yr)	-1.03E+10	-3.19E+09	-2.08E+10	-2.23E+10	-2.46E+10
Change in inter-basin channel inflow	Relative (%)	N/A	N/A	-19%	-16%	-14%
	Absolute (m^3/yr)	N/A	N/A	-1.35E+10	-2.08E+10	-2.23E+10
	As of outflow change (%)	N/A	N/A	65%	93%	90%
Change in net basin supply (NBS)	Relative (%)	-24%	-11%	-12%	-5%	-7%
	Absolute (m^3/yr)	-1.03E+10	-3.19E+09	-7.29E+09	-1.48E+09	-2.35E+09
	As of outflow change (%)	100%	100%	35%	7%	10%
Change in net direct GW discharge	Relative (%)	-7%	-3%	-3%	-3%	-1%
	Absolute (m^3/yr)	-7.73E+08	-1.37E+08	-2.00E+08	-1.29E+08	-4.69E+07
	As of NBS change (%)	7%	4%	3%	9%	2%
Change in on-lake net precipitation	Relative (%)	-51%	-61%	-47%	-31%	-27%
	Absolute (m^3/yr)	-7.86E+09	-3.65E+09	-6.26E+09	-1.76E+09	-1.52E+09
	As of NBS change (%)	76%	114%	86%	119%	65%
Change in basin runoff	Relative (%)	-10%	3%	-2%	2%	-4%
	Absolute (m^3/yr)	-1.69E+09	5.90E+08	-8.35E+08	4.05E+08	-7.81E+08
	As of NBS change (%)	16%	-18%	11%	-27%	33%

(d) WRF (A1B)

Changes in Water Budget Components		Superior	Michigan	Huron	Erie	Ontario
Change in lake surface elevation	Absolute (cm)	-4.96	-8.15	-8.59	-4.39	-8.37
Change in total outflow	Relative (%)	-15%	-12%	-14%	-15%	-14%
	Absolute (m^3/yr)	-6.39E+09	-3.43E+09	-1.83E+10	-2.38E+10	-2.81E+10
Change in inter-basin channel inflow	Relative (%)	N/A	N/A	-14%	-14%	-15%
	Absolute (m^3/yr)	N/A	N/A	-9.82E+09	-1.83E+10	-2.38E+10
	As of outflow change (%)	N/A	N/A	54%	77%	85%
Change in net basin supply (NBS)	Relative (%)	-15%	-12%	-14%	-18%	-14%
	Absolute (m^3/yr)	-6.39E+09	-3.43E+09	-8.45E+09	-5.53E+09	-4.26E+09
	As of outflow change (%)	100%	100%	46%	23%	15%
Change in net direct groundwater discharge	Relative (%)	0%	-3%	-4%	-8%	-3%
	Absolute (m^3/yr)	-4.88E+07	-1.39E+08	-2.81E+08	-3.65E+08	-1.34E+08
	As of NBS change (%)	1%	4%	3%	7%	3%
Change in on-lake net precipitation	Relative (%)	-40%	-58%	-49%	-38%	-32%
	Absolute (m^3/yr)	-6.18E+09	-3.45E+09	-6.49E+09	-2.17E+09	-1.84E+09
	As of NBS change (%)	97%	101%	77%	39%	43%
Change in basin runoff	Relative (%)	-1%	1%	-4%	-15%	-11%
	Absolute (m^3/yr)	-1.58E+08	1.64E+08	-1.68E+09	-3.00E+09	-2.28E+09
	As of NBS change (%)	2%	-5%	20%	54%	54%

Table 5-2: Standard deviation of hydrologic responses to the differences between RCMs and SRES scenarios. All data are for the future 2041-2070 period.

RCM outputs	Change in streamflow* (%)	Change in SW depth** (mm)	Change in WT elevation** (m)
CRCM (A2); HRM (A2)	7.4	5.9	0.52
HRM (A2); WRF (A2)	10.2	7.3	0.63
CRCM (A2); WRF (A2)	4.7	3.8	0.41
CRCM (A2); HRM (A2); WRF (A2)	8.2	6.5	0.62
WRF (A2); WRF (A1B)	2.9	1.6	0.19

*Average value of the 20 selected river gauging stations.

**Average value of all surficial nodes.

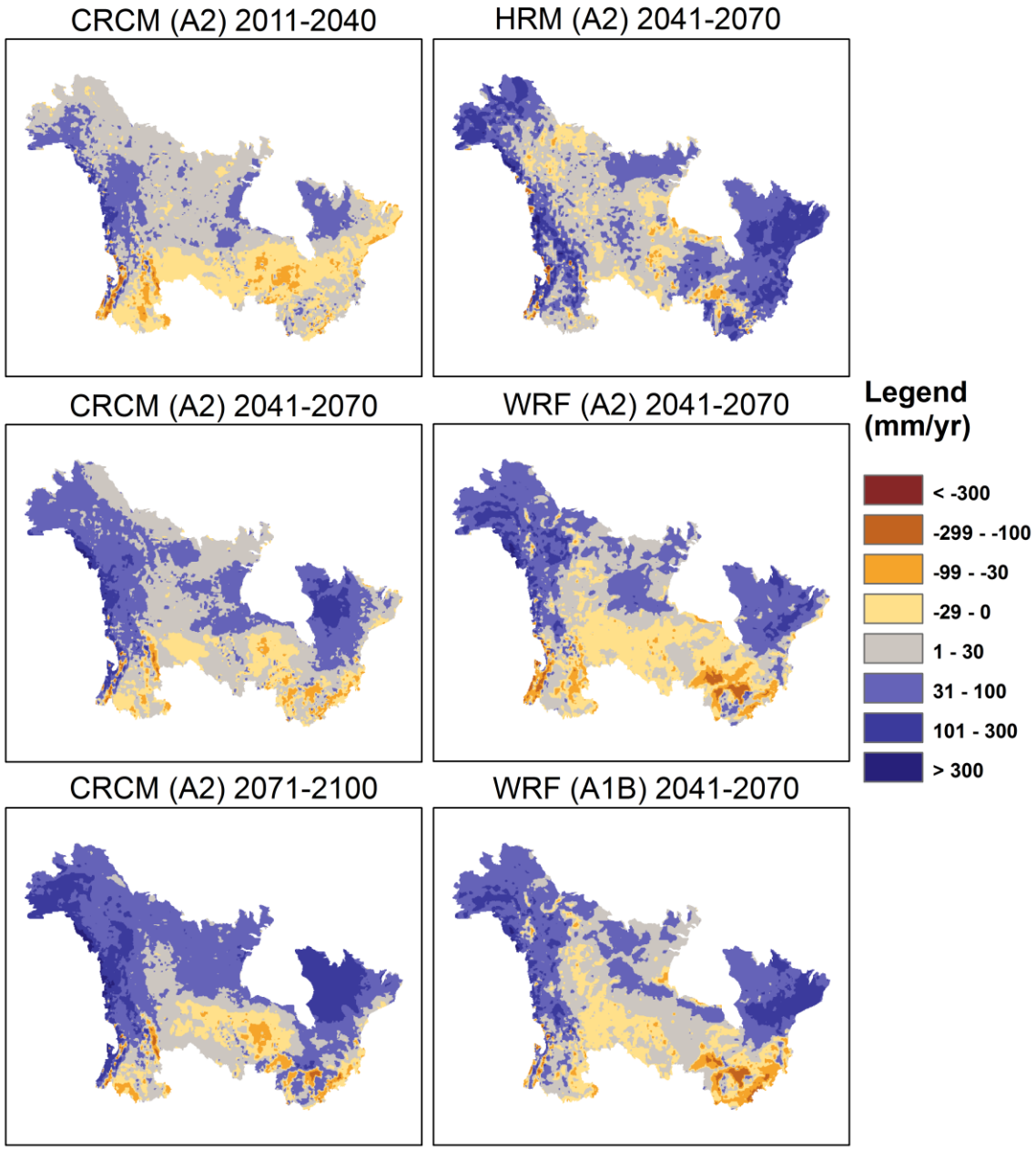

Figure 5-1: RCM based changes in mean annual net precipitation (mm/year) during the 21st century. Data are adjusted using the hybrid method described in this Chapter.

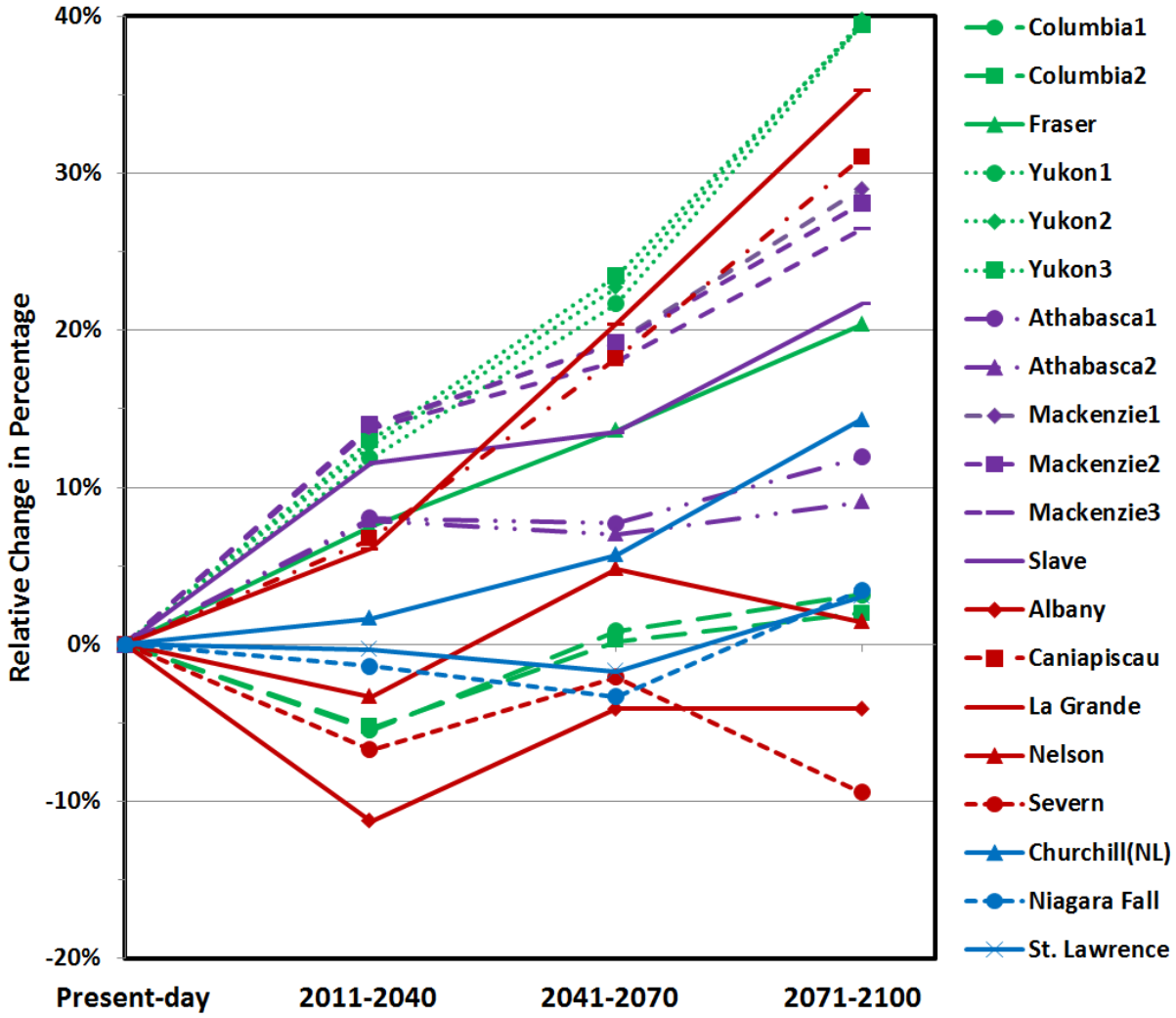

Figure 5-2: Predicted percentile changes in mean annual streamflow relative to present-day values based on CRCM (A2) projections. Further information of each gauging station can be found in Figure 2-2 and Table 4-1.

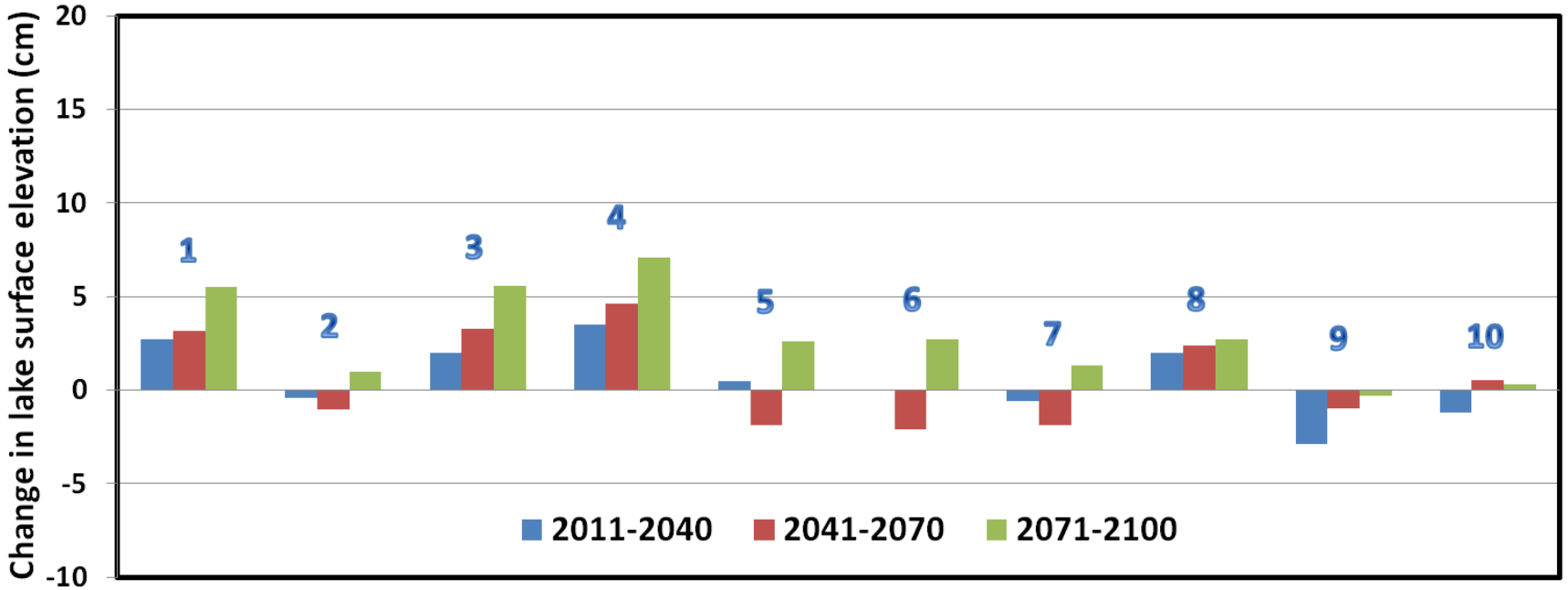

Figure 5-3: Predicted change in major lake surface elevations (cm) over the 21st century based on CRCM (A2) projections. Numbers on top of the bars denote the 10 largest lakes within the study domain as follows. 1: Athabasca; 2: Erie; 3: Great Bear; 4: Great Slave; 5: Huron; 6: Michigan; 7: Ontario; 8: Reindeer; 9: Superior; 10: Winnipeg.

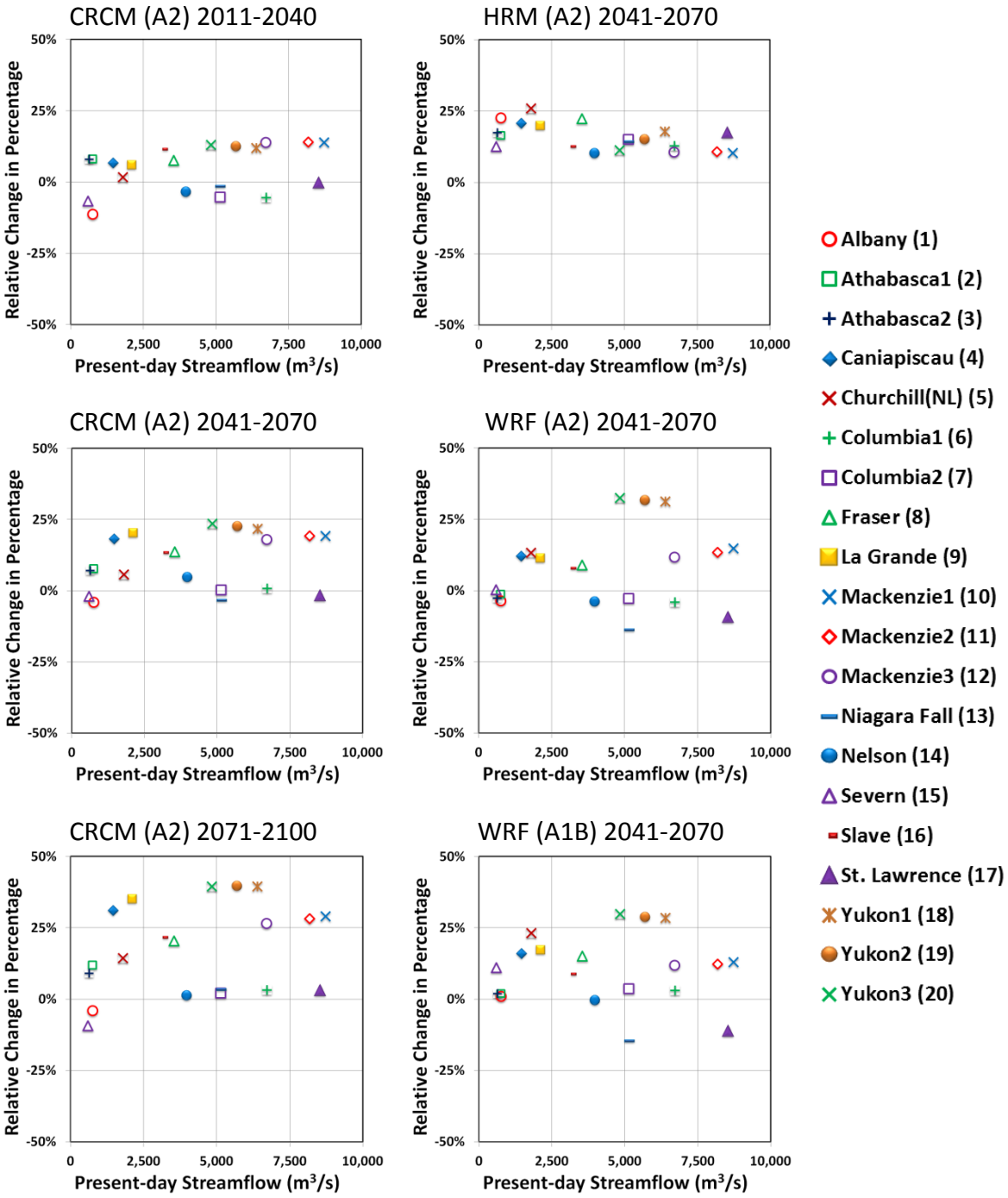

Figure 5-4: Predicted relative change in mean annual streamflow based on RCM future climate projections. Refer to Figure 2-2 for the location of each gauging station based on the number in parentheses.

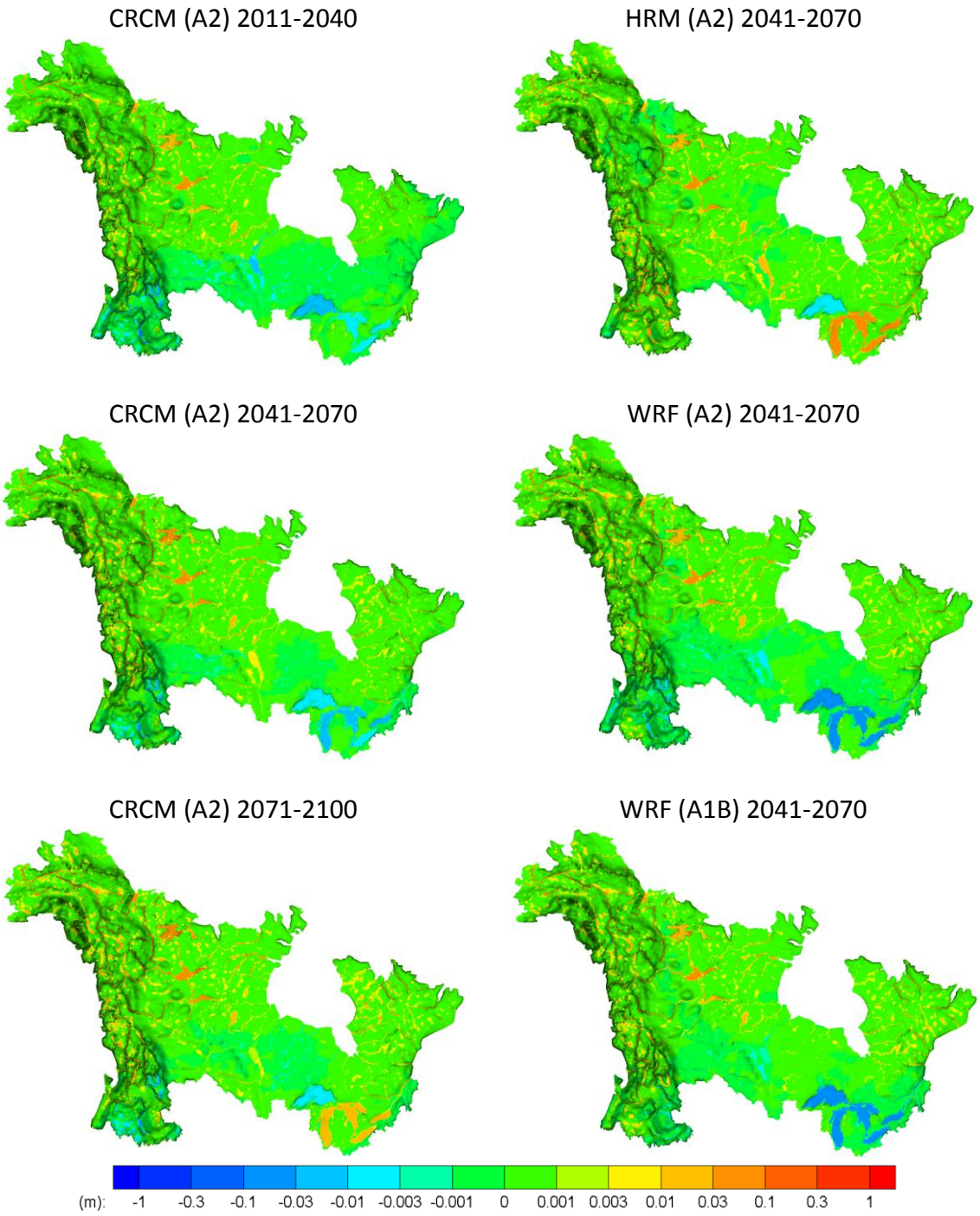

Figure 5-5: Predicted absolute change in surface water depth (m) based on RCM future climate projections. A positive change means an increase in surface water depth and a negative change represents a decrease in surface water depth.

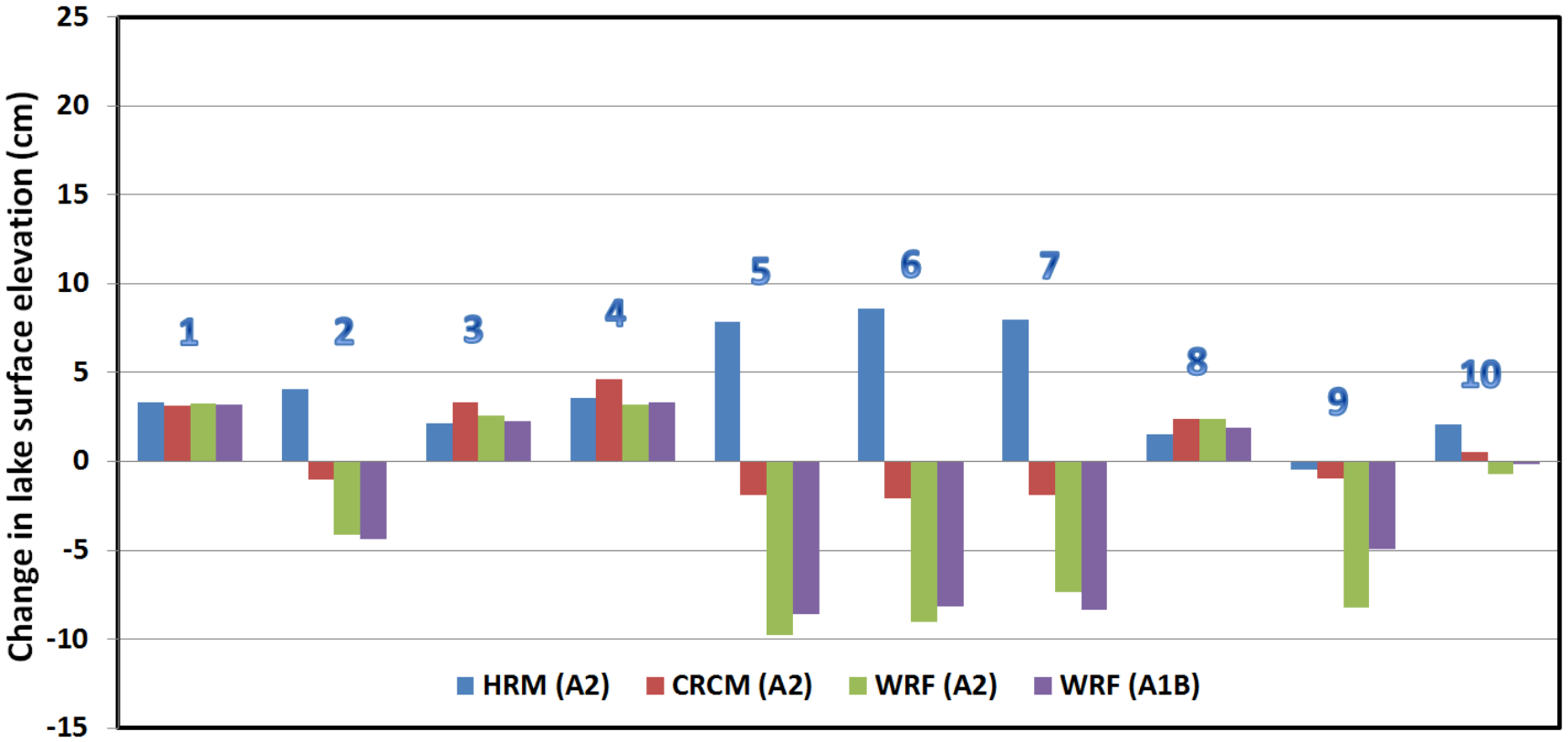

Figure 5-6: Predicted change in major lake surface elevations (cm) over the Mid-21st century (2041-2070) based on four RCM projections. Numbers on top of the bars denote the 10 largest lakes within the study domain as follows. 1: Athabasca; 2: Erie; 3: Great Bear; 4: Great Slave; 5: Huron; 6: Michigan; 7: Ontario; 8: Reindeer; 9: Superior; 10: Winnipeg.

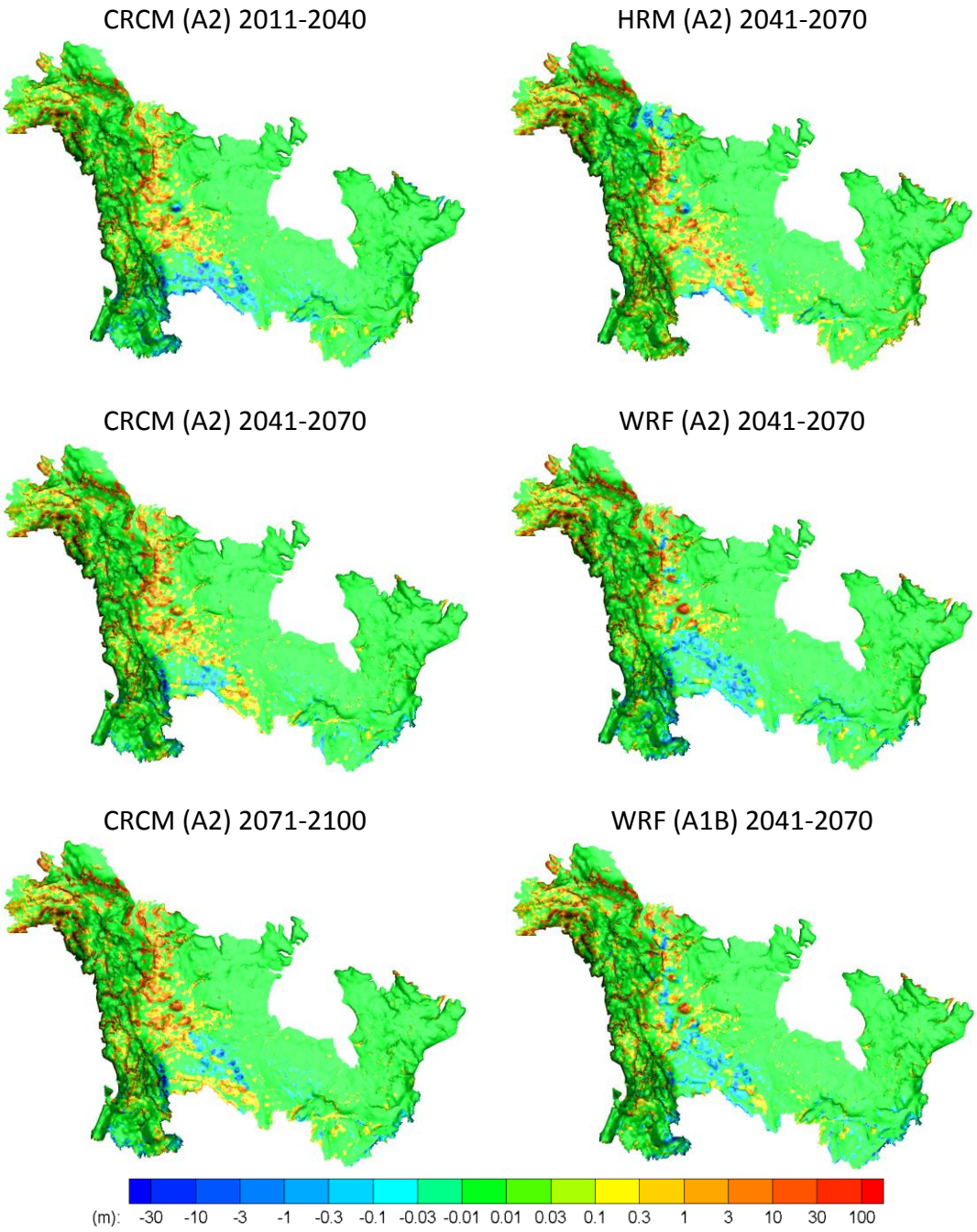

Figure 5-7: Predicted absolute change in watertable elevation (m) based on RCM future climate projections. A positive change means a rise in water table and a negative change represents a decline in water table.

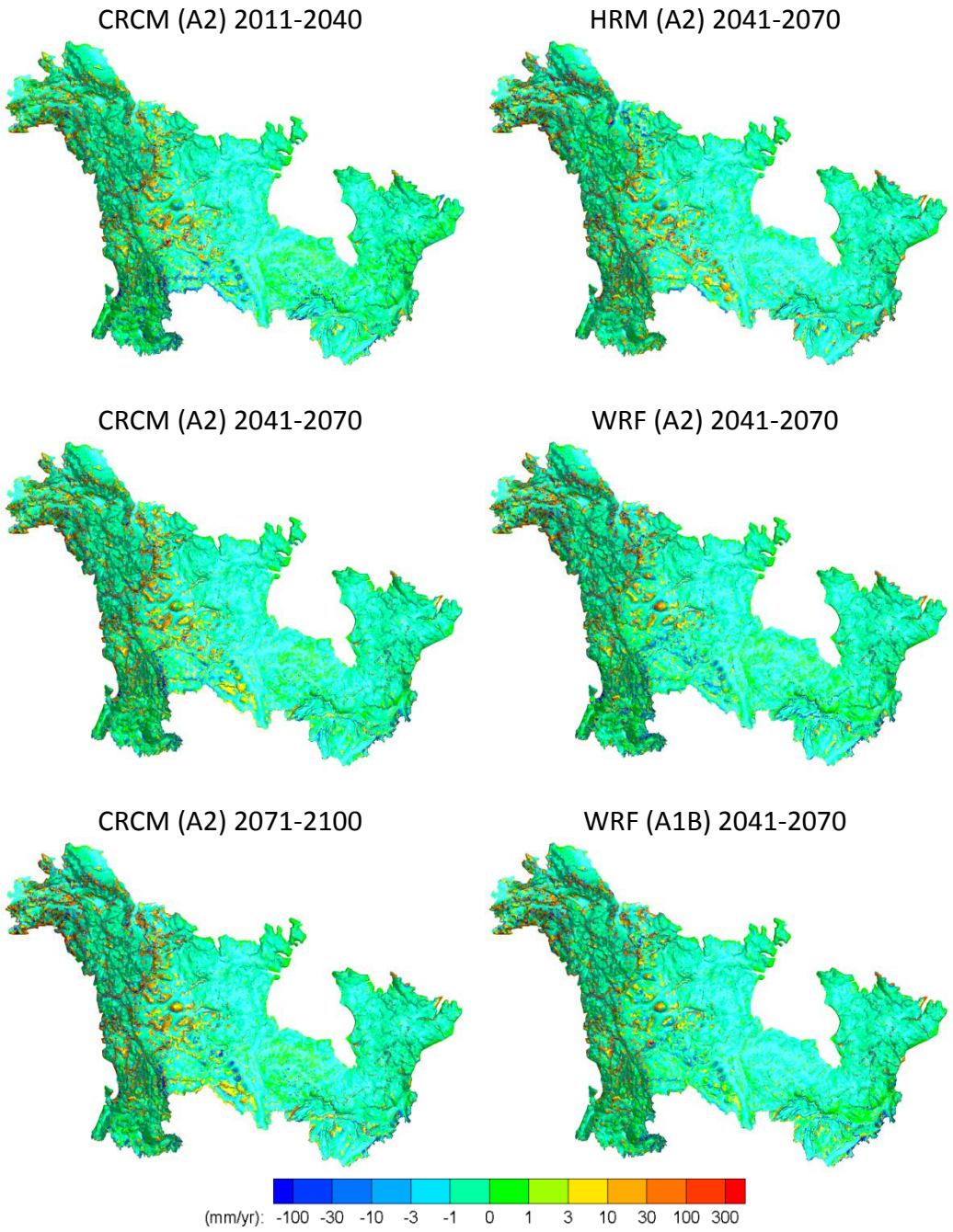

Figure 5-8: Predicted absolute change in rates of groundwater recharge (mm/yr) based on RCM future climate projections. A positive change means an increase in groundwater recharge and a negative change represents a decrease in groundwater recharge.

Chapter 6
Discussions and Conclusions

It is a well-known fact that the atmospheric component is the cornerstone for climate models and the meteorological variables are the primary targeted outputs. Although most current-generation climate models have begun to include an operational groundwater flow package, they have not yet incorporated a physically realistic representation of groundwater dynamics and storage, and hence their influence on the energy balance between land and the atmosphere. A comparison between HydroGeoSphere and CCSM3 simulated present-day infiltration / exfiltration results (Figure 4-6) demonstrates that the new-generation climate models may benefit from adopting a more sophisticated groundwater flow module and include a deeper soil column to better capture the feedbacks of both mass and energy from groundwater.

In this study, based on the HRM (a RCM without a lake model) output, lake levels are predicted to increase substantially for four of the five Great Lakes by 2041-2070. On the other hand, all Great Lakes are predicted to have a significant decrease in lake level based on the WRF (a RCM with a sophisticated lake model) projections (under both A2 and A1B scenarios). In addition, the CRCM (a RCM with a simple lake model) projection also forecasts a decrease in lake level for the five Great Lakes by 2041-2070, although the decrease is less significant than the WRF based predictions. The message discussed above is also upheld by the detailed breakdown in the water budget analysis for the Great Lakes

performed in this study. Thus, it is critically important for a regional climate model to couple to a lake model to capture the significant lake effect on regional climate.

The uncertainties in predictions of hydrologic responses to future climate change are mainly from: the biases embedded in climate models; the uncertainties associated with the underlying assumptions of the IPCC SRES emissions scenarios; and the errors associated with the model structures and the input parameters to the hydrologic models. In this study, no attempts are made to evaluate the uncertainties arising from the selection of hydrologic models. Minville et al. [2008] suggested that the uncertainty in hydrologic models is relatively minor in contrast to that induced by the choice of a climate model. On the other hand, Butt et al. [2004] showed that the uncertainty attributed to the choice of a hydrologic model is of the same order of magnitude as those associated with the selection of a climate model and the emissions scenario. Efforts are made to assess the uncertainties attributed to the first two sources in this study. Based on the limited number of comparisons made here, the uncertainties arising from the various climate models appear to dominate over the uncertainties associated with the emission scenarios. This result is in agreement with other impact studies [e.g. Kerkhoven and Gan, 2011; Choi et al., 2009; Minville et al., 2008]. More SRES scenarios, especially those with low emissions, should be investigated in the future to have a more comprehensive assessment of the sensitivity to different emissions scenarios. The uncertainties associated with climate models could be further separated to those arising from the particular RCM used during the downscaling process and to the GCM used for a global simulation. However, it is beyond the scope of this study to make this assessment. While quantification of the uncertainties in the hydrologic impacts due to climate change will

continue to be a meaningful and much needed research exercise, efforts that attempt to improve our understanding of the hydro-climatic system are much needed in the decision-making process [Pappenberger and Beven, 2006]. This work represents a first attempt on the continental scale and is thus a starting point for future studies.

While hydrologic impact studies at the watershed scale focusing mainly on surface water will probably continue to be the main focus in the literature for the years to come, the option of using a fully-coupled surface-subsurface flow model at the continental scale should be pursued. To the best of my knowledge, this study is the first continental-scale hydrologic impact study that couples surface water and groundwater flow, and the work undertaken here clearly demonstrates that a continental-scale hydrologic simulation of this type is feasible. Overall, the comprehensive 3D HydroGeoSphere model reasonably well reproduces the present-day hydrology over the continental-scale study domain. As faster computers become available and more efficient numerical algorithms are developed, hydrologically important features such as rivers, lakes and watersheds at the regional or local scale could be represented with a finer grid, both horizontally and vertically.

The hydrologic simulations presented in this study are steady-state in nature. Although steady-state results are meaningful in providing trends in the average hydrologic responses to climate evolution, it is a limitation that the steady-state model lacks the capacity to predict the hydrologic responses to seasonal variations as well as extreme weather events of relevance to a flooding and drought. A transient model with a higher grid resolution and more refined hydrologic properties should be developed to perform annual cycle simulations

in the future. The presence (or absence) of permafrost is known to have a significant influence on both surface water and groundwater flow regimes because of its vast extent and relatively low permeability. Global warming will have a direct influence on the distribution of permafrost, especially around its periphery and its upper layers. Thus, its hydraulic properties and distribution should ideally evolve with time for future-time simulations. However, in this work, these factors were not considered for the future-time simulations due to the lack of a projection of the 3D distribution of permafrost in the future. Similarly, LULC data ideally should also be updated as the climate system evolves but the vegetation cover, for example, is assumed to be stationary in this work.

In this study, six sets of mean annual net precipitation patterns derived from RCM projections were used as the forcing for the HydroGeoSphere model to assess the potential hydrologic impacts of climate change. The simulation results suggest that climate change may have a significant influence on water resources in portions of the study domain, such as the NW, the Great Lakes and the Prairie regions. All RCM projections forecast an increase in streamflow (by 8~40%) along major rivers in the Northern and North-western regions over the 21st century. As a result, flooding may be a concern during a rainy season for these regions. Predictions for the changes in streamflow for other rivers are less pronounced and thus unclear. Lake levels in the North are consistently forecasted to rise by a few cm over the next 90 years. Predictions for changes in lake levels are generally similar among various RCM projections for the major lakes located in the North of the study domain. However, predictions for the Great Lakes are inconsistent between the HRM and other RCMs. Most projections except for the HRM-based case forecast a decline in the water table for the

Prairie region. Results for all scenarios also reveal that watertable elevations may rise in some mountainous areas in the West, but are unlikely to change much over the 21st century for the central and Eastern parts of the study domain.

The predicted decrease in mean annual lake surface elevation for the Great Lakes based on three out of four RCM projections by 2041-2070 may result in significant subsequent socio-economic and environmental impacts. For example, historical shipping records show that low lake levels will lead to reduced vessel draft and cargos which in turn increase the operating cost for shipping around the Great Lakes [Millerd, 2011]. However, due to the coarse grid resolution and the steady-state simulation in nature, detailed adaptation and mitigation strategies for climate change cannot be recommended based on this study. A high-resolution transient impact modelling study driven by an ensemble of future climate scenarios is suggested for the Great Lakes region due to its social-economic importance.

Bibliography

Allen, M. R., and W. J. Ingram, 2002. Constraints on future changes in climate and the hydrologic cycle. Nature 419, 22432 2002.

Aquanty Inc., 2013. HydroGeoSphere 2013 User Manual, Release 1.0.

Arakawa, A., and V.R. Lamb, 1977. Computational design of the basic dynamical processes of the UCLA general circulation model. In: Methods in Computational Physics, 17 [J. Chang (ed.)]. Academic Press, New York, 173-265.

Barnola, J.M., D., Raynaud, Y.S. Korotkevich, and C. Lorius, 1987. Vostok ice cores provides 160,000-year record of atmospheric CO_2. Nature 329, 408–414.

Brown, J., O.J. Ferrians Jr., J.A. Heginbottom, and E.S. Melnikov, 1998. revised February 2001. Circum-Arctic map of permafrost and ground-ice conditions. Boulder, CO: National Snow and Ice Data Center/World Data Center for Glaciology. Digital Media.

Brunner, P., and C.T. Simmons, 2012. HydroGeoSphere: A Fully Integrated, Physically Based Hydrological Model, Ground Water, 50 (2), 170-176. doi:10.1111/j.1745-6584.2011.00882.x

Butts, B., J.T. Payne, M. Kristensen and H. Madsen, 2004. An evaluation of the impact of model structure on hydrological modelling uncertainty for streamflow simulation. J. Hydrol. (Amsterdam) 298 (1–4): 242–266.

Chen, F., and J. Dudhia, 2001. oupling and advanced land surface-hydrology model with the penn state-NCAR MM5 modeling system. Part I: Model implementation and sensitivity. Mon. Weath. Rev., 129, 569-585.

Chow, V. T., 1959. Open Channel Hydraulics, New York: McGraw-Hill.

Collins, W., C.M. Bitz, M.L. Blackmon, G.B. Bonan, C.S. Bretherton, J.A. Carton, P. Chang, S.C. Doney, J.J. Hack, T.B. Henderson, J.T. Kiehl, W.G. Large, D.S. McKenna, B.D. Santer, and R.D. Smith, 2006. The Community Climate System Model Version 3 (CCSM3). J. Climate, 19, 2122–2143. doi: http://dx.doi.org/10.1175/JCLI3761.1.

Cox, P.M., R.A. Betts, C.B. Bunton, R.L.H. Essery, P.R. Rowntree, and J. Smith, 1999. The impact of new land surface physics on the GCM simulation of climate and climate sensitivity. Climate Dyn., 15, 183–203.

d'Orgeville, M., W.R. Peltier, A.R. Erler, and J. Gula, 2014. Climate change impacts on Great Lakes Basin precipitation extremes, J. Geophys. Res. Atmos., 119, 10,799–10,812, doi:10.1002/2014JD021855.

Erler, A. R., W. R. Peltier, and M. D'Orgeville, 2015. Dynamically Downscaled High-Resolution Hydroclimate Projections for Western Canada. J. Climate, 28, 423–450, doi:http://dx.doi.org/10.1175/JCLI-D-14-00174.1.

Flato, G. M., and G. J. Boer, 2001. Warming asymmetry in climate change simulations. Geophys. Res. Lett., 28, 195-198.

Fouquart, Y., and B. Bonnel, 1980. Computation of solar heating of the earth's atmosphere: A new parameterization. Beitr. Phys., 53, 35-62.

Forsyth, P.A., 1991. A control volume finite-element approach to napl groundwater contamination. SIAM Journal on Scientific and Statistical Computing 12, no. 5: 1029–1057.

Fowler, H. J., S. Blenkinsop and C. Tebaldi, 2007. Linking climate change modelling to impacts studies: recent advances in downscaling techniques for hydrological modelling. Int. J. Climatol. 27: 1547-1578.

Freeze, R.A., and J.A. Cherry, 1979. Groundwater. Prentice-Hall.

Global Runoff Data Centre, 2011. Long-Term Mean Monthly Discharges and Annual Characteristics of GRDC Station / Global Runoff Data Centre. Koblenz, Germany: Federal Institute of Hydrology (BfG).

Goderniaux, P., S. Brouyere, H.H. Fowler, S. Blenkinsop, R. Therrien, P. Orban, A. Dassargues, 2009. Large scale surface-subsurface hydrological model to assess climate change impacts on groundwater reserves. Journal of Hydrology 373:122-138.

Gordon, C., C. Cooper, C.A. Senior, H. Banks, J.M. Gregory, T.C. Johns, J.F.B. Mitchell, and R.A. Wood, 2000. The simulation of SST, sea ice extents and ocean heat transports in a version of the Hadley Centre coupled model without flux adjustments, Clim. Dynam., 16, 147-168.

Goyette, S., N.A. McFarlane, and G. Flato, 2000. Application of the Canadian Regional Climate Model to the Laurentian Great Lakes Regions. Implementation of a Lake Model. Atmos. Oc., 38, 481-503.

Gula, J., and W.R. Peltier, 2012. Dynamical downscaling over the Great Lakes basin of North America using the WRF regional climate model: The impact of the Great Lakes system on regional greenhouse warming, J. Clim., 25(21), 7723–7742.

Hamilton, K., 2008. Numerical resolution and modeling of the global atmospheric circulation: A review of our current understanding and outstanding issues. High Resolution Numerical Modelling of the Atmosphere and Ocean: 7 2008.

Harris, S.A., H.M. French, J.A. Heginbottom, G.H. Johnston, B. Ladanyi, D.A. Sego and R.O. van Everdingen, 1988. Glossary of Permafrost and Related Ground-ice Terms. Permafrost subcommittee on Geotechnical Research, National Research Council of Canada, Ottawa, Canada. Technical Memorandum, No. 142.

Hwang, H.-T., Y.-J. Park, E.A. Sudicky and P.A. Forsyth, 2014. A parallel computational framework to solve flow and transport in integrated surface–subsurface hydrologic systems. Environmental Modelling and Software, 61(Complete), 39-58. doi:10.1016/j.envsoft.2014.06.024.

Hunter, T. S., and T. E. Croley, II, 1993. Great Lakes Monthly Hydrologic Data, NOAA Data Report ERL GLERL, National Technical Information Service, Springfield, Virginia, USA.

IPCC, 2007. Climate Change 2007: The Physical Science Basis. Contribution of Working Group I to the Fourth Assessment Report of the Intergovernmental Panel on Climate Change. Cambridge University Press, Cambridge, United Kingdom and New York, NY, USA, 996 pp.

IPCC, 2013. The Physical Science Basis. Contribution of Working Group I to the Fifth Assessment Report of the Intergovernmental Panel on Climate Change. Cambridge University Press, Cambridge, UK.

Jones, C.G., U. Wilen, A. Ullerstig and U. Hannsson, 2004. The Rossby centre regional atmospheric climate change results. J. Hydrol. (Amsterdam) 318 (1-4):163-172.

Jones, R.G., M., Noguer, D.C. Hassell, D. Hudson, S.S. Wilson, G.J. Jenkins and J.F.B. Mitchell, 2004. Generating high resolution climate change scenarios using PRECIS, Met Office Hadley Centre, Exeter, UK, 40 pp.

Kite, G.W., A. Dalton, and K. Dion, 1994. Simulation of streamflow in a macroscale watershed using general circulation model data. Water Resources Research 30, 1547-59.

Koutsoyiannis, D., A. Efstratiadis, N. Namassis and A. Christofides, 2008. On the credibility of climate predictions. Hydrol. Sci. J. 53:4, pp. 671-684. doi:10.1623/hysj.53.4.671.

Laske, G., and G. Masters, 1997. A Global Digital Map of Sediment Thickness, EOS Trans. AGU, 78, F483.

Lemieux, J.-M., 2006. Impact of the Wisconsinian glaciation on Canadian continental groundwater flow, Ph.D. thesis, Univ. of Waterloo, Waterloo, Ont., Canada.

Lemieux, J.-M., E.A. Sudicky, W.R. Peltier, and L. Tarasov, 2008. Dynamics of groundwater recharge and seepage over the Canadian landscape during the Wisconsinian glaciation, J. Geophys. Res., 113, F01011, doi:10.1029/2007JF000838.

Lofgren, B.M., F.H. Quinn, A.H. Clites, R.A. Assel, A.J. Eberhardt and C.L. Luukkonen, 2002. Evaluation of potential impacts on Great Lakes water resources based on climate scenarios of two GCMs. Journal of Great Lakes Research, 28, 537–554.

Matsuura, K., and C.J. Willmott, 2009a. Terrestrial Precipitation: 1900 - 2008 Gridded Monthly Time Series. (Available at: http://climate.geog.udel.edu/~climate/html_pages/Global2_Ts_2009/README.global_p_ts_2009.html)

Matsuura, K., and C.J. Willmott, 2009b. Terrestrial Air Temperature: 1900 - 2008 Gridded Monthly Time Series. (Available at: http://climate.geog.udel.edu/~climate/html_pages/Global2_Ts_2009/README.global_t_ts_2009.html)

Maxwell, RM, and S.J. Kollet, 2008. Interdependence of groundwater dynamics and land-energy feedbacks under climate change. Nature Geosci 1(10):665–669. doi:10.1038/ngeo31.

Mearns, L.O., et al., 2007, updated 2011. The North American Regional Climate Change Assessment Program dataset, National Center for Atmospheric Research Earth System Grid data portal, Boulder, CO. Data downloaded 2011-06-17. (Available at: http://www.earthsystemgrid.org/browse/viewProject.htm?projectId=ff3949c8-2008-45c8-8e27-5834f54be50f)

McFarlane, N.A., J. F. Scinocca, M. Lazare, R. Harvey, D. Verseghy, and J. Li, 2005. The CCCma third generation atmospheric general circulation model. CCCma Internal Rep., 25 pp.

Millerd, F., 2011. The potential impact of climate change on Great Lakes international shipping. Clim. Chang. 104 (3–4), 629–652.

Minville, M., F. Brissette and R. Leconte, 2008. Uncertainty of the impact of climate change on the hydrology of a nordic watershed. Journal of Hydrology 358 (1–2), 70–83. doi: 10.1016/j.jhydrol.2008.05.033.

Mironov, D., 2008. Parameterization of lakes in numerical weather prediction. Description of a lake model. COSMO Technical Report, No. 11, Deutscher Wetterdienst, Offenbach am Main, Germany, 41 pp.

Mironov, D., E. Heise, E. Kourzeneva, B. Ritter, N. Schneider, and A. Terzhevik, 2010. Implementation of the lake parameterisation scheme FLake into the numerical weather prediction model COSMO. Boreal Env. Res., 15, 218-230.

Morcrette, J.-J., 1984. Sur la parametrisation du rayonnement dans les modeles de circulation generale atmospherique, Ph.D. thesis, Universite des Sciences et Technique de Lille, 373 pp. (Available from Universite des Sciences et Technique de Lille, 59655 Villeneuve d'Asq Cedex, France)

Music, B., and D. Caya, 2007. Evaluation of the Hydrological Cycle over the Mississippi River Basin as Simulated by the Canadian Regional Climate Model (CRCM). J. Hydromet.,8(5), 969-988.

Nakicenovic, N., and R. Swart eds., 2000. IPCC Special Report on Emissions Scenarios, Cambridge University Press, Cambridge, United Kingdom, 612.

Neff, B. P., and J.R. Nicholas, 2005. Uncertainty in the Great Lakes Water Balance: U.S. Geological Survey Scientific Investigations Report 2004-5100, 42 p.

Nerem, R.S., D.P. Chambers, C. Choe and G.T. Mitchum, 2010. Estimating mean sea level change from the TOPEX and Jason altimeter missions. Mar. Geodesy 33, 435–446.

Nemec, J., and J. Schaake, 1982. Sensitivity of water resources system to climate variation. Hydrological Sciences Journal 27: 327– 343.

Neuman, S.P., 1994. Generalized scaling of permeabilities: Validation and effect of support scale, Geophys. Res. Lett., 21,349-352.

NGDC, 1988. Data Announcement 88-MGG-02, Digital relief of the Surface of the Earth. NOAA, National Geophysical Data Center, Boulder, Colorado, USA.

Noetinger, B., V. Artus, and G. Zargar, 2005. The future of stochastic and upscaling methods in hydrogeology. Hydrogeology Journal. 13 (1), 184-201.

Nuclear Waste Management Organization (NWMO), 2012. Adaptive Phased Management Used Fuel Repository Conceptual Design and Postclosure Safety Assessment in Crystalline Rock, Pre-Project Report, NWMO TR-2012-16. Toronto, Canada.

Pappenberger, F. and K. Beven, 2006, Ignorance is bliss: Or seven reasons not to use uncertainty analysis, Water Resour. Res., 42, W05302, doi:10.1029/2005WR004820.

Parrenin, F., et al., 2007. The EDC3 chronology for the EPICA Dome C ice core. Climate of the Past 3: 485-497.

Petit, J.R., et al., 1999. Climate and atmospheric history of the past 420,000 years from the Vostok ice core, Nature, 399, 429–436.

Randall, D.A., R.A. Wood, S. Bony, R. Colman, T. Fichefet, J. Fyfe, V. Kattsov, A. Pitman, J. Shukla, J. Srinivasan, R.J. Stouffer, A. Sumi and K.E. Taylor, 2007. Cilmate Models and Their Evaluation. In: Climate Change 2007: The Physical Science Basis. Contribution of Working Group I to the Fourth Assessment Report of the Intergovernmental Panel on Climate Change [Solomon, S., D. Qin, M. Manning, Z. Chen, M. Marquis, K.B. Averyt, M.Tignor and H.L. Miller (eds.)]. Cambridge University Press, Cambridge, United Kingdom and New York, NY, USA.

Rehana, S., and P.P. Mujumdar, 2011. River water quality response under hypothetical climate change scenarios in Tunga-Bhadra river, India, Hydrological Processes, 25 (22), 3373-3386.

Ross, M., M. Schumacher, J. Chen and E.A. Sudicky, 2010. Towards a seamless model of Quaternary sediments for continental-scale hydrogeology in North America, Abstract H21D-1081 presented at 2010 Fall Meeting, AGU, San Francisco, Calif., 13-17 Dec.

Skamarock, W., J. Klemp, J. Dudhia, D. Gill, D. Barker, W. Wang and J. G. Powers, 2007. A description of the Advanced Research WRF Version 2. NCAR Technical Note.

Spitz, K., and M. Joanna, 1996. A Practical Guide to Groundwater and Solute Transport Modeling. Wiley, New York.

Sushama, L., R. Laprise, D. Caya, A. Frigon, and M. Slivitzky, 2006. Canadian RCM projected climate-change signal and its sensitivity to model errors, Int. J. Climatol., 26, 2141–2159, doi:10.1002/joc.1362.

Tarasov, L., and W. R. Peltier, 2007. Coevolution of continental ice cover and permafrost extent over the last glacial-interglacial cycle in North America, J. Geophys. Res., 112, F02S08, doi:10.1029/2006JF000661.

U.S. Geological Survey, 2000. HYDRO1K Elevation Derivative Database, Cent. for Earth Resour. Obs. and Sci., Sioux Falls, S.D. (available at http://eros.usgs.gov/#/Find_Data/Products_and_Data_Available/gtopo30/hydro)

van Roosmalen, L., B.S.B. Christensen and T.O. Sonnenborg, 2007. Regional differences in climate change impacts on groundwater and stream discharge in Denmark. Vadose Zone J. 6 (3), 554–571.

van Vuuren, D.P. et al., 2011. The representative concentration pathways: an overview. Climatic Change 109 (1-2): 5-31. doi:10.1007/s10584-011-0148-z.

Verseghy, D. L., 1991. CLASS - A Canadian Land Surface Scheme for GCMS. I. Soil Model. Int. J. Climatol., 11, 111-113.

Verseghy, D. L., N. A. McFarlane, and M. Lazare, 1993. A Canadian Land Surface Scheme for GCMs: II. Vegetation model and coupled runs. Int. J. Climatol., 13, 347-370.

Wentz, F. J., L. Ricciardulli, K. Hilburn, and C. Mears, 2007. How much more rain will global warming bring? Science 317:233–235.

Wilby, R. L., L. E. Hay, W. J. Gutowski, R. W. Arritt, E. S. Takle, Z. Pan, G. H. Leavesley, and M. P. Clark, 2000. Hydrological responses to dynamically and statistically downscaled climate model output, Geophys. Res. Lett., 27(8), 1199–1202, doi:10.1029/1999GL006078.

Willmott, C.J. and S.M. Robeson, 1995. Climatologically aided interpolation (CAI) of terrestrial air temperature. International Journal of Climatology, 15(2), 221-229.

Xu, C.Y., 1999. From GCMs to river flow: a review of downscaling methods and hydrologic modelling approaches. Progress in Physical Geography 23, 2 pp. 229-249.

Xu, C.Y., 2000. Modeling the effects of climate change on water resources in Central Sweden. Water Resources Management 14: 177-189.

Xu, C.Y., E. Widen, and S. Halldin, 2005. Modelling hydrological consequences of climate change - progress and challenges. Adv Atmospheric Sci 22(6):789–797.

Zhang, K., J. S. Kimball, R. R. Nemani, and S. W. Running, 2010. A continuous satellite-derived global record of land surface evapotranspiration from 1983 to 2006, Water Resour. Res., 46, W09522, doi:10.1029/2009WR008800.